N
P

JOURNAL OF FOOD PROCESS ENGINEERING

D.R. HELDMAN
and
R.P. SINGH
COEDITORS

FOOD & NUTRITION PRESS, INC.

VOLUME 19, NUMBER 2 JUNE 1996

JOURNAL OF FOOD PROCESS ENGINEERING

All articles for publication and inquiries regarding publication should be sent to DR. D.R. HELDMAN, COEDITOR, *Journal of Food Process Engineering*, Food Science/Engineering Unit, University of Missouri-Columbia, 235 Agricultural/Engineering Bldg., Columbia, MO 65211 USA; or DR. R.P. SINGH, COEDITOR, *Journal of Food Process Engineering*, University of California, Davis, Department of Agricultural Engineering, Davis, CA 95616 USA.

All subscriptions and inquiries regarding subscriptions should be sent to Food & Nutrition Press, Inc., 6527 Main Street, P.O. Box 374, Trumbull, CT 06611 USA.

One volume of four issues will be published annually. The price for Volume 19 is $149.00, which includes postage to U.S., Canada, and Mexico. Subscriptions to other countries are $172.00 per year via surface mail, and $183.00 per year via airmail.

Subscriptions for individuals for their own personal use are $119.00 for Volume 19, which includes postage to U.S., Canada and Mexico. Personal subscriptions to other countries are $142.00 per year via surface mail, and $153.00 per year via airmail. Subscriptions for individuals should be sent directly to the publisher and marked for personal use.

The *Journal of Food Process Engineering* (ISSN:0145-8876) is published quarterly (March, June, September and December) by Food & Nutrition Press, Inc.—Office of Publication is 6527 Main Street, P.O. Box 374, Trumbull, Connecticut 06611 USA.

Second class postage paid at Bridgeport, CT 06602.

POSTMASTER: Send address changes to Food & Nutrition Press Inc. 6527 Main Street. P.O. Box 374, Trumbull, Connecticut 06611 USA.

JOURNAL OF FOOD PROCESS ENGINEERING

JOURNAL OF FOOD PROCESS ENGINEERING

Journal of FOOD PROCESS ENGINEERING

VOLUME 19
NUMBER 2

Coeditors: D.R. HELDMAN
R.P. SINGH

FOOD & NUTRITION PRESS, INC.
TRUMBULL, CONNECTICUT 06611 USA

ISSN 0145-8876

Printed in the United States of America

CONTENTS

CHANGES IN THE VISIBLE/NEAR-INFRARED SPECTRA OF CHICKEN CARCASSES IN STORAGE[1]

YUD-REN CHEN[2], ROY W. HUFFMAN and BOSOON PARK

U.S. Department of Agriculture, Agricultural Research Service
Beltsville Agricultural Research Service
Instrumentation and Sensing Laboratory
Beltsville, Maryland 20705-2350

Accepted for Publication September 29, 1995

ABSTRACT

A spectrophotometer was used to measure the visible/near-infrared (Vis/NIR) spectra of post-mortem chicken carcasses freshly slaughtered, 1, 2, 3, 4, 8, 11, and 14 days after storage at 0, 4, and 20C. The spectrum of a carcass after storage was compared with the spectra of freshly slaughtered carcasses and the spectra of carcasses stored at the different temperatures. The method of comparison was performed by computing the Mahalanobis distance of the sample's second central difference spectrum from the group means of the second central difference spectra of all the carcasses measured shortly after slaughter (about 1 h) and the set of second central difference spectra of the carcasses stored at each temperature. The results showed the spectra of the chicken carcasses changed 24 h after removal from the slaughter plant, even though they were stored at 0C. The spectra of the carcasses stored at 20C were different from those of the carcasses stored at 0 and 4C. The spectra of the carcasses stored at 0 and 4C for the first 8 days remained in the same class of the spectra of the carcasses at 1 day of storage at 0C. However, the spectra changed dramatically after 8 days of storage. The pattern of change of the spectra coincided with that of the myoglobin and oxymyoglobin changes of chicken carcasses at various storage temperatures and durations. It was suggested that Vis/NIR spectroscopy has the potential to be used as a rapid, nondestructive method for monitoring the freshness of chicken carcasses.

[1] Mention of any company or trade name does not imply endorsement of the products by the U.S. Department of Agriculture. It is for the purpose of description only.

[2] Address correspondence to: Y.R. Chen, USDA-ARS, NRI, ISL, Bldg. 303, BARC-EAST, Beltsville, MD 20705-2350, Phone: (301) 504-8450 FAX: (301)504-9466.

INTRODUCTION

Poultry products have increased in popularity with U.S. consumers in recent years. Per capita consumption of chicken products increased from 18.5 kg in 1970 (USDA 1975) to 32 kg in 1993 (USDA 1994). Similarly, the number of chicken slaughtered at federally inspected establishments increased from 3.1×10^9 in 1973 (USDA 1975) to 6.9×10^9 birds in 1993 (USDA 1994). The export market increased even more dramatically, the United States exported 92.3×10^6 kg in 1973 (USDA 1975) and 919×10^6 kg in 1993 (USDA 1994).

The development of accurate, reliable, and economical sensors is of paramount importance to the industry's goal of improved poultry product quality. A system that is capable of detecting spoilage of chicken carcasses at the distribution center, grocery store, and even at home will be very useful in improving consumer's confidence in poultry products and, in turn, will further increase the products acceptance because the system will ensure food freshness to the public. Such an instrument to detect the changing quality of poultry products will also provide the USDA/State Inspectors a tool for objective evaluation of poultry quality. The system will also benefit the U.S. poultry industry to compete in world markets. For practical purposes the testing of quality has to be rapid and has to be performed on-site. Modern technologies of spectrophotometry, electronics, computer science, and pattern recognition will be used to make such a system possible.

Chen and his co-worker (Chen 1992; Chen and Massie 1993) worked on a project to develop a rapid technique to detect certain abnormal poultry carcasses on-line at slaughter plants. They have developed classifiers to separate chicken carcasses into normal, septicemic, and cadaver classes, based on the visible/near-infrared (Vis/NIR) spectra of the chicken carcasses. They concluded that the classifiers based on Vis/NIR reflectance and interactance of chicken carcasses can be used effectively in separation of normal carcasses from abnormal (septicemic and cadaver) carcasses. The spectral reflectance and interactance were defined as the ratio of the light energy returning from a sample to the energy returning from a reference material. For the reflectance measurement, the probe which receives the returning light was placed a certain distance away from the sample. For the interactance measurement, the probe was placed directly against the sample.

There can be a considerable lapse between the time chicken products leave processing plants and the time they are purchased by the consumer. During this time the poultry products are subjected to different methods of transportation and cold-storage, which will change the product's quality. There is a great need to monitor the quality of the carcasses during this time. We are therefore interested in constructing a portable instrument that could be used to rapidly detect if the quality of poultry carcass has changed. The changes of quality can indirectly be

measured by the changes in the chemical and physical states of the carcasses. Since Vis/NIR spectroscopy of the carcass varies with the chemical condition of the carcass, the objective of this research was to determine the feasibility of the Vis/NIR spectral measurement of chicken carcasses as a function of aging and storage temperatures.

MATERIALS AND METHODS

Diode-Array Spectrophotometer

A transportable diode-array spectrophotometer system (Oriel 60000, ORIEL Co., Stratford, CT) was assembled and tested. This system is capable of measuring optical spectra of poultry products in the laboratory, poultry slaughter plants, distribution centers (cold storage houses), and grocery stores in a dark room. Chen and Massie (1993) developed a system based on a photodiode array spectrophotometer system to obtain optical spectra of the breasts of poultry carcasses in the visible and near-infrared regions.

The transportable system consists of a tungsten halogen light source, bifurcated fiber optic probe assembly, spectrograph (Oriel 77400, ORIEL Co., Stratford, CT), photodiode array detector (Oriel 77111, ORIEL Co., Stratford, CT), personal computer with a photodiode array computer interface card (Oriel 77112, ORIEL Co., Stratford, CT) and 16 bits A/D converter installed, and a lamp power supply (Oriel 68830, ORIEL Co., Stratford, CT) as shown in Fig. 1. The photodiode array detector was thermoelectrically cooled to a temperature of 20 $\pm$ 0.1C.

Light from a 100 W quartz tungsten halogen light bulb was focused on the light source circular end of a fiber optic bundle (see Fig. 2). A constant current DC power supply was used to keep the light intensity constant and minimize color temperature shift as a result of power line fluctuations.

This light energy travels through the fiber optic bundle (1.2 m) and exits by means of a 5-mm diameter aperture in the center of a concentric optical probe (see Fig. 2). In this study, interactance at each wavelength was defined as the ratio of energy returning from a sample to the energy returning from a reference material (Teflon™ block, DuPont, Wilmington, DE). Unlike reflectance, when taking the interactance measurements, the probe was in direct contact with the sample.

After interacting with the skin and muscle tissue of the carcass, the light energy was collected through a concentric ring of optical fibers (2 mm thick at a diameter of 10 mm) at the circular end of a fiber optic bundle (see Fig. 2). The collected energy was transmitted back through the same bifurcated fiber optic cable to a 4 $\times$ 20 mm exit rectangle (slit). The fixed entrance slit of the spectrograph was 25 μm wide.

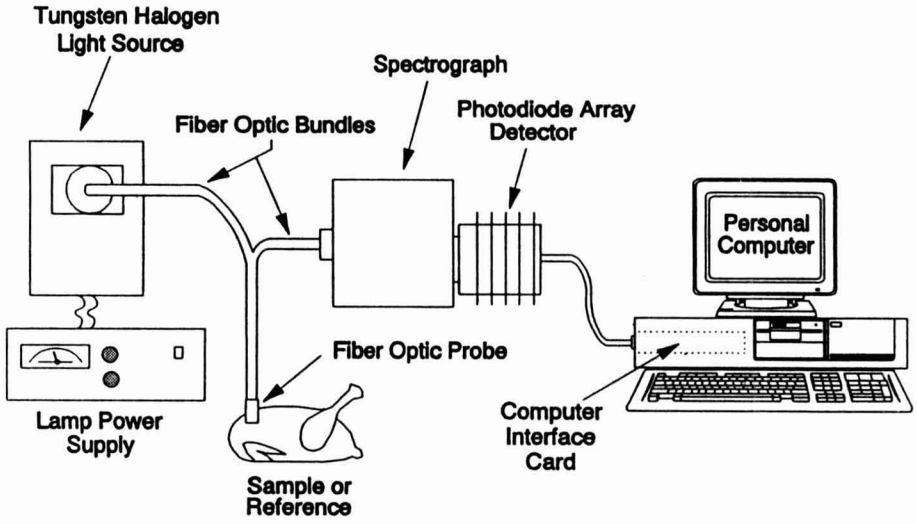

FIG. 1. A SCHEMATIC DIAGRAM OF THE DIODE ARRAY SPECTROPHOTOMETER

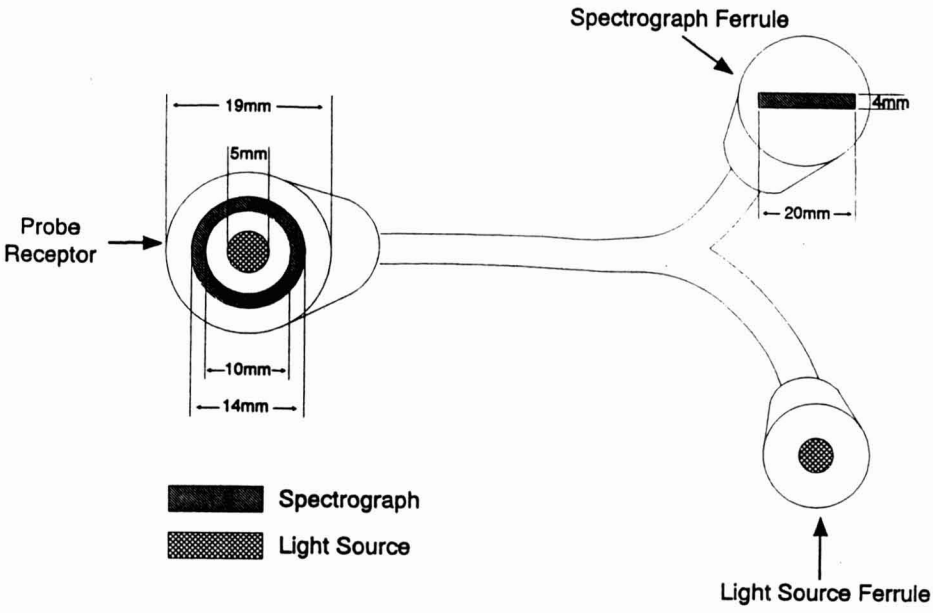

FIG. 2. A SCHEMATIC DIAGRAM OF THE FIBER OPTIC BIFURCATED CABLE

Calibration of the Spectrophotometer System

The wavelength calibration was done by using a high intensity short wave UV light source (Hg(Ar) Penray™, UVP Inc., San Gabriel, CA) placed near the probe receptor. This ensured the accuracy of the spectral calibration. The spectra emissions of the mercury lamp were measured at the mercury doublet at 577 and 579.1 nm and at the peak of 546.1 nm. A dark reference (background measurement) was taken to compensate for the zero energy signal. A reference measurement was provided by using a ground pressed Teflon™ block placed against the probe receptor with the light source on to establish a spectrally flat repeatable high energy reference.

Procedures

Thirty normal fresh chicken carcasses were selected by a Food Safety and Inspection Service (FSIS) plant veterinarian from the processing line at a poultry slaughter plant located on Maryland's Eastern Shore.

The spectrophotometer system was set up in a dark room near the processing floor at the chicken slaughter plant. Thirty normal carcasses were removed from the processing line right after they went through the chill tank (about 0C). The spectra (Vis/NIR) of the left and right breasts with skin on of the whole chicken carcasses were then measured in the dark environment at the slaughter plant (designated as Day 0). The spectrophotometer measured the spectral interactance of each carcass in the wavelength range of 471 to 963.7 nm in increments of 0.4816 nm. For the interactance measurements, each spectrum was the mean of 50 scans of the diode array where each scan was a result of 0.2 s photodiode array exposure. A reference reading (Teflon™) was taken at the beginning and at intervals of 10 chickens thereafter.

The carcasses were placed into plastic picnic coolers (in lots of 10 filled with ice) and transported to USDA's Instrumentation and Sensing Laboratory in Beltsville, Maryland. At the laboratory the ice was removed from the coolers and the chickens were stored in the coolers with the lids closed to minimize dehydration in the following environments: (1) 0C cold room, (2) 4C refrigerator, and (3) 20C.

The following afternoon, 24 h post-mortem (designated as Day 1), interactance measurements were obtained on both sides of the breast of each carcass. The room was in complete darkness when the measurements were taken for the carcasses stored at 0 and 4C. For the measurements of the chickens stored at 20C, the room was kept as dark as possible and the carcass and probe were covered with a black cloth. After the measurements were taken, the carcasses were returned to their original storage environments until measurements were to be taken again. The same measurements were repeated 2 days

post-mortem (Day 2), 3 days postmortem (Day 3), and 4 days postmortem (Day 4) on all chickens at the three different storage temperatures.

On Day 4, the chickens stored at 20C were disposed of due to extreme deterioration of the carcass. Spectral measurements on the cold room and refrigerator chickens continued, taken on 8 days postmortem (Day 8), 11 days postmortem (Day 11), and 14 days postmortem (Day 14).

Data Analysis

To classify an unknown sample, the Mahalanobis distance (D_M) from the unknown to the class to be classified against was calculated. Second central difference interactance were used in the following computation, because as found in a previous study (Chen and Massie 1993), the second central difference spectra were better indicators of the condition of the carcass, when interactance was measured.

The spectral interactance with wavelengths from 530 to 920 nm were smoothed with 11 points averaging and the gap size of the second difference was 20 points. For a more detailed description of second central difference, see Chen and Massie (1993).

The Principal-Component-Analysis (PCA) Method and Mahalanobis-Distance (D_M) Classifier were used for the data analysis. The PCA method expresses the spectral vector of any carcass as a linear combination of a set of orthogonal (uncorrelated) vectors, called factors. The first factor, a vector of second difference interactances, is chosen to account for the largest possible fraction of the variance of the interactances in the class. Each successive factor is then chosen to account for the largest possible fraction of the remaining variance. A few factors can usually account for most of the variance. The optimal number of factors were determined by the Malinowski's indicator (Galactic Industries Corp. 1989). When a spectrum is expressed as a linear combination of these factors, the coefficients are called the factor scores. Each spectrum can be adequately represented by a few scores in factor space instead of many interactances in wavelength space.

A set of factors was developed for the class to be tested against by other spectra. Any spectrum was tested against the class to see whether the spectrum belongs to the class, based on its Mahalanobis distance (D_M) from the class group mean. Theoretically, for the unknown spectrum to be classified as in the class, the D_M of the unknown sample should be less than three times the D_M of the class group mean. However, Mark and Tunnell (1985) stated that because of small variations in the size, shape, or orientation between the two samples, small changes in the physical nature of the samples, drifts in the instrument, etc., samples of the same group could be beyond the three standard deviation limit. Mark and Tunnell further showed that, for two spectra not to be in the

same group, the minimum D_M must lie between 10 and 15. To make sure that is on the conservative side, 15 was chosen to be the cut-off D_M in the paper.

The vector was first expressed in terms of the linear combination of the factors for that class. The scores and the residue error not modeled by PCA were used to compute the Mahalanobis distance from the centroid of each class. The Mahalanobis distance, unlike the Euclidean distance, is measured in units of standard deviation. The Mahalanobis distance provides a measurement of the likelihood of similarities between the vector and the class mean, and it assigns a statistical probability to that measurement. To improve the sensitivity of the classifier, the Mahalanobis distances were further scaled by the Root Mean Square Group (RMSG) size of each class.

The RMSG is determined by calculating the Mahalanobis distance for every sample in the class from the class mean:

$$RMSG = \sqrt{\frac{\sum_{i=1}^{n} d_i^2}{n-1}} \qquad (1)$$

where D_i is the Mahalanobis distance of vector i from the class mean and n is the number of patterns in the class in the set. The scaled Mahalanobis distance (D_M) was assigned to the vector.

The pattern vectors consisted of the second central differences of each spectrum. The second central difference was computed by:

$$S''(\lambda_n, g) = S(\lambda_n + 0.4816g) - 2S(\lambda_n) + S(\lambda_n - 0.4816g) \qquad (2)$$

where $S''(\lambda_n, g)$ is the second central difference value of the spectrum at wavelength λ_n, g is the "gap" measured in points (0.4816 nm per point interval). In this study, "Lab Calc™" (Galactic Industries Corp. 1989) was used to determine number of factors, mean, and variance of the class to be tested against, and the D_M of testing vectors. The factors were determined using within-group co-variance matrix.

RESULTS AND DISCUSSION

The means for the interactance spectra of the carcasses stored at 0, 4, and 20C for the different days of measurement are shown in Fig. 3 to 5, respectively. As indicated in these figures, there were two distinct interactance valleys (a and b) in the early stages of storage. These valleys could be an indication of oxymyoglobin or oxyhemoglobin absorption bands, however, the myoglobin might be the main pigment because the chicken carcasses were well bled (Francis and Clydesdale 1975). The spectral changes due to the combination of these two pigments might be major indicators to monitor the changing

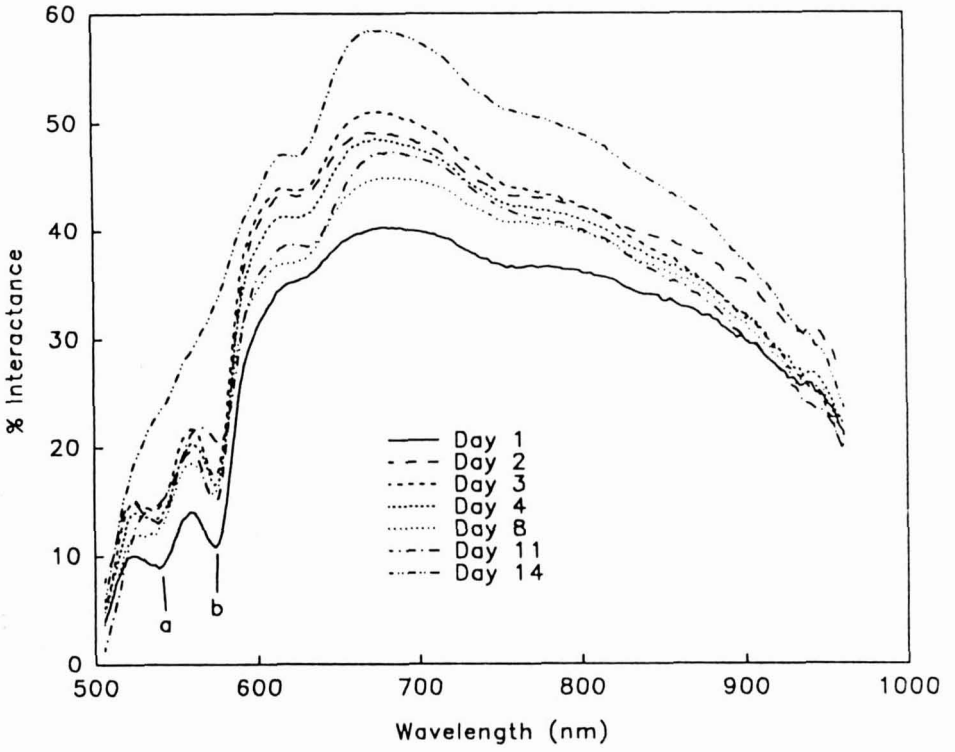

FIG. 3. MEAN INTERACTANCE SPECTRA OF THE CARCASSES STORED AT 0C CHANGED WITH STORAGE DURATION

composition of chicken carcasses since the two pigments undergo identical reactions that are of concern to meat color.

After 4 days of storage (Day 4) there was a clear indication of metmyoglobin formation by the diminishing of the interactance valleys (Points a and b of Fig. 3 to 5). This loss continued until Day 14 where the interactance valleys have completely disappeared in the 0 and 4C temperature. This indicates that metmyoglobin is the predominant pigment and muscle tissue of the chicken at this stage of storage.

The D_M of the spectra of the chicken carcasses at 0, 4, and 20C measured on subsequent days were computed and compared with the class of the spectra measured at the slaughter plant (Day 0). Table 1 presents the mean, minimum, and maximum D_M of the carcasses stored at room temperature (20C) at Day 1 through Day 4, and the carcasses stored at 0 and 4C at Day 1 through Day 14. Also given in Table 1 are numbers of the carcasses in each group having $D_M <$

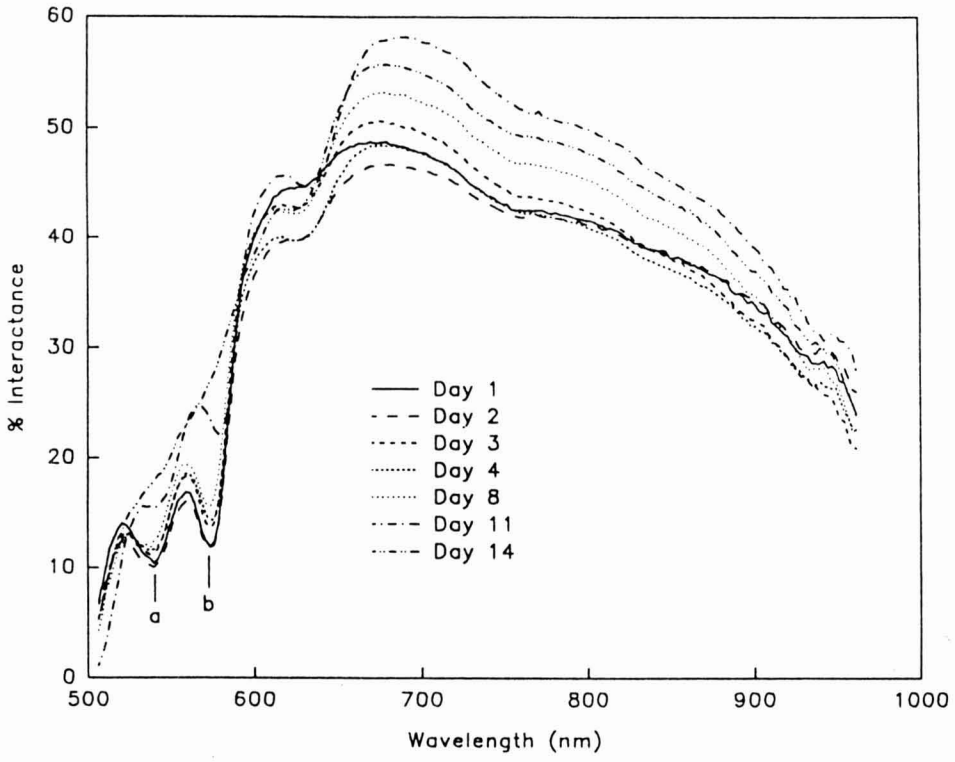

FIG. 4. MEAN INTERACTANCE SPECTRA OF THE CARCASSES STORED AT 4C CHANGED WITH STORAGE DURATION

15. Except Day 1 at 0 and 4C, most of the D_M in the three different temperature ranges were substantially greater than 15. At Day 1, there were 9 out of 20 spectra of the carcasses stored at 0C and 8 out of 20 spectra of the carcasses stored at 4C having a D_M greater than 15, i.e., these spectra no longer remained in the same group of the spectra obtained at the Day 0. These results showed that some carcasses have changed their chemical state during transport and storage in the laboratory, despite the fact that the carcasses were packed in ice during transportation and stored at 0 and 4C in the laboratory.

Table 2 presents the mean D_M, minimum and maximum D_M, and numbers of the spectra having $D_M < 15$ in each group of the carcasses stored at room temperature (20C) at Day 1 through Day 4, and the carcasses stored at 0 and 4C at Day 1 through Day 14, as compared to the class of 0C carcasses at Day 1. At Day 1, for the carcasses stored at 20C, 7 out of 20 had spectra completely different from the Day 1's spectra of carcasses at 0C. At Day 2, the number of

carcasses different from those stored at 0C doubled. However, for the carcasses stored at 0C and 4C, almost all spectra remained in the class up to Day 8 (D_M remaining below 15). At Day 8, 17 of the 20 carcasses at 0 and at 4C remained in the group of carcasses at Day 1 stored at 0C. Figure 6 is the plot of the mean D_M of the carcasses stored at different temperatures, as they were compared with the class of the carcasses after 1 day of transportation and storage at 0C. It was shown that the spectra of the carcasses stored at room temperature (20C) were very different from the Day 1's spectra of the carcasses stored at 0C.

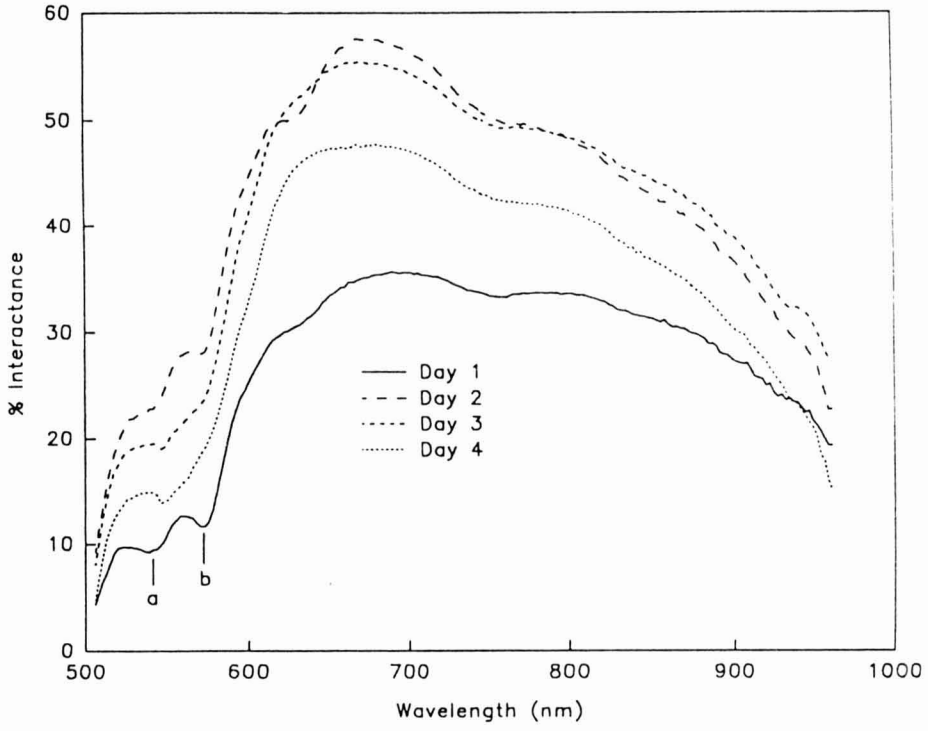

FIG. 5. MEAN INTERACTANCE SPECTRA OF THE CARCASSES STORED AT 20C CHANGED WITH STORAGE DURATION

TABLE 1.
MEAN D_M MAXIMUM AND MINIMUM D_M, NUMBER OF SPECTRA WITH D_M LESS THAN 15 OF THE CARCASSES STORED AT DIFFERENT TEMPERATURES AND DATES WHEN THE SPECTRA WERE MEASURED, AS COMPARED TO THE CLASS OF CARCASSES AT DAY 0

Temperature (°C)	Day 1	2	3	4	8	11	14
0	23.2 (6.4, 108) [11]	26.7 (8.3, 95.7) [4]	75.8 (14.8, 447) [0]	77.9 (6.6, 519) [4]	82.8 (35.4, 211) [0]	950 (39.0, 4050) [0]	23,298 (1208, 137400) [0]
4	17.5 (6.9, 55.8) [12]	32.3 (6.8, 68.1) [3]	49.9 (6.4, 173) [2]	67.5 (9.5, 260) [1]	101.6 (24.8, 358) [0]	1,956 (478, 12290) [0]	14,177 (111.3, 35740) [0]
20	6,850 (9.2, 134670) [2]	1,904 (20.5, 19020) [0]	595 (85.4, 3449) [0]	143,434 (158, 2459000) [0]	--	--	--

Note: The first and second numbers in ( ) are the minimum and maximum D_M in the group, respectively. The number in [ ] is the number of spectra with $D_M < 15$ in the group of 20.

TABLE 2.
MEAN D_M, MAXIMUM AND MINIMUM D_M, NUMBER OF SPECTRA WITH D_M LESS THAN 15 OF THE CARCASSES STORED AT DIFFERENT TEMPERATURES AND DATES WHEN THE SPECTRA WERE MEASURED, AS COMPARED TO THE CLASS OF 0C CARCASSES AT DAY 1

Temperature (°C)	Day 1	2	3	4	8	11	14
0	--	2.6 (0.5, 14.5) [20]	5.5 (0.52, 39.3) [18]	9.1 (0.77,93.0) [18]	11.1 (5.9, 42.3) [17]	525 (2.13, 1561) [4]	1,920 (284, 75437) [0]
4	2.2 (0.37, 11.3) [20]	2.8 (1.01, 5.40) [20]	5.3 (0.49, 65.1) [19]	6.2 (1.45, 29.1) [19]	13.2 (4.46, 79.6) [17]	1,085 (389, 5905) [0]	1,374 (62.7, 3102) [0]
20	7,237 (1.61, 143686) [13]	2,808 (1.99, 53592) [6]	472 (24.5, 4884) [0]	145,190 (139, 2613670) [0]	--	--	--

Note: The first and second numbers in ( ) are the minimum and maximum D_M in the group, respectively. The number in [ ] is the number of spectra with $D_M < 15$ in the group of 20.

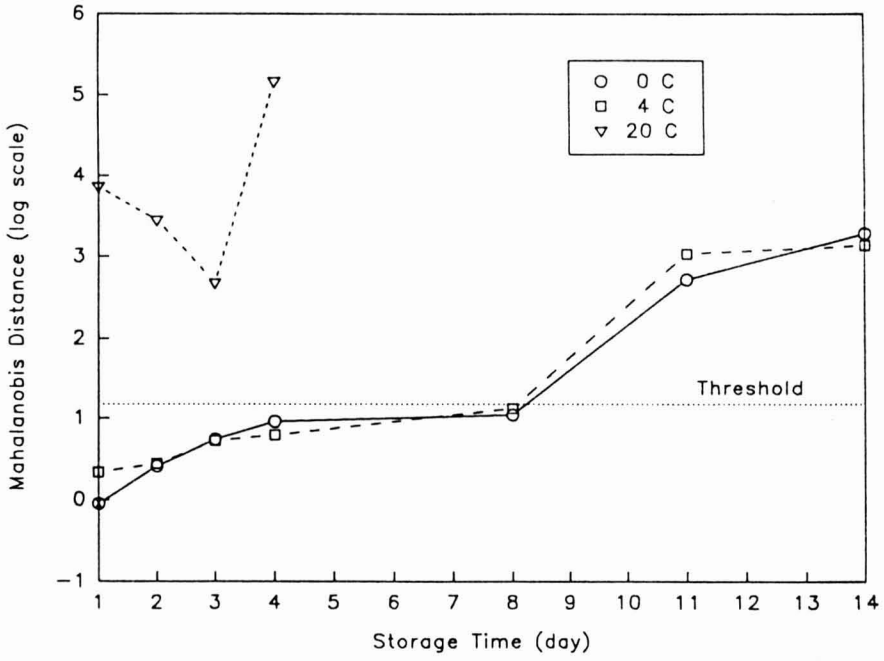

FIG. 6. MEAN MAHALANOBIS DISTANCE CHANGED WITH THE STORAGE TIME
Mahalanobis distance was computed on the second difference of the spectra of the carcass from the class of carcasses 24h postmortem (Day 1), stored at 0C. The threshold line is with $D_M = 15$

It was also observed that when the carcasses became slimy and malodorous the spectral characteristics became very different from the carcasses stored up to 4 days at 0C. This slimy and malodorous condition indicated that the carcasses have bacterial spoilage microbiologically.

When the mean D_M of the carcasses stored at different temperatures was compared to the class of 0C carcasses at Day 2, the second difference spectra of the carcasses stored at the room temperature (20C) were different from those of the 0C carcasses at Day 2, and the spectra of the carcasses stored at 0 and 4C remained in the class of those of the 0C carcasses at Day 2 up to Day 4. At Day 8 the 0 and 4C carcasses did not belong to the class of 0C carcasses at Day 2 and, after Day 11, the spectra with very large D_M were clearly very different from those of the carcasses stored at 0 and 4C and measured at Day 2.

When the spectra of carcasses were compared to the spectrum of Day 3 and Day 4 carcasses, similar results were obtained. The results showed that the spectrum of carcasses stored at 0 and 4C belong to same class as Day 1 to Day 4. However, by Day 8, the spectra of the carcasses had changed from those at Day 1 to Day 4. The spectra were dramatically different from those of carcasses at Day 11 and Day 14.

The results of this study indicate that the Vis/NIR spectroscopy of the carcasses has the potential to be used as a rapid, nondestructive method for monitoring the biochemical conditions of the chicken carcasses. Further work is needed to correlate the changing Vis/NIR spectroscopy with pH and bacterial load of the carcasses stored at different temperatures and durations, and to study the effects of ambient light on measurements.

ACKNOWLEDGMENTS

The chicken carcasses used in this experiment were obtained from Allen Family Foods Inc. in Cordova, Maryland. The authors highly appreciate the technical assistance of Ajay Dhuria and the cooperation of Mr. Dale Harrison and Dr. Christopher Robinson in making this work possible.

REFERENCES

CHEN, Y.R. 1992. Classifying diseased poultry carcasses by visible and near-IR reflectance spectroscopy. Optics in Agriculture and Forestry. SPIE *1836*, 46–55.

CHEN, Y.R. and MASSIE, D.R. 1993. Visible/near-infrared reflectance and interactance spectroscopy for detection of abnormal poultry carcasses. Trans. of the ASAE. *36*(3), 863–869.

FRANCIS, F.J. and CLYDESDALE, F.M. 1975. The chemistry of meat color. In *Food Colorimetry: Theory and Application*, pp. 279–291, Van Nostrand Reinhold/AVI, New York.

Galactic Industries Corp. 1989. Lab Calc™ User's Guide, Salem, NH.

MARK, H.L. and TUNNELL, D. 1985. Qualitative near-infrared reflectance analysis using Mahalanobis Distances. Anal. Chem. *57*, 1449–1456.

USDA, 1975. Agricultural Statistics. 621 pages. United States Government Printing Office, Washington, D.C.

USDA, 1992. Agricultural Statistics. 524 pages. United States Government Printing Office, Washington, D.C.

USDA, 1994. Agricultural Statistics. 486 pages. United States Government Printing Office, Washington, D.C.

APPLICATION OF LASER DOPPLER ANEMOMETRY TO MEASURE VELOCITY DISTRIBUTION INSIDE THE SCREW CHANNEL OF A TWIN-SCREW EXTRUDER

MUKUND V. KARWE[1]

Food Science Department and
Center for Advanced Food Technology
P.O. Box 231, Cook College
Rutgers University
New Brunswick, New Jersey 08903

AND

VALENTINAS SERNAS

Mechanical Engineering Department
Rutgers University
New Brunswick, New Jersey 08903

Accepted for Publication June 30, 1995

ABSTRACT

Velocity measurements inside the screw channels of a co-rotating, self-wiping twin-screw extruder (ZSK-30) have been carried out using the noninvasive technique of Laser Doppler Anemometry. A two-dimensional Argon-ion laser Doppler system was used to measure tangential and axial velocity components in one of the screws, away from the intermeshing zone. Heavy corn syrup with naturally occurring particles was used in the extrusion experiments. The measured tangential velocity distribution agreed with the expected distribution for a Newtonian fluid. Measurements also indicated that near the screw root and away from the flights, shear rates were substantially lower as compared to the shear rates near the barrel. The results indicated that this technique is suitable for making velocity measurements in a twin-screw extruder using model fluids.

INTRODUCTION

Extrusion is one of the widely used industrial processes in the manufacture of food, plastic and pharmaceutical products. In the food industry, extrusion is used to make a variety of products such as pasta, ready-to-eat breakfast cereals, snacks and candy. It is also used to manufacture animal feed and pet products.

[1]To whom all correspondence should be addressed.

Journal of Food Process Engineering **19** (1996) 135–152.

Both single and twin-screw extruders are used depending upon the processing requirements such as mixing and shear intensity, conveying capacity, energy input to the product, degree of starch conversion, etc. (Harper 1989). In some situations, the use of a twin-screw extruder is advantageous because of its flexibility and ease of control (Miller 1993). In twin-screw extrusion of food materials, co-rotating screws are more commonly used because of their high shear cooking potential and capacity, less wear and enhanced mixing capability. Extrusion of plastics has been described in detail by several authors (Fenner 1980; Rauwendaal 1990; Tadmor and Gogos 1979; Tadmor and Klein 1970). The subject of extrusion cooking has been discussed at length by several investigators and the information has been compiled in a few volumes (Harper 1981; Mercier *et al.* 1989; Kokini *et al.* 1992).

In the last two decades there has been a substantial effort made to develop rigorous mathematical models of the extrusion process. Due to the complicated geometry of the screws and complex behavior of the flowing materials, the task of mathematical modeling is very challenging. Often, one has to resort to many simplifying assumptions in order to develop a model which will adequately describe overall performance of the extrusion process. However, these models are not sufficient to describe local transport, mixing, etc., accurately. Further, in most cases, the solutions to the governing transport equations have to be obtained numerically on a computer.

Modeling of a single-screw extruder is relatively less difficult as compared to modeling of a twin-screw extruder. In a few of the very early studies (Carley and Strub 1953; Carley *et al.* 1953; McKelvey 1953), simplified models for Newtonian fluids were developed for isothermal situations. Recently, many investigators have developed mathematical models and numerical simulations to understand the transport phenomena in a single-screw extruder for power-law fluids under nonisothermal situations (Elbirli and Lindt, 1984; Fenner 1980; Karwe and Jaluria 1990). Gopalakrishna *et al.* (1992) have attempted to simulate starch conversion in a single-screw extruder by incorporating kinetics of starch gelatinization and melting reactions.

Modeling of transport phenomena in a twin-screw extruder has been attempted by a few investigators (Yacu 1985; Janssen 1986; van Zuilichem *et al.* 1992; Sastrohartono *et al.* 1992; Tayeb *et al.* 1992). Due to the complicated geometry of twin-screw extruders, one often has to resort to simplifications in order to make mathematical modeling possible. The solutions of these models are often obtained by numerical programs using discretization methods such as finite difference or finite element, which are computer time and memory intensive.

All of the mathematical models developed for single or twin-screw extruders should be validated with experiments. Very often the comparison is made in terms of global quantities such as die pressure or die temperature,

power required, and average residence time because of the relative ease of measurement of these quantities. Comparison of experimental results with the numerical predictions on a local scale has not been attempted by many investigators. One such comparison is in terms of local velocity distribution within the screw channel.

Eccher and Valentinotti (1958) were the first ones to measure the velocity distribution in a single-screw extruder which had a rotating glass barrel and a stationary screw. In their experiments, polyisobutylene mixed with paraffin oil containing small aluminum particles was used as a fluid for microscopic observations. Velocity measurements were made at very low screw speeds (0.146 rpm). Their measurements did show cross-wise circulatory motion within the single-screw channel. Mohr *et al.* (1961) measured the velocity distribution in a single-screw extruder in which the screw was held stationary and the barrel made of transparent Lucite was rotated. Flow patterns were observed by injecting black India ink in the screw channel for corn syrup (Newtonian) and 2.8% hydroxyethyl cellulose in water (non-Newtonian), for barrel rotational speeds between 0-10 rpm. Velocity measurements were carried out by tracing trajectories of white resin beads. They concluded that non-Newtonianism of the fluid did not greatly alter the picture of flow distribution in the screw channel as based upon the equations developed for Newtonian fluids. This was because the nominal shear rate in their experiments was of the order of 0.6 s^{-1} which is considerably less than those encountered in a typical extruder (10-100 s^{-1}), as pointed out by the authors. Choo *et al.* (1980) measured the velocity distribution in a deep channel single-screw extruder by taking streak photographs of tracers through Perspex window simultaneously from two perpendicular directions. They used a concentrated glucose solution which is a Newtonian fluid. Their data were in reasonably good agreement with the expected distributions for a Newtonian fluid, though the data were scattered. Their data also indicated that it was relatively difficult to make measurements near the screw root. Recently, McCarthy *et al.* (1992) have measured the velocity distribution in a specially designed single screw extruder, using a noninvasive NMR imaging technique. The motion of a magnetically marked band of fluid across the barrel diameter was monitored. Velocity measurements were carried out for CMC, which is a non-Newtonian fluid. The results were compared with a simplified mathematical model in which the viscosity was assumed to be constant. Two extreme cases, namely, (1) open die and (2) closed die, were considered.

This paper deals with the application of the noninvasive Laser Doppler Anemometry (LDA) technique to make velocity measurements in the screw channels of a twin-screw extruder. The emphasis in this paper is on the application of the LDA technique to make measurements in the screw channels of a twin-screw extruder using model fluids, which is not possible using other techniques or which have not been reported in the literature.

LASER DOPPLER ANEMOMETRY

The technique of Laser Doppler Anemometry has been in use for over two decades by researchers dealing with flows of air and water. The technique is described in detail in a book by Durst *et al.* (1981). It is a noninvasive technique consisting of two monochromatic laser beams which are made to intersect at a point in space where the velocity is to be measured. This is shown schematically in Fig. 1 for a one-dimensional situation. The measurement volume formed by the two intersecting laser beams has an ellipsoidal shape which looks somewhat like an American football having approximate dimensions of 0.9 mm $\times$ 0.1 mm $\times$ 0.1 mm. These dimensions can be changed by changing the diameters of the laser beams and/or by changing the focal length of the lens which is used to make the two beams intersect. Since the two beams are monochromatic and coherent, a fringe pattern consisting of alternate dark and bright fringes is formed (Fig. 1) in the intersection volume. When a naturally occurring particle in the fluid passes through this measurement volume, cutting across the dark and bright fringes, it intermittently scatters the incident light in all directions. The scattered light from the particle is collected by an optical system, then processed further by a photo multiplier to convert it into an electronic signal. The frequency of flashing of the scattered light from the particle is directly proportional to the velocity of the fluid particle. The velocity of the fluid particle is given by

$$U = \frac{f \cdot \lambda}{2 \sin(\Theta)} \tag{1}$$

where U is the velocity of the particle, f is flashing frequency of the scattered light from the particle, λ is the wave length of the laser beams and Θ is half angle between the two beams.

It is not necessary to know the exact size of the scattering particle. It can be anywhere between a few microns to few hundred microns. Naturally occurring particles in any fluid are usually adequate to get a good measurement signal. However, artificial polymer particles can be added to get a better signal, if necessary. To some extent, the more the number of particles, the better is the signal leading to a more accurate velocity measurement.

The measured velocity is the velocity component normal to the bisector of the two laser beams and is in the plane formed by the two laser beams. In order to know the direction of the velocity vector, a Bragg cell is used. The Bragg cell causes a slight shift in the frequency of one of the laser beams with respect to the other beam, which gives rise to a moving fringe pattern within the measurement volume. Thus, the flashing frequency of a particle moving to the right in Fig. 1 will be different than that of a particle moving with the same speed but to the left.

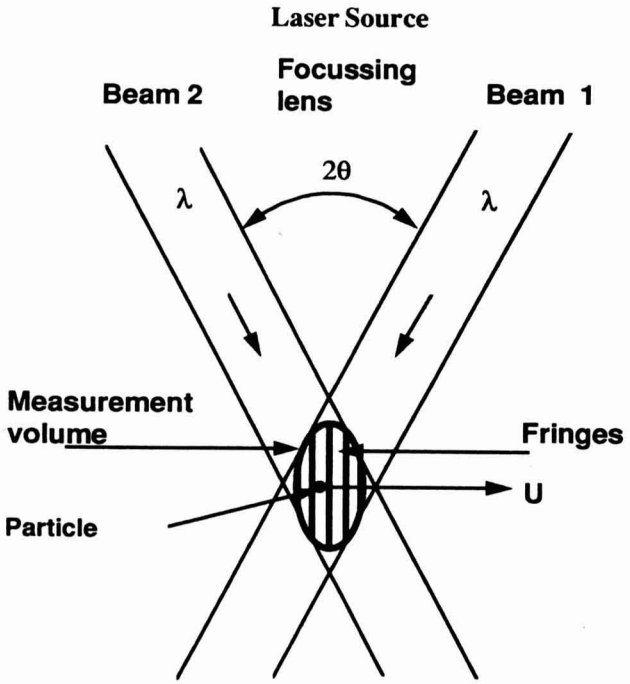

FIG. 1. SCHEMATIC DIAGRAM OF ONE-DIMENSIONAL LASER DOPPLER ANEMOMETER (LDA) SYSTEM SHOWING THE TWO INTERSECTING LASER BEAMS, THE MEASUREMENT VOLUME AND THE INTERFERENCE FRINGES

A two-dimensional LDA system is an extension of the one-dimensional system. Two other coherent, monochromatic laser beams having a different wavelength from the first two beams, are made to intersect at the same point in space as the first two beams. The plane of the second pair of beams is normal to the plane formed by the first pair of beams. Recently, three-dimensional LDA systems have also been developed. These are not as easy to use as the two-dimensional or one-dimensional systems, and are also very expensive.

An LDA system is capable of measuring velocities ranging from a few millimeters per second to hundreds of meters per second. Also, the response time of an LDA system is extremely short, i.e., of the order of nanoseconds. The fluid in which velocity measurements are to be made by the LDA system, must be optically transparent to the laser light. This means that for extruders, "model" fluids such as corn syrup or CMC must be used.

MATERIALS AND METHODS

The overall measurement system is shown in Fig. 2.

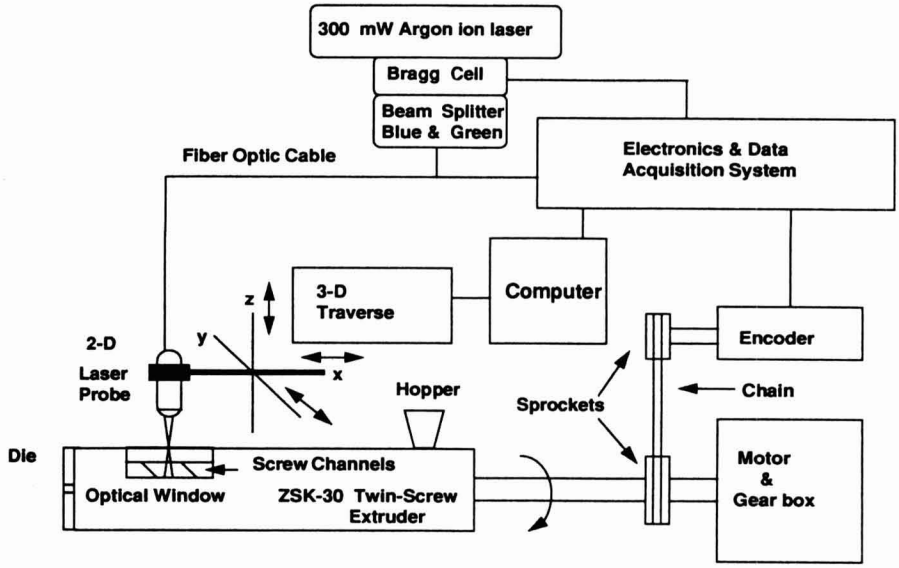

FIG. 2. OVERALL MEASUREMENT SYSTEM SHOWING VARIOUS COMPONENTS OF THE LDA SYSTEM, THE ZSK-30 EXTRUDER WITH OPTICAL WINDOW AND THE ENCODER

Extruder

Velocity measurements were made inside the screw channels of a ZSK-30 twin-screw extruder (WERNER & PFLEIDERER CORP., Ramsey, NJ). It is a co-rotating twin-screw extruder with 30.7 mm diameter screws and an L/D ratio of 29. The screw channel depth is 4.77 mm. In order to gain access for velocity measurements inside the screw channels, an optical window of Plexiglas (refractive index of 1.49) was constructed and fitted into the vent port of the extruder. The window was about 200 mm from the die end of the extruder (see Fig. 2). The size of the optical window was about 35 mm $\times$ 115 mm. Thus, through this window, one of the two screws could be seen entirely, and slightly more than half of the other screw could also be seen.

LDA System

A four beam 300 mW Argon-ion Laser Doppler Anemometer system (Dantec Measurement Technology, Inc., Mahwah, NJ) was used to make the velocity measurements. The system is schematically shown in Fig. 2 along with the extruder. The system consists of a laser, a beam splitter which splits the laser beam into two blue and two green beams, a Bragg cell, a portable probe (lens) of known focal length along with a fiber optic cable, two photo multipliers, a flow velocity analyzer (electronics) and a microcomputer. This system has the following characteristics:

Lasers: Blue (λ = 488 nm) and Green (λ = 514.5 nm)
Bragg Cell Frequency Shift: 40 MHz
Portable Probe with Fiber Optic Cable, focal length = 120 mm
Beam intersection angle (2Θ): 18°
Measurement Volume $\cong$ 0.9 mm $\times$ 0.1 mm $\times$ 0.1 mm
No. of Fringes: 60
Fringe Spacing: 1.6 μm
Mode: Back Scatter
Traverse: 3-D, spatial resolution of 0.1 mm

The portable fiber optic probe is mounted on a 3-dimensional (X-Y-Z) traverse which can be controlled through a microcomputer. The scattered light from a particle in the flow is picked by the probe, processed by the photo multipliers and finally converted into a velocity signal by appropriate software in the computer. The velocity data are stored and later processed to obtain information in terms of velocity profiles, moments, vector plots and contours.

Encoder

An encoder is a device which keeps track of the angular position of the screw shaft. On the ZSK-30 extruder, the back end of one of the screw shafts was fitted with a sprocket which was connected to an encoder by a 1:1 chain drive (Fig. 2). One rotation of the encoder is divided into 500 equal parts. The encoder sends out a 2.5 VDC pulse at every 0.72 degree of rotation of the screw and 5 VDC reset pulse for every full rotation. The signal from the encoder is read by the flow velocity analyzer (FVA) and for every velocity signal coming from a particle in the fluid, the corresponding angular position of the screw shaft is also recorded. From the angular position of the shaft and knowing the depth at which the beams intersect, the exact location within the screw channel where the velocity measurement is being made, can be identified.

Fluid

Globe corn syrup (Corn Products, CPC International, Summit-Argo, IL) was used as the working fluid in the extrusion experiments. Some of the relevant properties of this syrup are given in Table 1.

TABLE 1.
PROPERTIES OF GLOBE CORN SYRUP 1132

Type	regular conversion, ion-exchanged, normal viscosity syrup
Density	1425 kg/m^3
Refractive Index	1.49
Viscosity	74.0 Pa.s at 26.6C
	17.5 Pa.s at 37.8C
	0.54 Pa.s at 48.9C

Since the values of refractive indices of the Plexiglas and the corn syrup are very close (1.49), the problems due to the changes in the refractive index at the fluid/wall interface were minimized. The only correction needed was in the actual depth of the measurement location, with respect to the portable probe, which is given as follows:

$$\text{actual depth} \approx (\text{apparent depth}) \times (\text{refractive index})$$

where the apparent depth is the depth at which the laser beams would intersect in air.

Measurement Geometry

As seen through the Plexiglas window, the measurement geometry is shown in Fig. 3(a). It shows double start screw elements having pitch(mm)/length(mm) of 28/28. The velocity measurements are made at the center of the cross shown in Fig. 3(a). The four arms of the cross represent the four beams, namely, two green and two blue, as the beams traverse through the fluid. The four beams meet at the center of the cross to form the measurement volume. The front view is shown in Fig. 3(b) in which the radial depth at which the measurement is made, is indicated.

The spatial resolution of the LDA measurement system along the vertical direction (from screw root to the barrel) was estimated from the optics of the system to be about 0.5 mm or less. The spatial resolution in the other two directions was less than 0.1 mm. Thus, the number of locations along the vertical direction where the velocity measurements could be made, for a channel depth of 4.77 mm, were limited to 8 or 9.

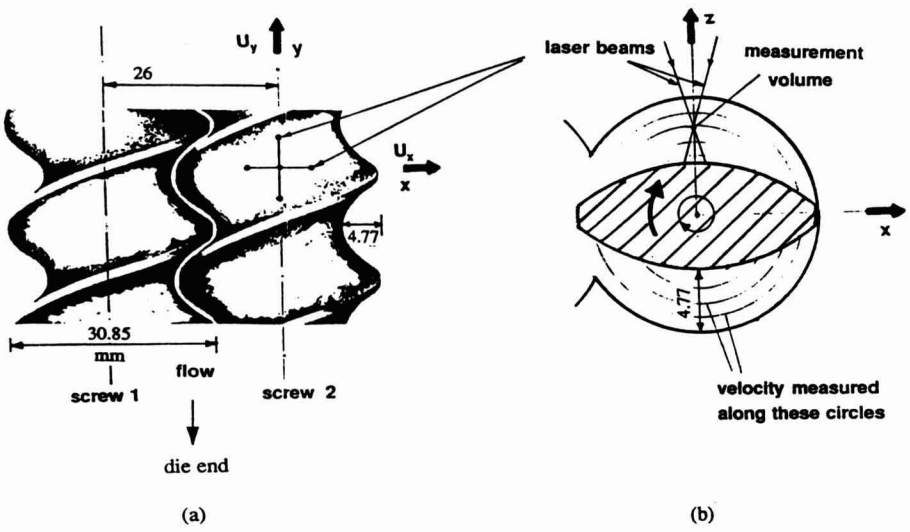

FIG. 3. MEASUREMENT GEOMETRY: (a) TOP VIEW AS SEEN THROUGH THE OPTICAL WINDOW (b) SECTION TAKEN NORMAL TO THE AXIS OF ONE OF THE SCREWS

RESULTS AND DISCUSSION

The LDA system was tested by measuring the velocity distribution in corn oil placed between two concentric cylinders with the inner cylinder rotating at constant angular speed. The geometry of the concentric cylinders apparatus is shown in Fig. 4(a). For a Newtonian fluid with constant properties, the theoretical distribution for $u_\phi(r)$ is given as (White 1980):

$$u\,\phi = \frac{\omega\, r_i^2}{(r_o^2 - r_i^2)} \frac{(r_o^2 - r^2)}{r}$$

where r_i is the radius of inner cylinder rotating with angular velocity ω and r_o is the radius of the stationary outer cylinder. The measured tangential velocity (u_ϕ) as a function of radial distance (r) between the two cylinders is shown in Fig. 4(b). Appropriate correction factors due to refraction and curvature were taken into account as described by Boadway and Karahan (1981) and Bicen (1982). It can be seen from Fig. 4(b) that the measured distribution of $u_\phi(r)$ agreed very well with the theoretically predicted distribution. This simple experiment validated the measurement and calculation procedures.

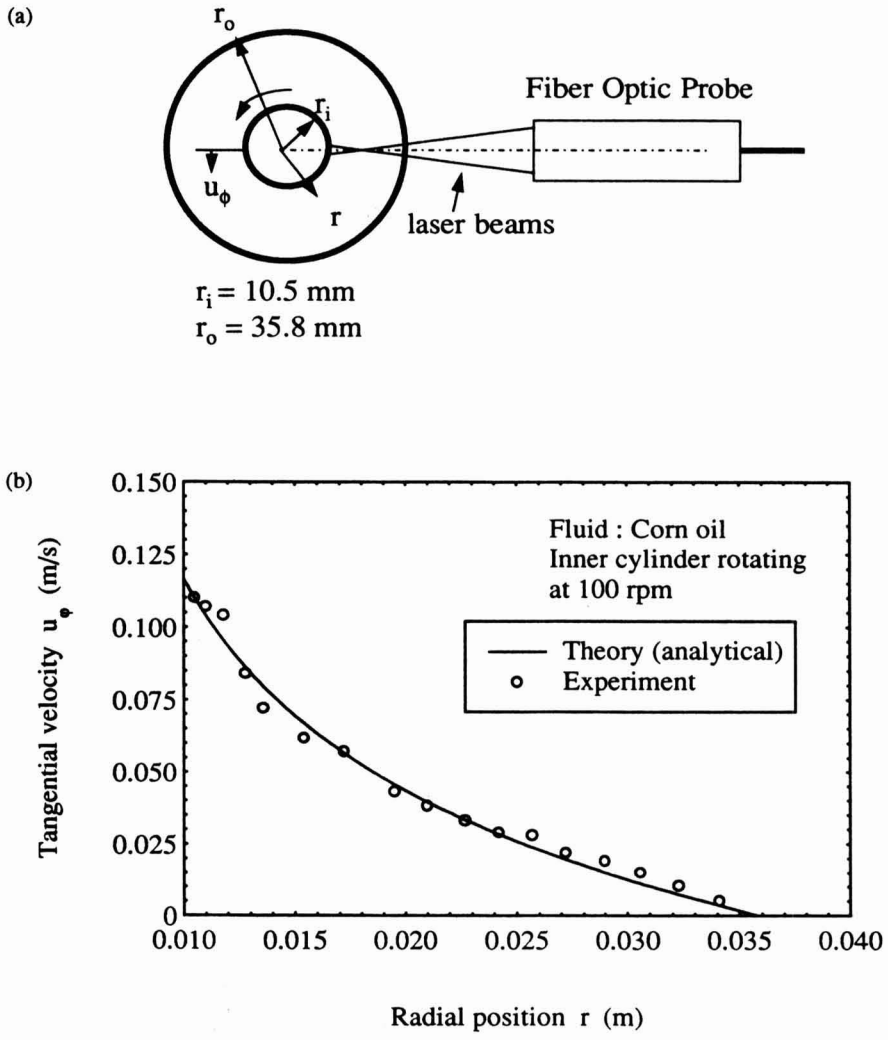

FIG. 4. COMPARISON BETWEEN LDA MEASURED AND THEORETICAL TANGENTIAL VELOCITY COMPONENT (u_ϕ) AS A FUNCTION OF THE RADIAL DISTANCE, FOR CORN OIL BETWEEN TWO CONCENTRIC CYLINDERS WITH INNER CYLINDER ROTATING AT 100 RPM
(a) Measurement Apparatus (b) Measured Velocity Distribution

In the extrusion experiments, the measured velocity components are the tangential component U_x and the axial component U_y, as shown in Fig. 3. Measurements were made at a given radial location within the screw channel over nine revolutions of the screw. As the screw rotates, the relative position of

the measurement location with respect to the screw flight changes continuously. When the screw flight cuts the laser beams, no signal is obtained, thus there is a gap in the velocity data when plotted as a function of angular position of the screw. By making measurements at several radial depths, the velocity field in the channel can be obtained and the velocity profile between the screw root and the barrel, at a given angular position, can be generated.

Figures 5(a) and (b) show typical measured variations of the tangential velocity component, U_x, as a function of angular position, at two different fixed radial distances from the barrel, for a screw speed of 30 rpm. Fig. 5(a) shows the variation of U_x at a point near the screw flight tip at about 0.5 mm away from the inside of the barrel wall. Fig. 5(b) shows the variation of U_x at a point on the screw root. As can be seen from Fig. 5(a) the U_x goes through four maxima and two minima in one full revolution. The measured maximum velocity is near the tip of the rotating screw flight which is very close to the calculated velocity of the screw flight tip (0.048 m/s). The minimum velocity is in the middle of the screw channel. There appear to be two local maxima corresponding to the points just before and just after the screw flight tip. This is confirmed by calculating the angular separation between the two local maxima which corresponds to the flight tip width measured along the circumferencial direction. Also, seen in Fig. 5(a) is a local minimum between the two peaks, which corresponds to the U_x velocity in the clearance between the flight tip and the barrel. Since the size of the measurement volume is larger than the clearance between the screw flight tip and the barrel, an average velocity in the clearance is measured which is smaller than the velocity of the screw flight tip.

From Fig. 5(b) it can be seen that at the screw root, the tangential velocity does not change significantly with the angular position. In fact, the measured velocity is very close to the calculated screw root velocity (0.033 m/s) obtained from the solid body rotation. This is because the self-wiping screw profile is flatter near the screw root. Comparing the magnitudes of measured tangential velocities in Figs. 5(a) and (b), it can be seen that the magnitude of velocity near the barrel, at an angular position midway between the two flight tips, is lower than that near the screw root.

Velocity distributions similar to those shown in Fig. 5(a) and (b), were obtained at different channel depths. From these distributions, the variation of the tangential velocity along the depth of the screw channel was obtained at a fixed angular position, which was chosen as the middle of the right screw channel in Fig. 3(a). Such a distribution is shown in Fig. 6, for a screw speed of 30 rpm. As can be seen from Fig. 6, the tangential velocity is zero at the barrel due to no-slip and is close to the screw root velocity near screw root, also due to no-slip condition. The maximum tangential velocity occurs in the middle, but nearer to the screw root. This is expected because the pressure gradient along the tangential direction, along x in Fig. 3, is favorable, i.e., pressure is

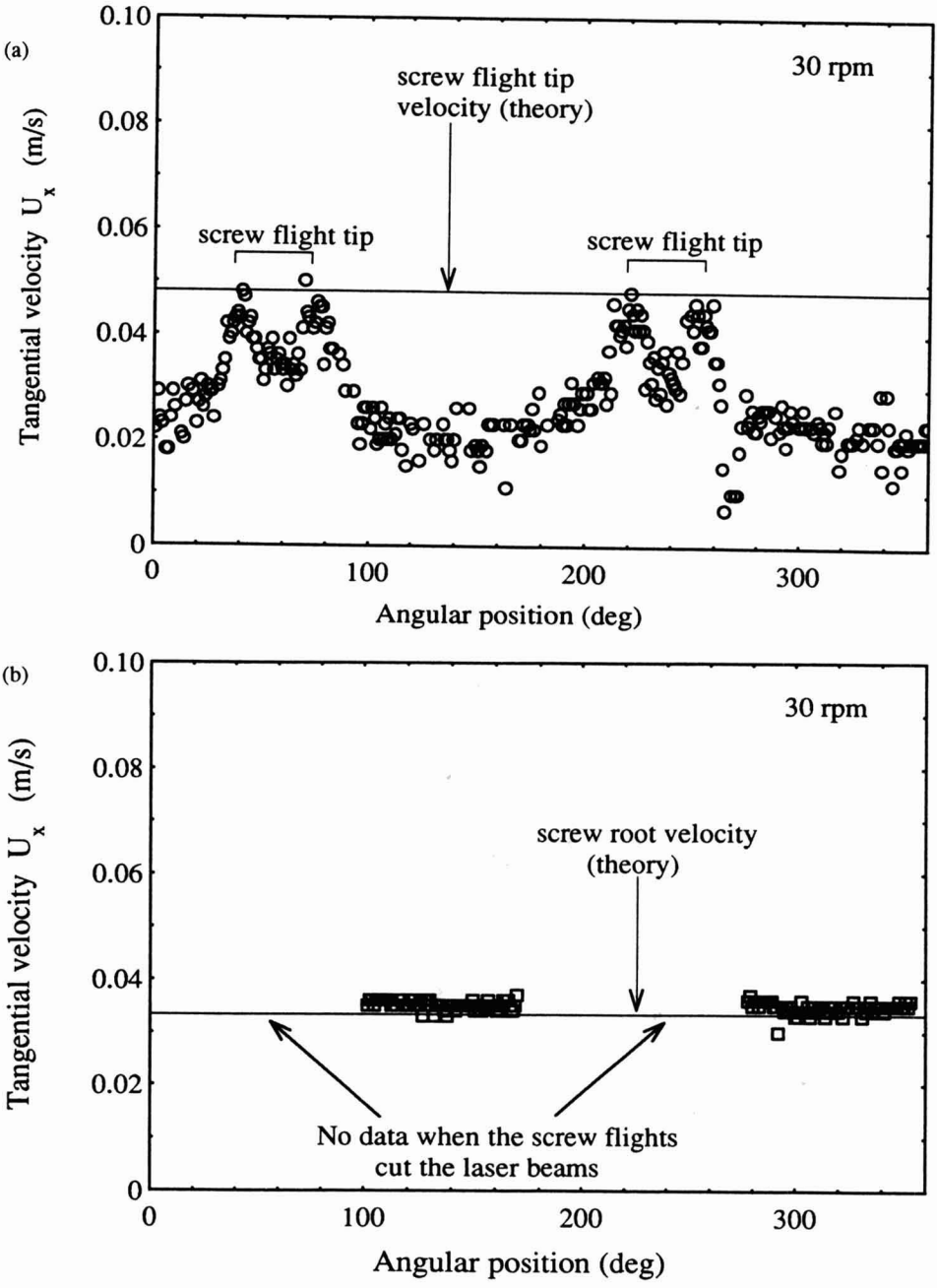

FIG. 5. VARIATION OF TANGENTIAL VELOCITY COMPONENT (U_x) WITH ANGULAR POSITION OF THE SCREW SHAFT FOR THE SCREW SPEED OF 30 RPM, MASS FLOW RATE OF 12 kg/h AT 27C
(a) Near the barrel (b) Near the screw root.

higher towards the die. Similar trends can be obtained from theoretical considerations and have been discussed by several authors (Harper 1981; Fenner 1980). Also shown in Fig. 6 is the numerically predicted U_x velocity distributions shown by the solid line. These predictions were obtained by finite-difference numerical simulation which is described in detail elsewhere (Chiruvella *et al.* 1995). In the mathematical model, 3-dimensional effects and the leakage flows were neglected. Also, for the ZSK-30 screws used in the experiments, the ratio of channel depth (H) to channel width (W) was about 0.43, whereas, in the mathematical model, this ratio was assumed to be much less than 1. It can be seen that the two profiles show similar trends, though the model seems to somewhat under predict the velocity, due to reasons mentioned above.

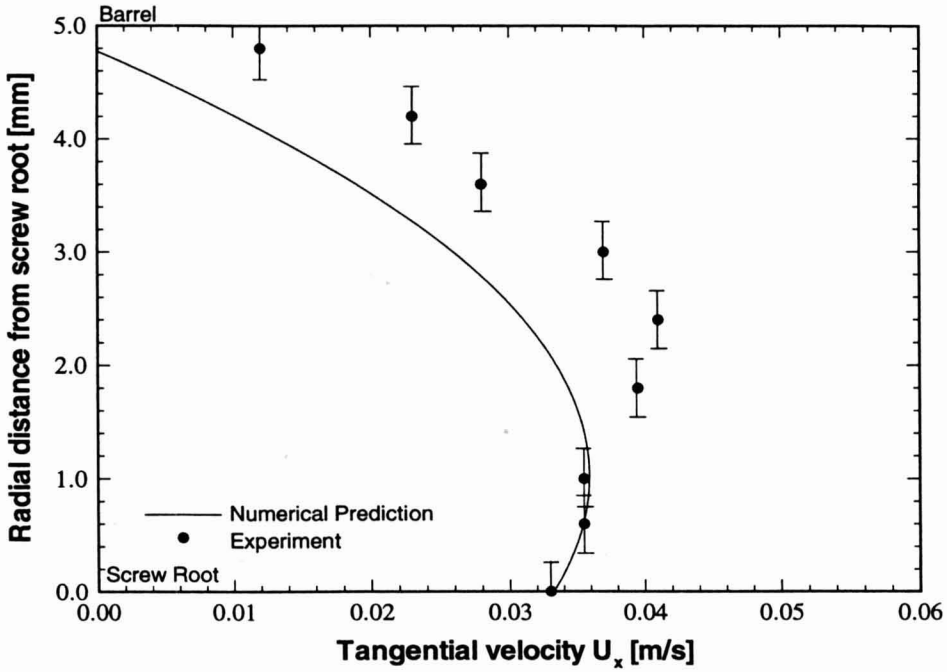

FIG. 6. COMPARISON BETWEEN MEASURED AND NUMERICALLY PREDICTED (CHIRUVELLA *ET AL.* 1995) VARIATIONS OF THE TANGENTIAL VELOCITY (U_X) WITH THE CHANNEL DEPTH AT THE CENTER OF THE RIGHT SCREW CHANNEL FOR SCREW SPEED OF 30 RPM, MASS FLOW RATE OF 12 kg/h AT 27C

Figure 7 shows variation of axial velocity U_y with angular position, near the screw root for screw speed of 30 rpm. Again, as in Fig. 5, no velocity signal is obtained when the screw flight cuts the laser beams. It can be seen from Fig. 7 that small but finite axial velocity exists near the screw root. The negative sign indicates that the flow is towards the die (see Fig. 3), which is expected. The scatter in the data for U_y is much larger than the scatter in the data for U_x. The reasons for this scatter are not known and are being investigated.

Figure 8 shows typical measured distributions of U_x velocity as a function of channel depth at locations 1, 2 and 3 which are shown on the top in Fig. 8. It can be seen from Fig. 8 that the variation of tangential velocity component with channel depth is similar at all three locations except that the profile gets squeezed as one gets away from the mid-plane. In all cases, the shear rates near

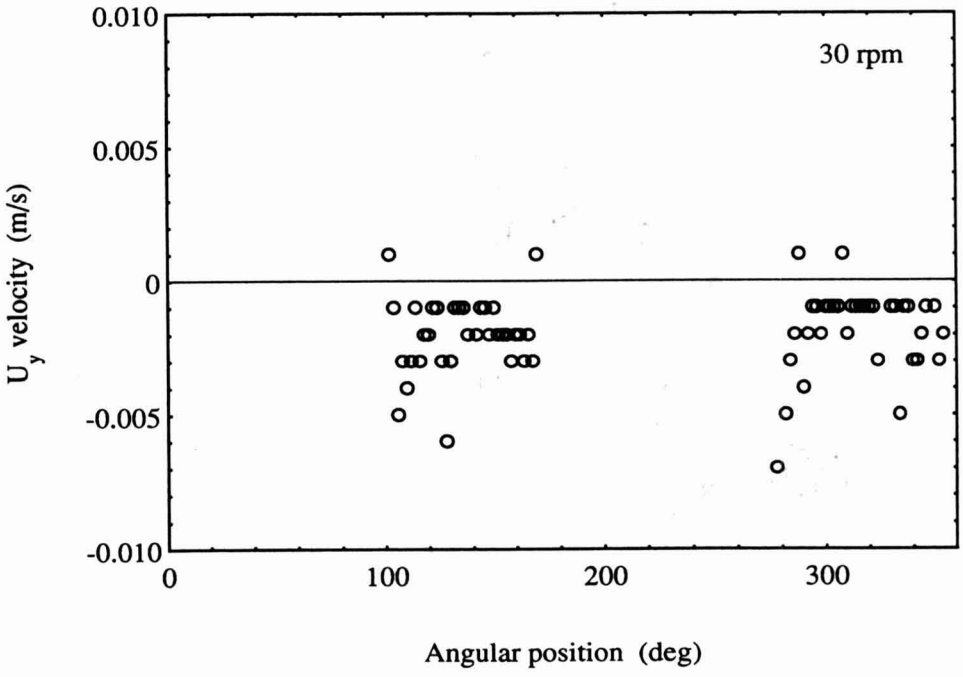

FIG. 7. VARIATION OF AXIAL VELOCITY COMPONENT (U_y) WITH ANGULAR POSITION OF THE SCREW SHAFT, NEAR THE SCREW ROOT FOR SCREW SPEED OF 30 RPM, MASS FLOW RATE OF 12 kg/h AT 27C

the barrel (as exemplified by the velocity gradient) are substantially higher as compared to the screw root. Also, shear rates near the barrel become higher as one moves away from the mid-plane, i.e., shear rates near the barrel for locations (1) and (3) are higher than the shear rates near the barrel at the central location (2).

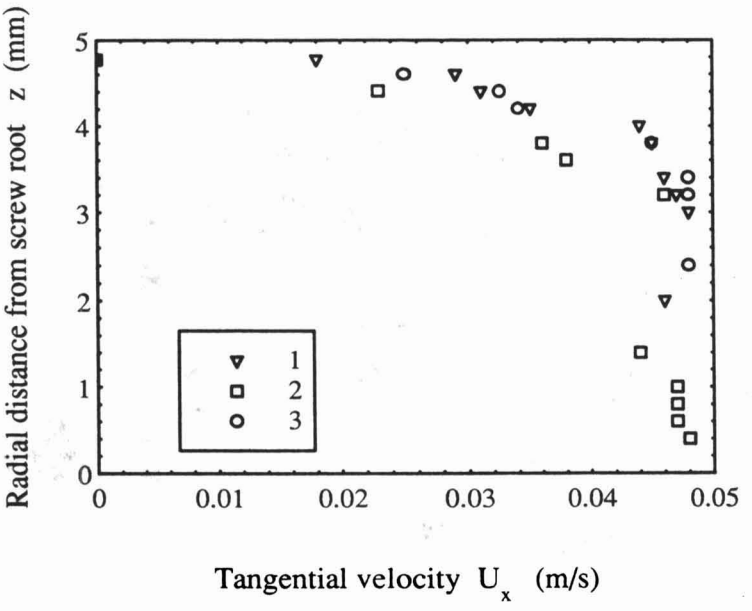

FIG. 8. VARIATION OF TANGENTIAL VELOCITY COMPONENT (U_x) AT THREE DIFFERENT LOCATIONS IN THE SCREW CHANNEL AT SCREW SPEED OF 41 RPM, MASS FLOW RATE OF 15 kg/h AT 28C
Locations 1, 2, and 3 are along the screw axis and the separation distance between them is 2 mm. Location 2 is in the middle of the screw channel.

All the measurements reported here were carried out at a location away from the intermeshing region between the two screws (also called the nip region). Therefore, the effect of one screw on the velocity profiles in the other screw is expected to be small as one gets away from the nip region. Within the nip region, the flow is affected by rotations of both the screws and hence the relative position of one screw with respect to the other screw must be known when a measurement is made. Research in progress is focused on these measurements to investigate the flow field in the nip region and also for different types of screw profiles.

CONCLUSIONS

Laser Doppler Anemometry (LDA) was used to measure velocity distribution in the screw channel of a self-wiping, co-rotating, twin-screw extruder (ZSK-30), using corn syrup. Both tangential and axial components of the velocity were measured as a function of angular orientation of the screw at different channel depths. Measured tangential velocity was maximum before and after the screw flight, and was minimum but nonzero in the middle of the screw channel. Measured values of the tangential velocity were slightly higher than the numerically predicted values. Tangential velocity gradients were always higher at the barrel as compared to screw root. Tangential velocity gradients at the barrel were lower in the middle of the screw channel.

ACKNOWLEDGMENT

This is publication No. D-10544-4-94 of the New Jersey Agricultural Experiment Station supported in part by the State Funds and the Center for Advanced Food Technology. The Center for Advanced Food Technology is a New Jersey Commission on Science and Technology Center and supported in part by the U.S. Army Research Office. Authors would like to thank Professor Y. Jaluria and Dr. R.V. Chiruvella for several discussions on this problem.

REFERENCES

BICEN, A.F. 1982. Refraction correction for LDA measurements in flows with curved optical boundaries. TSI Quarterly, *VIII*(2), 10–12.

BOADWAY, J.D. and KARAHAN, E. 1981. Correction of Laser Doppler Anemometer readings for refraction at cylindrical interfaces. DISA Information, 26.

CARLEY, J.F., MALLOUK, R.S. and McKELVEY, J.M. 1953. Simplified flow theory for screw extruders. Ind. Eng. Chem. *45*(5), 974–977.

CARLEY, J.F. and STRUB, R.A. 1953. Basic concepts of extrusion. Ind. Eng. Chem., 45(5), 970-973.

CHIRUVELLA, R.V., JALURIA, Y. and ABIB, A.H. 1995. Numerical simulation of fluid flow and heat transfer in a single-screw extruder with different dies. Polymer Engineer. Sci. *35*, 261–273.

CHOO, K.P., NEELAKANTAN, N.R. and PITTMAN, J.F.T. 1980. Experimental deep channel velocity profiles and operating characteristics for a single-screw extruder. Polymer Engineer. Science, 20(5), 349–356.

DURST, F., MELLING A. and WHITELAW J.H. 1981. *Principles and Practices of Laser Doppler Anemometry*, Academic Press, New York.

ECCHER, S. and VALENTINOTTI, A. 1958. Experimental determination of velocity profiles in and extruder screw. Ind. Eng. Chem. *50*(5), 829–836.

FENNER, R.T. 1980. *Principles of Polymer Processing*, Chemical Publishing, New York.

GOPALAKRISHNA, S., JALURIA, Y. and KARWE, M.V. 1992. Heat and mass transfer in a single-screw extruder for non-Newtonian materials. Int. J. Heat and Mass Transfer *35*(2), 493–511.

HARPER, J.M. 1981. *Extrusion of Foods*, Vol. 1, CRC Press, Boca Raton, Florida.

HARPER, J.M. 1989. Food Extruders and Their Applications. In *Extrusion Cooking* (C. Mercier, P. Linko and J.M. Harper, eds.) pp. 1–16, American Association of Cereal Chemists, Inc., St. Paul, Minnesota.

JANSSEN, L.P.B.M. 1986. *Twin Screw Extrusion*, Chemical Engineering Monographs, 7, Elsevier, New York.

KARWE, M.V. AND JALURIA, Y. 1990. Numerical simulation of fluid flow and heat transfer in a single-screw extruder for non-Newtonian materials. Num. Heat Trans., Part A *17*, 167–190.

KOKINI, J.L., HO, C.-T. and KARWE, M.V. (eds.). 1992. *Food Extrusion Science and Technology*, Marcel Dekker, New York.

McCARTHY, K.L., KAUTEN, R.J. and AGEMURA, C. 1992. Application of NMR imaging to the study of velocity profiles during extrusion processing. Trends in Food Sci. Tech. *3*, 215–219.

MCKELVEY, J.M. 1953. Experimental studies of melt extrusion. Ind. Eng. Chem., *45*(5), 982–986.

MILLER, R.C. 1993. A primer on cooking extruders. SUSTAIN NOTES, *5*(3), NCBA-USAID, Washington D.C.

MOHR, W.D., CLAPP, J.B. and STARR, F.C. July, 1961. Flow patterns in a non-Newtonian fluid in a single-screw extruder. SPE Transactions, 113–120.

SASTROHARTONO, T., KARWE, M.V. and JALURIA, Y. 1992. Numerical simulation of transport phenomena in co-rotating twin-screw extruders for non-Newtonian fluids. Num. Meth. in Ind. Form. Proc. NUMIFORM92, (J.-L. Chenot, R.D. Wood and O.C. Zienkiewicz, eds.) Balkema, Rotterdam, Netherlands.

TADMOR, L. and KLEIN, I. 1970. *Engineering Principles of Plasticating Extrusion*, Van-Nostrand-Reinhold, New York.

TADMOR, Z. and GOGOS, C.G. 1979. *Principles of Polymer Processing*, John Wiley & Sons, New York.

TAYEB, J., DELLA VALLE, G., BARNES, C. and VERGNES, B. 1992. Simulation of transport phenomena in twin-screw extruders. In *Food Extrusion Science and Technology*, (J.L. KOKINI, C.-T. HO, and M.V. KARWE, eds.) pp. 41–70, Marcel Dekker, New York.

VAN ZUILICHEM, D.J., VAN DER LAAN, E., STOLP, W. and VAN'T RIET, K. 1992. Modeling of heat transfer in a co-rotating twin-screw extruder. In *Food Extrusion Science and Technology* (J.L. KOKINI, C.-T. HO and M.V. KARWE, eds.) pp. 149–164, Marcel Dekker, New York.

WHITE, F.M. 1980. *Viscous Fluid Flow*, McGraw-Hill, New York.

YACU, W.A., 1985. Modeling a twin screw co-rotating extruder. J. Food Engineer. *8*, 1–21.

EFFECT OF SCREW CONFIGURATION AND SPEED ON RTD AND EXPANSION OF RICE EXTRUDATE

SIEW YOONG LEE

Food Technology Research Center
Malaysian Agricultural Research and Development Institute
50774 Kuala Lumpur, Malaysia

AND

KATHRYN L. MCCARTHY[1]

Department of Food Science and Technology
University of California
Davis, CA 95616

Received for Publication August 21, 1995

ABSTRACT

The influence of screw configuration and screw speed on the residence time distribution and product expansion was determined for rice meal processed in a corotating twin screw extruder. Screw speed had strong effect on the E(t)- and F(t)-diagrams, with the mean residence time varying inversely with screw speed from 206 s to 256 s. The F-diagram was modeled by the combination of perfect mixing and plug flow. The P estimates, which express the fraction of material in plug flow, varied inversely with screw speed from 0.41 to 0.55 for the operating conditions in this study. Both screw configuration and screw speed were statistically significant to the expansion ratios of rice extrudate, with the expansion in the height ranging from 2.98 to 4.13.

INTRODUCTION

Extrusion cooking of foods can be described as a process whereby moistened, starchy, and/or proteinaceous foods are cooked and worked into a viscous, plastic-like dough. Cooking is accomplished through the application of heat, either directly by steam injection or indirectly through jackets, and by dissipation of the mechanical energy through shearing of the dough (Harper 1981).

[1] To whom correspondence should be addressed. Tel.: 916-752-1487; Fax: 916-752-4759.

Journal of Food Process Engineering **19** (1996) 153–170.

Although both single screw extruders and twin screw extruders are used in the food and feed industries, there are several advantages of twin screw extruders over single screw extruders. The throughput of the twin screw extruders is independent of feed rate and fluctuations in production rate can be accommodated by the positive displacement action of the screws. They can also provide better mixing and more uniform temperature distribution.

Although extrusion of food materials is based on the development of this process in the plastics industry, food materials tend to be more complex due to their biological nature. They consist of carbohydrates, proteins, lipids, salts, water, and vitamins which undergo complex physico-chemical changes when they are subjected to high temperature, pressure and shear in the extruder barrel (Senounci and Smith 1988). These extrusion cooking conditions will ultimately cause some transformation in textural properties as well as some nutritional loss in the extruded products. Therefore, it is important to understand how changes in extrusion operating conditions affect the extrusion process.

Extrusion cooking of food materials containing mainly starch has been widely used for corn and wheat products, while rice extrusion has been studied only in recent years. Similarly, there are fewer extruded rice products on the market than extruded corn or wheat products.

Nevertheless, extruded rice snacks have been gaining popularity in Western markets during recent years (Pan *et al.* 1992). Rice has the ability to expand well and makes an excellent extruded snack. The bland flavor of rice makes it desirable for preserving more expensive flavor attributes (Huber and Rokey 1990).

The residence time distribution (RTD) in an extruder is a useful means of determining optimal processing conditions for mixing, cooking and shearing reactions during the process. From the RTD functions one can estimate the degree of mixing, the residence time of mass flow and the average total strain exerted on the mass during its transition and thus provide a clear picture of how an extruder behaves as a chemical reactor (Fichtali and van de Voort 1989). These results coupled with the knowledge of the operating variables such as temperature, screw speed, screw configuration, and moisture content provide necessary information to predict what fraction of the material will undergo specific reactions.

It is possible to analyze and compare the mixing and conveying behavior of different types of twin screw extruders by fitting the RTD data to an appropriate mathematical model. The most widely reported model is based on the combination of perfect mixing and plug flow developed by Wolf and White (1976). In their study using a single screw plasticating extruder, they found that RTD functions of solid conveying process were very close to plug flow ($P = 1$), and that the mixing conditions, flow patterns, and RTD in a plasticating extruder

had significant effects on the product. Under their extrusion conditions, screw speed had no significant effect on the RTD.

Wolf *et al.* (1986) and Lin and Armstrong (1990) studied the RTD in a counterrotating twin screw extruder. Their experimental results showed counterrotating twin screw extruders have unusually near plug flow profiles with $P \approx 1$ and $P = 0.92$, respectively. Lin and Armstrong (1990) found that changes in screw speed affected the residence time.

Altomare and Ghossi (1986), Kao and Allison (1984), Ollett *et al.* (1989), Vergnes *et al.* (1992), Kirby *et al.* (1988) and Yeh *et al.* (1991) studied the RTD of corotating twin screw extruders. All of these investigators concluded that screw speed was significant to the RTD, either $E(\theta)$ or $F(\theta)$ and/or the mean residence time. Yeh *et al.* (1991) concluded that increasing screw speed reduced the mean residence time. In these studies, Altomare and Ghossi (1986), Kao and Allison (1984) and Kirby *et al.* (1988) found that screw configuration had a significant effect on the RTD. However, Ollett *et al.* (1989) and Vergnes *et al.* (1992) found that screw configuration did not significantly affect the RTD. Kao and Allison (1984) concluded that the flow characteristics of the more severe screw configuration was closer to the plug flow than the plain screw configuration. Yeh *et al.* (1991) concluded that decreasing screw speed caused the flow pattern to approach plug flow. Altomare and Ghossi (1986) and Meuser *et al.* (1987) concluded that flow in the extruder approaches the P estimate of laminar flow in a pipe ($P = 0.5$).

In starchy extrudates, such as expanded snacks and RTE (ready-to-eat) cereals, one of the most important textural properties is the ability of the material to expand at the die. During the expansion stage the extrudate reaches its maximum size as it is formed into the general shape of the product by the die. In order to achieve the desired physical properties of the extrudate, it is necessary to understand how the independent variables and system variables interact with each other. Mercier and Feillet (1975) and Bhattacharya *et al.* (1986) concluded that the highest expansion ratio was obtained at highest screw speeds in the extrusion cooking of corn grits. Also, Bhattacharya *et al.* (1986) found that screw geometry, screw speed and shear within an extruder all affected the expansion of starch. Park (1976) concluded that screw speed had a positive effect on the expansion ratio and total expansion in the extrudates. Vergnes *et al.* (1987) found that the expansion varied from 1.36 to 5.44 as speed increased.

The objective of this research was to study the effects of screw configuration and screw speed on the residence time distribution and expansion of rice extrudate in a twin screw extruder and slit die. Parameters that characterize the residence time distribution and expansion were evaluated statistically; the F-distribution was characterized by the perfect mixing/plug flow model.

MATERIALS AND METHODS

Extrusion tests were performed with a System90 torque rheometer (Haake Buhler, Paramus, NJ) that provided computer control and data acquisition for a MPC/V-30 corotating twin screw extruder (APV, Staffordshire, England), length to diameter ratio (L/D) of 13. The slit die (Haake Buhler, Paramus, NJ) had dimensions of 1.47 mm × 20 mm × 150 mm. The MPC/V-30 had a clam-shell barrel consisting of three independent temperature zones controlled by electrical heating and compressed air cooling. A computerized data acquisition system was used to record five set temperatures and rotor speed and to acquire four melt temperatures, three pressures at the slit die, and torque data; data acquisition rate was every six seconds. Note that the actual extruder screw speed is 2.5 times the rotor speed due to the torque converter between the torque rheometer and the twin screw extruder. Therefore, rotor speeds of 25, 35, 45, 55 and 65 rpm used in this study correspond to 62.5, 87.5, 112.5, 137.5 and 162.5 rpm, respectively.

Screw configurations incorporated left-handed feed screws with a 30 mm double lead, mixing paddles, and a 1.0 L/D camelback discharge screw with a 7.5 mm single lead. The mixing paddles with an L/D of 0.25 were incorporated to increase agitation and retention time.

Rice meal at 25% wb (Pacific Grain Products, Woodland, CA) was metered at a rate of 30 g/min by a K-Tron volumetric feeder (Model T-20, K-Tron Corp., Pitman, NJ). Its fractional wet weight basis moisture content of the rice meal was determined by the AOAC official method 925.09 (AOAC 1990). To prepare the material for extrusion runs, the amount of water to be added to bring the samples to the required moisture content of 25% wb was added slowly to the samples while being mixed at medium speed in a Hobart mixer (Model N-50, Hobart Corp., Troy, OH).

For each experimental run, 15 kg of rice meal was prepared. The sample was sealed in polyethylene bags and stored in the cold room at 5C for a minimum of 24 h but not more than 72 h for moisture equilibration. The feed material was then allowed to equilibrate to room temperature prior to extrusion. This preconditioning procedure was employed to ensure uniform mixing and hydration and to minimize variability in the state of the feed material.

The set temperatures for the extruder and die were the same for each extruder run. The set temperatures for the extruder barrel were 30C at the first section, 60C at the second section, 100C at the third section, 130C at the adapter piece into the die and 130C at the die. During the experimental runs, melt temperatures were recorded at 40 ± 5, 60 ± 5, 85 ± 10C for the barrel sections and 135 ± 2C at the die section.

Experiment Design

The experimental design was carried out as a split plot design (Table 1). Three screw configurations were chosen to achieve a range of die pressures from 3000 kPa to 4200 kPa; they were designated Low, Medium, and Severe (Fig. 1). The Low screw configuration had six pieces of 1.5 L/D feed screws, followed by three 1.0 L/D feed screws and 1.0 L/D discharge screw downstream. The Medium screw configuration had six pieces of 1.5 L/D feed screws, three mixing paddles oriented at 30°, 60° and 90° feed forward, one 1.0 L/D feed screw, followed by one mixing paddle oriented at 90° feed forward, and 1.0 L/D discharge screw downstream. The Severe screw configuration had six pieces of 1.5 L/D feed screws, two 1.0 L/D feed screws, and four mixing paddles oriented at 30°, 60°, 90° and 30° feed forward and 1.0 L/D discharge screw.

Within the three replicates, the three screw configurations were randomly assigned. For each screw configuration, the rotor speeds of 25, 35, 45, 55 and 65 rpm were then randomly assigned. This grouping of five rotor speeds is referred to as an "experiment" because all the data was collected on the same day, hence the split plot design. Barrel temperatures toward the end of the day were systematically higher; however due to the randomization procedure, each rotor speed was affected equally.

Residence Time Distribution

Based on a calibration curve for rice meal extrudate, 0.025g of red dye sodium erythrosine (Sigma Chemical Co., St. Louis, MO) was mixed with 10.0g of rice meal and the amount of water needed to bring the moisture content of the tracer to that of the feed material (25% wb). These tracer samples were sealed

TABLE 1.
EXPERIMENTAL DESIGN

Replicate 1			Replicate 2			Replicate 3		
EXP 1	EXP 2	EXP 3	EXP 4	EXP 5	EXP 6	EXP 7	EXP 8	EXP 9
L	S	M	M	L	S	M	S	L
55	55	25	55	35	35	35	45	25
65	65	65	45	55	45	65	65	55
45	35	35	35	25	55	45	25	65
25	25	45	25	65	25	25	55	35
35	45	55	65	45	65	55	35	45

Screw Configuration: L=Low; M=Medium; S=Severe
Rotor speed = 25, 35, 45, 55, 65 rpm
Screw speed = Rotor speed * 2.5

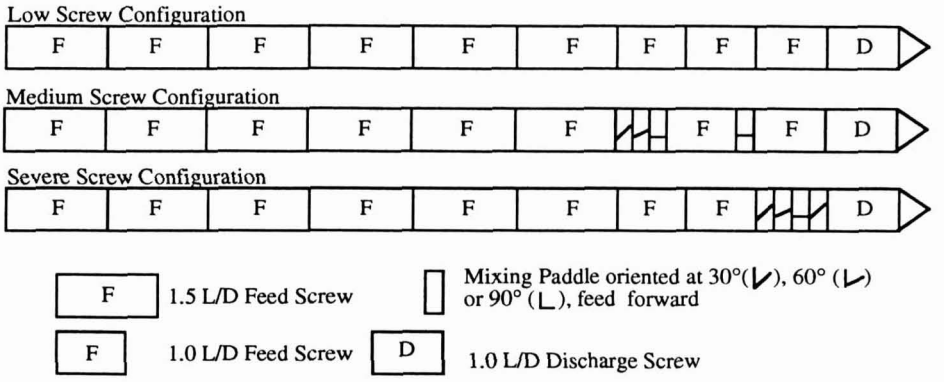

FIG. 1. DIAGRAM OF SCREW CONFIGURATIONS

in polyethylene cups and stored in the cold room at 5C for a minimum of 24 h but not more than 72 h to equilibrate. The tracer samples were then allowed to equilibrate to room temperature prior to extrusion. Once steady state conditions were achieved on the extruder as indicated by constant temperature, pressure and torque measurements, a strip of the extrudate was cut as a control for color intensity. The tracer sample was added as a pulse input through the inlet port of the extruder. At the same instant, a timer was started and a length of extrudate was cut at an interval of 20 s for a duration of 15 min. All samples for the first five min and then every third sample for the next 10 min were selected for color measurement.

All the samples, including the control, were dried overnight in a force air oven at 60C to equilibrate the moisture. The dried samples were ground in a IKA-analytical mill A10 (Type A10S2, Staufen, Germany). The ground material was then sieved through a 50 US standard sieve (Newark Wire Cloth Co., Newark, NJ). The uniform powder was analyzed for color on a Spectrophotometer CM-2002 (Minolta Corp., Ramsey, NJ). Measurements were calculated based on the 2° Standard Observer D65 illuminant. Measurement results were then displayed in L*, a*, b* values which were registered and stored in the memory card. The L* value refers to lightness, a* refers to redness-greenness and b* refers to yellowness-blueness (Hunter 1975). Each measurement was averaged from three readings. These values were then used in the calculations of the RTD functions. The values of a* and b* were subtracted from the standard values of the control. The red color intensity was calculated as the 'Index of Saturation' (Francis and Clydesdale 1975) as follows:

$$c = [(\Delta a)^2 + (\Delta b)^2]^{1/2} \quad (1)$$

where, Δa = a*standard - a*; Δb = b*standard - b*.

RTD Functions

RTD can generally be described with two functions which are closely related: the E(t)- and F(t)-diagrams (Levenspiel 1972). The response of the extruder to a pulse at the inlet is given by an E(t) diagram, which represents the age distribution of the material in the extruder.

$$E(t) = \frac{c}{\int_0^\infty c\,dt} \approx \frac{c_i}{\sum_{i=0}^{\infty} c_i \Delta t} \tag{2}$$

where c is the tracer concentration at time t.

The F(t)-diagram is related to the E(t)-diagram and it represents the cumulative distribution function in the exit stream at any time. It is given by

$$F(t) = \int_0^t E(t)dt \cong \frac{\sum_{i=0}^{i=t} c_i \Delta t}{\sum_{i=0}^{i=\infty} c_i \Delta t} \tag{3}$$

The mean residence time ($\bar{t}$), which represents the mean time the material spent in the extruder, is given by

$$\bar{t} = \int_0^t tE(t)dt \cong \frac{\sum_{i=0}^{\infty} t_i c_i \Delta t}{\sum_{i=0}^{\infty} c_i \Delta t} \tag{4}$$

Since it is common to plot residence time distributions in a normalized form, the normalized time, E-diagram and F-diagram are

$$\Theta = \frac{t}{\bar{t}} \tag{5}$$

$$E(\Theta) = \bar{t}E(t) \tag{6}$$

$$F(\Theta) = F(t) \tag{7}$$

respectively. For this study, the dependent variables that characterized the residence time and residence time distribution were $E(\Theta)$ maximum, Θ at $E(\Theta)$ maximum, mean residence time, $\bar{t}$, and $F(\Theta)$ at $\Theta = 1$. In addition, the P estimate, which characterizes the fraction of material in plug flow, was evaluated from the $F(\Theta)$-diagram.

Expansion Ratios of Extrudate

Two expansion ratios characterized the rice meal extrudate. The expansion

ratio in the width direction (E_w) is expressed as the ratio of the measurement of the width of the extrudate to the width of the slit die (Bhattacharya *et al.* 1986). The expansion ratio in the height direction (E_h) is expressed as the ratio of the measurement of the height of the extrudate to the height of the slit die.

When steady state extrusion conditions were achieved, a 50 cm continuous length of extrudate was cut for the evaluation of expansion ratios of the extrudate. From this length, 10 pieces of 5 cm length were further cut. These samples were dried overnight in a forced air oven at 60C to equilibrate moisture. These samples were removed from the oven and stored in the dessicator for further analysis. Samples were randomly chosen for the determination of expansion ratios. The reported results were the average of ten measurements. Based on thermal curves using Differential Scanning Calorimetry, the starch in these extrudate samples was 100% gelatinized under all experimental conditions (Lee 1994).

RESULTS AND DISCUSSION

The dependent variables in this study were $E(\Theta)$ maximum, Θ at $E(\Theta)$ maximum, mean residence time, $\bar{t}$, $F(\Theta)$ at $\Theta = 1$, the P estimate, and expansion ratios. A split plot design using SuperANOVA (Abacus Concepts, Inc., Berkeley, CA) was used for statistical analysis. For each of the variables, the statistical analysis included the variance table, means table, Duncan New Multiple Range for the significant variables, plots of predicted and experimental values as well as scattergram of residuals.

RTD Functions

The RTD dependence on screw speed is shown in Fig. 2-4. As illustrated, as the screw speed increased the peak of the $E(\Theta)$ diagram decreased. The $E(\Theta)$ diagrams were characterized by their peaks of $E(\Theta)$ values and also the normalized time when the peak occurred. Screw speed was highly significant with regards to the peak of $E(\Theta)$ diagram with a statistical p-value of 0.0002. The means of $E(\Theta)$ maximum indicated that as the rotor speed (screw speed = 2.5 $\times$ rotor speed) increased from 25 rpm to 65 rpm, $E(\Theta)$ maximum decreased from 0.907 to 0.766. Refer to Table 2 for the summary of RTD functions. The Duncan New Multiple Range of the effect of speed on the $E(\Theta)$ maximum indicated that 65, 55, 45 and 35 rpm were significantly different from 25 rpm and that only 25 and 65 rpm were significantly different from 35 rpm. In addition, the scattergram of residuals of $E(\Theta)$ maximum showed that all the residuals are randomly distributed within the region of less than $\pm$ three standard deviations which indicated that the assumptions of normality and constancy of variance were valid.

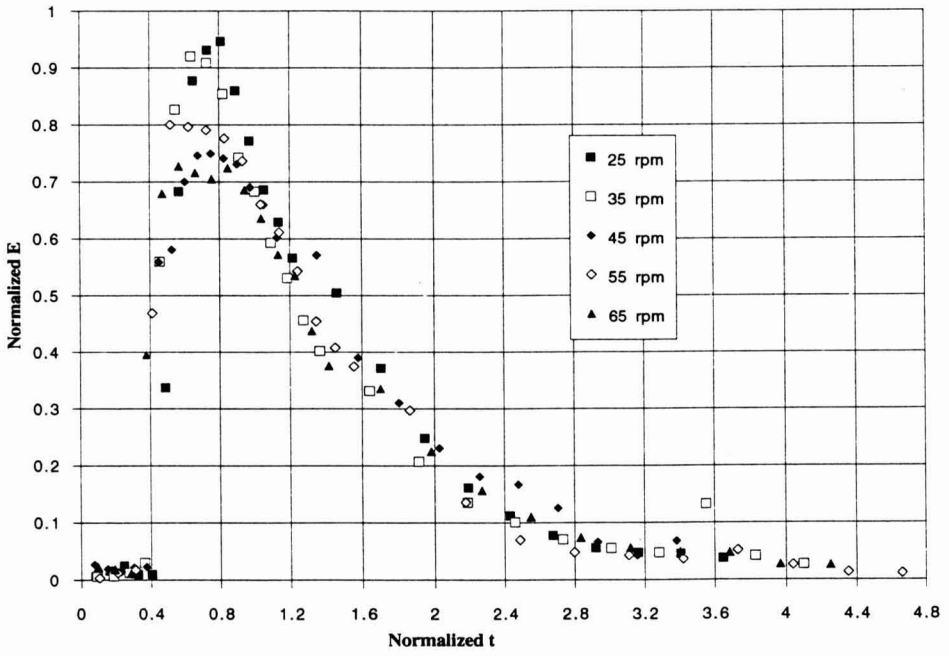

FIG. 2. E-DIAGRAM FOR LOW SCREW CONFIGURATION

As mentioned above, the time, Θ, when the peak of $E(\Theta)$ value occurred characterized the $E(\Theta)$ diagram. Screw speed was highly significant to the time, Θ at $E(\Theta)$ maximum with a p-value of 0.0021. Screw speed was inversely proportional to the time, Θ at $E(\Theta)$ maximum. Table 2 shows that as rotor speed increases from 25 to 65 rpm, Θ decreases from 0.754 to 0.641. The Duncan New Multiple Range of the effect of speed on Θ at $E(\Theta)$ maximum indicated that 65, 55 and 45 rpm were significantly different from 25 rpm but not 35 rpm. The scattergram of residuals of Θ at $E(\Theta)$ maximum indicated that all the residuals were within ± 0.125 which was $\pm$ two standard deviations. As with $E(\Theta)$ maximum, the assumptions of normality and constancy of variance were valid for Θ at $E(\Theta)$ maximum.

Screw speed had a high significance with a p-value of 0.0001 on the mean residence time, $\bar{t}$ (Table 2). Similar results were obtained by Kao and Allison (1984), Altomare and Ghossi (1986) and Yeh *et al.* (1991). The Duncan New Multiple Range of the effect of speed on mean time showed that rotor speed of 65 and 55 rpm were significantly different from 45, 35 and 25 rpm. Scattergram of residuals indicated that all residuals were randomly distributed within less than $\pm$ three standard deviations. The assumptions of normality and constancy of variance were valid.

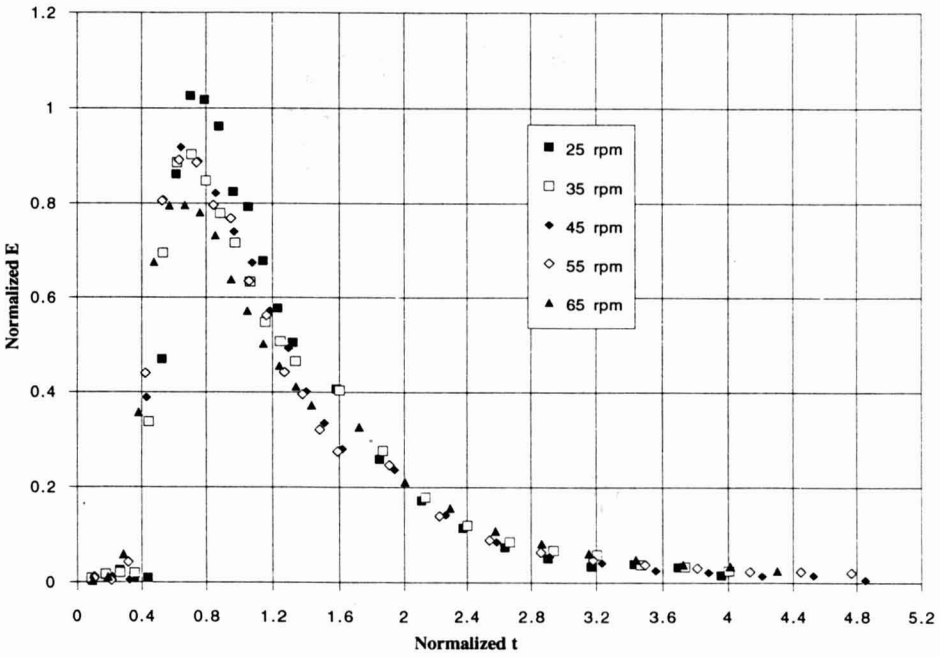

FIG. 3. E-DIAGRAM FOR MEDIUM SCREW CONFIGURATION

The F(Θ)-diagrams as shown in Fig. 5 - 7 superimpose data from all screw speeds for each of the three screw configurations. As indicated in each of the figures, the overall mixing pattern and shape of F(Θ) did not change. The F-diagram is characterized by the value of F(Θ) at $\Theta = 1$. Statistically, it was found that screw speed had a significant effect on the F(Θ) at $\Theta = 1$ (Table 2). The Duncan New Multiple Range of the effect of speed on F(Θ) at $\Theta = 1$ indicated that rotor speed of 65 and 55 rpm were significantly different from 45 and 25 rpm and only 55 rpm was significantly different from 35 rpm. Scattergram of residuals showed that all the residuals were within $\pm$ 0.03 which was about $\pm$ two standard deviations. The assumptions of normality and constancy of variance were valid.

RTD Flow Models

The experimental F(Θ)-diagrams were characterized using the Wolf and White model (1976); flow is modeled by considering extrusion as a combination of perfect mixing and plug flow. This model is expressed as

$$F(\theta) = 1 - e^{[-(1/(1-P))(\theta-P)]} \quad \text{for } \theta \geq P \tag{8}$$

$$F(\theta) = 0 \quad \text{for } 0 < \theta < P \tag{9}$$

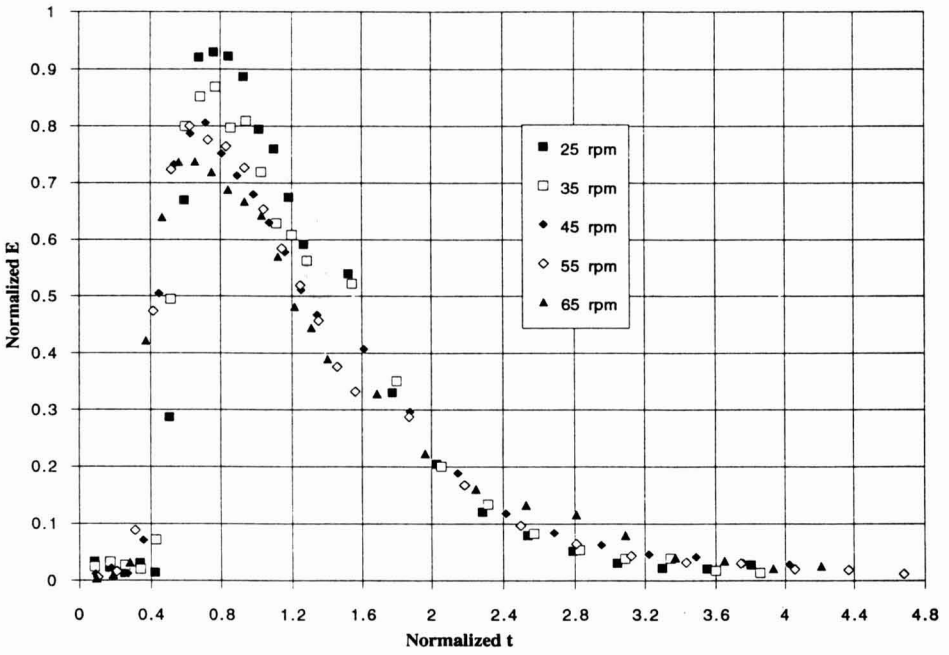

FIG. 4. E-DIAGRAM FOR SEVERE SCREW CONFIGURATION

TABLE 2.
SUMMARY TABLE OF RTD FUNCTIONS

Rotor Speed (rpm)	E(Θ)max*	Θ at E(Θ)max*	F(Θ)at Θ = 1*	t̄ (sec)*
25	0.907 ± 0.028	0.754 ± 0.022	0.438 ± 0.005	256 ± 10
35	0.838 ± 0.036	0.712 ± 0.017	0.452 ± 0.008	236 ± 9
45	0.789 ± 0.020	0.668 ± 0.019	0.447 ± 0.006	240 ± 11
55	0.790 ± 0.016	0.635 ± 0.028	0.472 ± 0.004	199 ± 4
65	0.766 ± 0.021	0.641 ± 0.018	0.465 ± 0.005	206 ± 6

*Mean ± Standard Error of nine readings
Screw Speed = Rotor Speed * 2.5

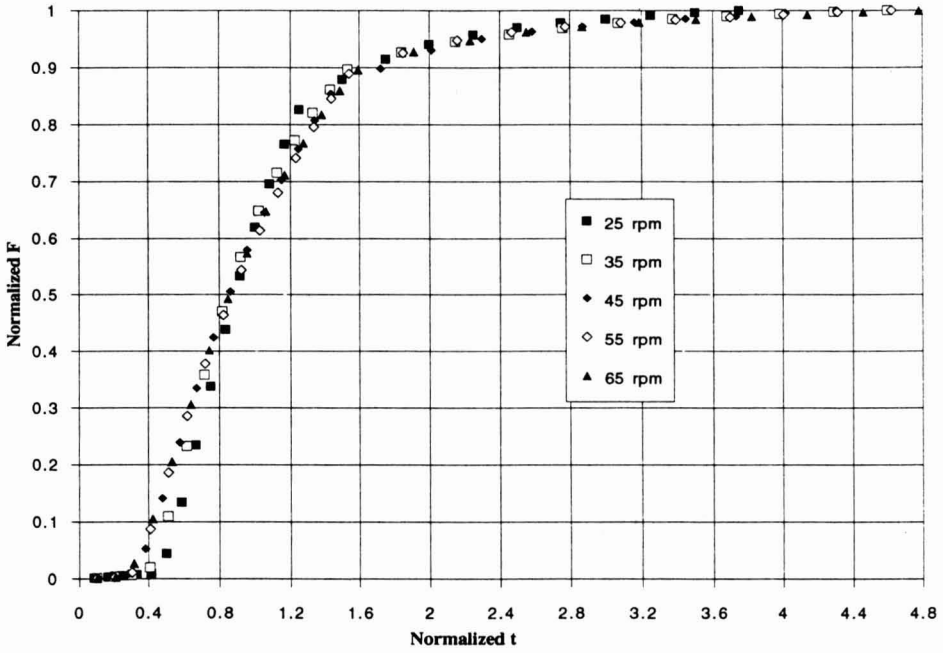

FIG. 5. F-DIAGRAM FOR LOW SCREW CONFIGURATION

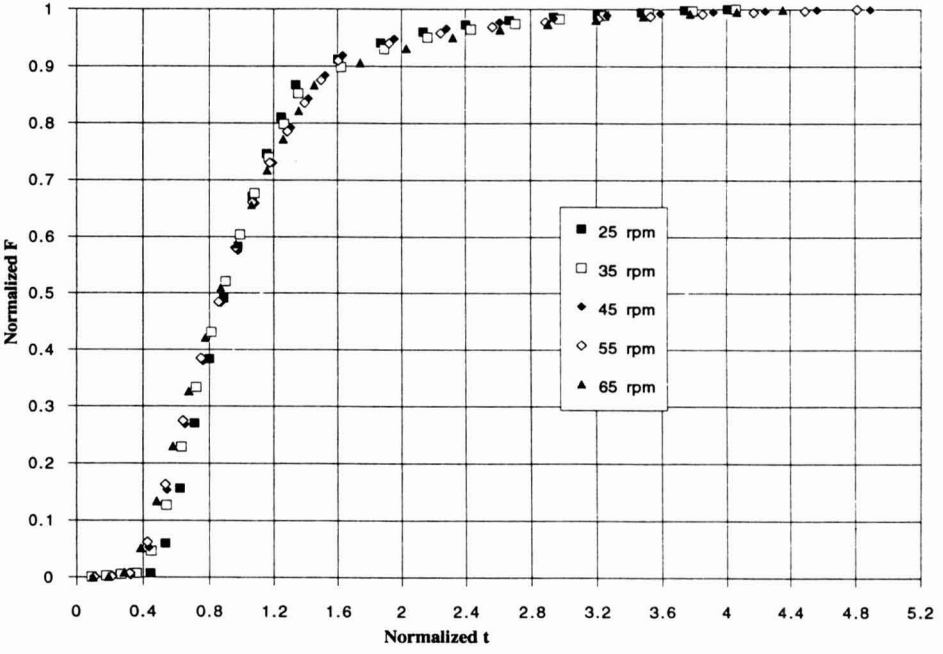

FIG. 6. F-DIAGRAM FOR MEDIUM SCREW CONFIGURATION

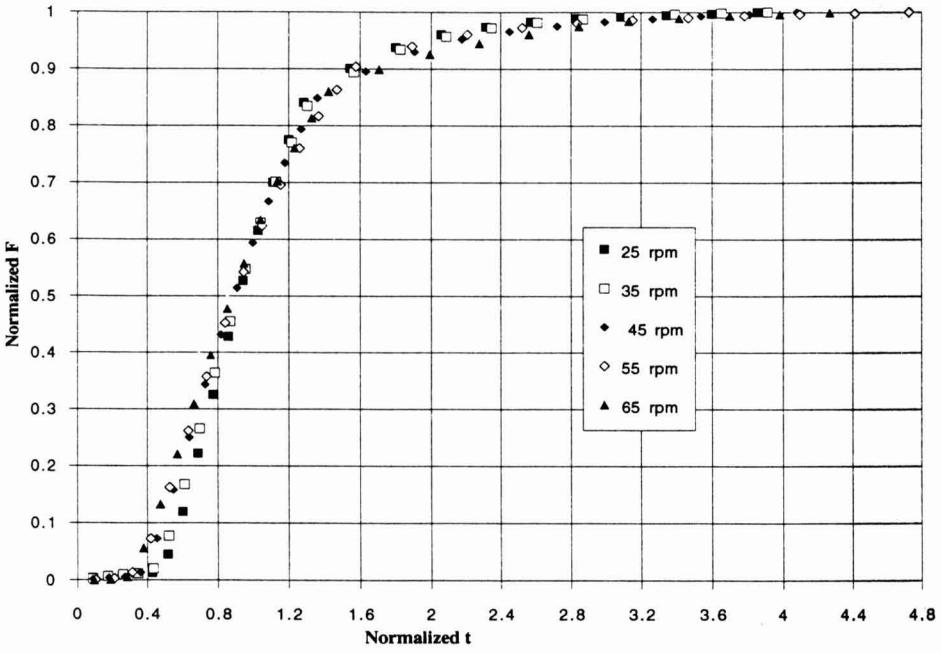

FIG. 7. F-DIAGRAM FOR SEVERE SCREW CONFIGURATION

where P is the fraction of material in plug flow. AR - Derivative-free nonlinear regression (BMDP Statistical Software, Inc., Los Angeles, CA) was used to analyze the P estimate for each F-diagram. Screw speed was highly significant to the P estimate with a p-value of 0.0001. Table 3 shows the inverse relationship of speed and the P estimate. As rotor speed increased from 25 to 65 rpm, the P estimate decreased from 0.551 to 0.406. A P estimate of 0.48 was found to give a reasonable fit to all experimental data obtained in this study. This value indicated that the flow in the extruder approached the P estimate of laminar flow in a pipe ($P = 0.5$) under these experimental conditions. Similar results were obtained by Altomare and Ghossi (1986) and Meuser *et al.* (1987). For comparative purposes, the curves for perfect mixing, plug flow, laminar flow in a pipe, and a representative curve from this study are shown in Fig. 8, as well as the curve for the fitted F ($P = 0.48$).

The Duncan New Multiple Range of the effect of speed on the P estimate of RTD flow models showed that all speeds were significantly different from each other except 65 rpm was not significantly different from 55 rpm; and 45 rpm was not significantly different from 35 rpm. The scattergram of residuals of the P estimate showed that all the residuals were within $\pm$ 0.05 which was less than $\pm$ two standard deviations.

TABLE 3.
P ESTIMATE FOR THE RTD FLOW MODELS

Rotor Speed (rpm)	P estimate*	Std. Deviation
25	0.551 ± 0.006	0.018
35	0.486 ± 0.013	0.040
45	0.479 ± 0.011	0.034
55	0.419 ± 0.011	0.032
65	0.406 ± 0.009	0.026

* Mean ± Standard Error of nine readings
Screw Speed = Rotor Speed * 2.5

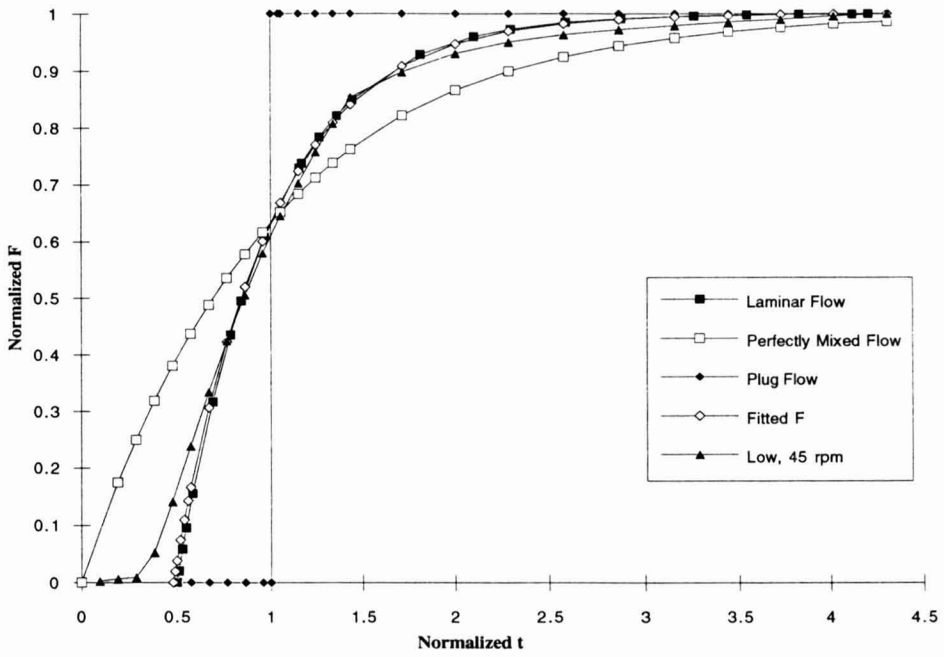

FIG. 8. COMPARISON OF F-DIAGRAMS FOR: LAMINAR FLOW, PERFECTLY MIXED FLOW, PLUG FLOW, A REPRESENTATIVE EXPERIMENTAL CURVE, AND THE P=0.48 CURVE THAT REPRESENTS THE FIT FOR ALL EXPERIMENTAL DATA IN THIS STUDY

Expansion Ratios

Unlike the residence time variables, the expansion ratios were functions of screw configuration, as well as screw speed. The screw configuration and speed were highly significant to the expansion ratio in the width dimension (E_w); the p-value was 0.0001 for each. As the severity of the screw configuration increased, E_w increased from 1.029 to 1.094 with each screw configuration significantly different from the others (Table 4). With respect to screw speed, E_w increased from 1.022 to 1.087 as the screw speed increased (Table 5). All speeds were significantly different from each other except for 35 rpm, which was not significantly different from 45 rpm. The scattergram of residuals of expansion ratio (E_w) showed that all the residuals were within $\pm$ 0.025 which was less than $\pm$ two standard deviations.

TABLE 4.
EFFECT OF SCREW CONFIGURATION ON EXPANSION RATIOS

Screw Configuration	Expansion (E_w)*	Expansion (E_h)*
Low	1.029 $\pm$ 0.004	3.189 $\pm$ 0.083
Medium	1.049 $\pm$ 0.006	3.464 $\pm$ 0.128
Severe	1.094 $\pm$ 0.011	4.038 $\pm$ 0.143

*Mean $\pm$ Standard Error of 15 readings

TABLE 5.
EFFECT OF SCREW SPEED ON EXPANSION RATIOS

Rotor Speed (rpm)	Expansion (E_w)*	Expansion (E_h)*
25	1.022 $\pm$ 0.005	2.978 $\pm$ 0.095
35	1.046 $\pm$ 0.010	3.311 $\pm$ 0.127
45	1.054 $\pm$ 0.008	3.573 $\pm$ 0.149
55	1.076 $\pm$ 0.013	3.824 $\pm$ 0.162
65	1.087 $\pm$ 0.016	4.132 $\pm$ 0.177

* Mean $\pm$ Standard Error of nine readings
Screw Speed = Rotor Speed * 2.5

Likewise, the screw configuration and screw speed were significant to the expansion ratio in the height direction, (E_h), with p-values of 0.0025 and 0.0001, respectively. The value of E_h increased with the severity of screw configuration, i.e., from 3.189 for the Low screw configuration to 4.038 for the Severe screw configuration (Table 4). The screw configurations were significantly different, with the exception of the Low and Medium screw configurations. In other words, the Low and Severe configurations were statistically different, as were the Medium and Severe configurations. Table 5 illustrates the relationship between the screw speed and E_h, with all screw speeds significantly different from each other. The scattergram of residuals of expansion ratio (E_h) showed that all the residuals were within $\pm$ 0.316 which was less than $\pm$ two standard deviations.

CONCLUSIONS

The experimental studies reported here using the dye technique enabled us to study the effects of screw configuration and speed on the residence time distribution. In addition, expansion ratios were evaluated as functions of screw configuration and screw speed. The following significant findings in this study were:

(1) Screw speed was highly significant to the residence time variables: $E(\Theta)$ maximum, time at $E(\Theta)$ maximum, mean residence time, and $F(\Theta)$ at $\Theta = 1$. As screw speed increased, $E(\Theta)$ maximum decreased, time at $E(\Theta)$ maximum decreased, mean residence time decreased, and $F(\Theta)$ at $\Theta = 1$ increased.

(2) With respect to modeling the $F(\Theta)$-diagram, the P estimate ranged from 0.406 at 65 rpm rotor speed to 0.551 at 25 rpm. The P estimate of 0.48 represented all experimental data, which is close to the P estimate of 0.5 for laminar flow in a pipe.

(3) The expansion ratios were strong functions of screw configuration and screw speed, both in the width and height directions. These properties were much more sensitive to changes in screw configuration than the residence time variables.

ACKNOWLEDGMENTS

This research was funded by NSF Grant BES-9057676.

REFERENCES

ALTOMARE, R.E. and GHOSSI, P. 1986. An analysis of RTD patterns in a twin screw cooking extruder. Biotechnol. Prog. *2*, 157–163.

AOAC 1990. *Official Methods of Analysis of the Association of Official Analytical Chemists*, 15 Ed. Arlington, VA.

AR-*Derivative-free Nonlinear Regression*. 1990. BMDP Statistical Software, Inc., Los Angeles, CA.

BHATTACHARYA, M., HANNA, M.A. and KAUFMAN, R.E. 1986. Textural properties of extruded plant protein blends. J. Food Sci. *51*(4), 988–993.

BRUIN, S., VAN ZUILICHEM, D.J. and STOLP, W. 1978. A review of fundamental and engineering aspects of extrusion of biopolymers in a single screw extruder. J. Food Process Engineering *2*, 1–37.

FICHTALI, J. and VAN DE VOORT, F.R. 1989. Fundamental and practical aspects of twin screw extrusion. Cereal Foods World *34*(11), 921–929.

FRANCIS, F.J. and CLYDESDALE, F.M. 1975. *Food Colorimetry: Theory and Applications*, Van Nostrand Reinhold/AVI, New York.

HARPER, J.M. 1981. *Extrusion of Food, Vol. 1.*, CRC Press, Boca Raton, FL.

HUBER, G.R. and ROKEY, G.J. 1990. Extruded snacks. In *Snack Food*, (R.G. Booth, ed.) Van Nostrand Reinhold, New York.

HUNTER, R.S. 1975. *The Measurement of Appearance*. John Wiley & Sons, Canada.

KAO, S.V. and ALLISON, G.R. 1984. Residence time distribution in a twin screw extruder. Polymer Eng. Sci. *24*, 645–651.

KIRBY, A.R., OLLETT, A.L., PARKER, R. and SMITH, A.C. 1988. An experimental study of screw configuration effects in a twin screw extrusion cooking of maize grits. J. Food Eng. *8*, 247–272.

LEE, S.Y. 1994. Effect of screw configuration and speed on the extrusion of rice meal. M. Sc. thesis, University of California, Davis, CA.

LEVENSPIEL, O. 1972. *Chemical Reaction Engineering*, 2nd Ed., Wiley, New York.

LIN, J.K. and ARMSTRONG, D.J. 1990. Process variables affecting residence time distributions of cereals in an intermeshing, counter rotating twin screw extruder. Trans. ASAE *33*(6), 1971–1978.

MERCIER, C. and FEILLET, P. 1975. Modification of carbohydrate components by extrusion-cooking of cereal products. Cereal Chem. *52*(3), 283–297.

MEUSER, F., PFALLER, W. and VAN LENGERICH, B. 1987. Technological aspects regarding specific changes to the characteristic properties of extrudates by HTST-extrusion cooking. In *Extrusion Technology For The Food Industry*, (C. O'Connor, ed.) Elvesier Applied Science, London.

OLLETT, A.L., LI, Y., PARKER, R. and SMITH, A.C. 1989. A comparative study of the conveying performance of screws in a twin screw corotating extrusion-cooker. J. Food Eng. *10*, 165–181.

PAN, B.S., KONG, M.S. and CHEN, H.H. 1992. Twin screw extrusion for expanded rice products: Processing parameters and formulation of extrudate properties. In *Food Extrusion Science and Technology*, (J.L. Kokini, C.T. Ho and M.W. Karwe, eds.) Marcel Dekker, New York.

PARK, K.H. 1976. Elucidation of the extrusion puffing process. Ph. D. thesis, University of Illinois, Urbana, IL.

SENOUNCI, A. and SMITH, A.C. 1988. An experimental study of food melt rheology. I. Shear viscosity using a slit die viscometer and a capillary rheometer. Rheol. Acta. *27*, 546–554.

SuperANOVA. 1991. *Accessible General Linear Modeling*. Abacus Concepts, Berkeley, CA.

VERGNES, B., BARRES, C. and TAYEB, J. 1992. Computation of residence time and energy distributions in the reverse screw element of a twin screw extrusion cooker. J. Food Eng. *16*, 215–237.

VERGNES, B., VILLEMAIRE, J.P., COLONNA, P. and TAYEB, J. 1987. Interrelationships between thermomechanical treatment and macromolecular degradation of maize starch in a novel rheometer with preshearing. J. Cereal Sci. *5*, 189–202.

WOLF, D., HOLIN, N. and WHITE, D.H. 1986. Residence time distribution in a commercial twin screw extruder. Polymer Eng. and Sci. *26*, 640–646.

WOLF, D. and WHITE, D.H. 1976. Experimental study of the RTD in plasticating screw extruders. AIChEJ *22*, 122–131.

YEH, A.I., HWANG, S.J. and GUO, J.J. 1991. Effects of screw speed and feed rate on residence time distribution and axial mixing of wheat flour in twin screw extruder. J. Food Eng. *17*, 1–13.

DRAG ON MULTIPLE SPHERE ASSEMBLIES SUSPENDED IN NON-NEWTONIAN TUBE FLOW

K.P. SANDEEP[1] and CARLOS A. ZURITZ

Department of Agricultural and Biological Engineering
The Pennsylvania State University
University Park, PA 16802

Received for Publication August 17, 1995

ABSTRACT

The drag forces experienced by single and multiple sphere assemblies suspended in non-Newtonian tube-flow were investigated under different levels of fluid viscosity of aqueous CMC solutions ($m=2.0$ to 21.1 Pa-s^n and $n=0.73$ to 0.82), flow rate (0.02 to 0.86 kg/s) and particle concentrations (1.53 to 11.01% on a volume basis). It was found that an increase in particle concentration resulted in an increase in drag force experienced by each sphere in an assembly. It was also observed that the presence of identical assemblies upstream and downstream of the single test assembly (multiple assembly case), resulted in drag force increases per sphere from 14% for low concentration to 25% for high concentration. An equation was developed to predict a drag correction factor for Stokes' equation for the multiple assembly configuration based on particle concentration.

INTRODUCTION

In continuous sterilization of particulate food suspensions, the product, heated in a heat exchanger, passes through a holding tube assembly where the liquid loses heat to the particles and they both achieve the desired degree of sterility. However, in the holding tube section, all particles do not experience the same drag force and therefore they have different retention times. Thus the thermal treatment achieved at the center of the particles is not the same for all of them. Continuous aseptic sterilization of low-acid foods (which can support the growth of *Clostridium botulinum* if not properly sterilized) containing particulates of major dimension larger than 3.2mm has not yet been approved by the FDA since neither mathematical models nor biological tests available to

[1]Research Assistant; Author to whom correspondence should be addressed

Journal of Food Process Engineering **19** (1996) 171–183.

date are sufficiently reliable to accurately predict or measure the lethality accumulated at the center of each particle. The accuracy of mathematical models rests largely in a precise description of the drag force experienced by different particles while flowing through the holding tube section of the system. The problem encountered here involves the determination of the force experienced by individual particles in the presence of other particles for different flow conditions. It would appear then that a single-particle analysis might not provide appropriate information.

Early work on the force experienced by a sphere suspended in a fluid was performed by Stokes (1901). He developed an equation to calculate the drag force on a settling sphere in an unbounded fluid under creeping flow conditions. This was probably the first step towards understanding particulate flows.

Smoluchowski (1912) developed a mathematical approximation to represent the motion of a cluster of particles using the method of reflections. Burgers (1940a,b) extended Smoluchowski's procedure to one order higher. He developed equations for the drag correction factors, 'K', for some regular assemblies of identical spheres; the expression for each sphere in a cubic assembly was given as:

$$K = \frac{1}{1 + 5.7\ (a/b) - 0.34\ (a/b)^2} \tag{1}$$

where 'a' is the radius of the particle and 'b' is the distance between adjacent spheres in the assembly.

This suggests that the drag force on any one sphere is less than that on an isolated sphere in Stokesian flow. The correction factor is used to modify Stokes' equation for single spheres as follows:

$$C_d = \frac{24K}{Re} \tag{2}$$

Hasimoto (1959) derived solutions to the Stokes equation for a viscous fluid flowing past a periodic array of spheres arranged in cubic lattices using a Fourier series. Kawase and Ulbrecht (1981) obtained an approximate solution for the motion of an assemblage of spheres moving in a power-law fluid using a free surface model and the boundary layer theory.

Acharya *et al.* (1976) performed an approximate momentum integral boundary layer analysis to determine the drag coefficient for a sphere moving through a power-law fluid in the presence of a flat wall.

Frankel and Acrivos (1967) derived the functional dependence of effective viscosity on concentration for a suspension of uniform solid spheres. Their result was intended to complement the classical Einstein formula which is valid only at infinite dilution. Their results were found to be in good agreement with published values.

Zick and Homsy (1982) developed a mathematical approximation for the drag force exerted on periodic cubic arrays of spheres in an unbounded Newtonian flow for low Reynolds numbers. They used the following expression for the drag correction factor in Eq. (2) to modify the Stokes' law depending on the particle concentration (Φ):

$$K = 10^{\frac{\Phi^{1/3}}{1-\Phi}} \tag{3}$$

Goren (1983) made corrections to Stokes' law (first order in a/b and a/h, where 'b' is the center to center spacing of the spheres translating at a distance 'h' from a no-slip wall). He found that when h/b was small, the drag was greater than that given by Stokes' law.

Satish and Zhu (1992) and Jaiswal *et al.* (1993) obtained numerical solutions for the slow flow of a power-law fluid through an assemblage of spheres. They found that the drag force decreases with decrease in the flow behavior index. All these studies were done for unbounded-type flow conditions.

Greenstein (1980) developed expressions to compute the drag forces on spherical particles translating in a cylindrical tube filled with an incompressible Newtonian fluid. They obtained interaction and wall correction factors based on the distance between particles and the distance between the particles and the tube wall.

Slattery and Bird (1961) conducted terminal velocity experiments to determine drag coefficients of single spheres falling in carboxymethylcellulose (CMC) solutions within different diameter tubes.

Subramaniam and Zuritz (1990) studied the drag force experienced by individual spherical particles suspended in solutions of CMC in a tube of circular cross-section. They developed a correlation relating the drag coefficient with the generalized particle Reynolds number based on streamline velocity. Subramaniam *et al.* (1991) later expanded the previous correlation to include particle to tube diameter ratio.

In a later work, Subramaniam and Zuritz (1994) studied the drag force on single cubic assemblies of spheres and, using average fluid velocity, developed the following equation for the correction factor for drag coefficient based on concentration (volume fraction):

$$K = 11.42\ \Phi + 2.493 \tag{4}$$

With their study, as with any other study using a single assembly of spheres, the question arises whether this type of experiment provides a true representation of the effect of particle concentration on the drag correction factor for continuous flow of a homogeneous suspension (probably better represented by the presence of similar upstream and downstream assemblies). In order to answer this question, the present study was conducted with the objective of

investigating the influence of upstream and downstream assemblies on the drag force experienced by the single test assembly.

MATERIALS AND METHODS

The experiments conducted involved the measurement of drag force on cubic arrays of spheres placed in the flow regime of a Pseudoplastic fluid (carboxymethylcellulose; CMC 6000C; TIC Gums Inc.) under horizontal laminar flow conditions in a cylindrical tube with a diameter of 10cm. A strain gauge (P-3500; Measurements Group), connected to a load cell protected with a polyurethane coating was used to measure the drag force on the sphere assemblies. The range of parameters studied is shown in Table 1. A schematic diagram of the experimental system is shown in Fig. 1. Experiments were first conducted with single assemblies of spheres. The two arrangements of spheres used are shown in Fig. 2. The location of spheres on the frame are such that the distance between two adjacent spheres on any face is the same as the distance between the two faces of the frame.

TABLE 1.
RANGE OF PARAMETERS STUDIED

Fluid			
Viscosity		Density	Flow Rate
m (Pa-s^n)	n	kg/m^3	kg/s
2.0 to 21.1	0.73 to 0.82	1000-1008	0.02 to 0.86
Particle			
	Arrangement 'A'		Arrangement 'B'
Diameter (mm)	12, 14, 25.4		12, 14
Concentration (%)	1.53, 2.2, 11.01		6.16, 8.85
Reynolds number			
0.0062 to 1.15			

Arrangement 'A' contains eight spheres (four spheres on each face of the frame) and arrangement 'B' is made up of twenty four spheres (twelve spheres on each face of the frame). Both these arrangements represent cubic arrays of spheres. Three different assemblies, one for each particle size (12, 14 and 25.4mm in diameter) were used in arrangement 'A' and two different assemblies (particle sizes 12 mm and 14 mm in diameter) were used in arrangement 'B'.

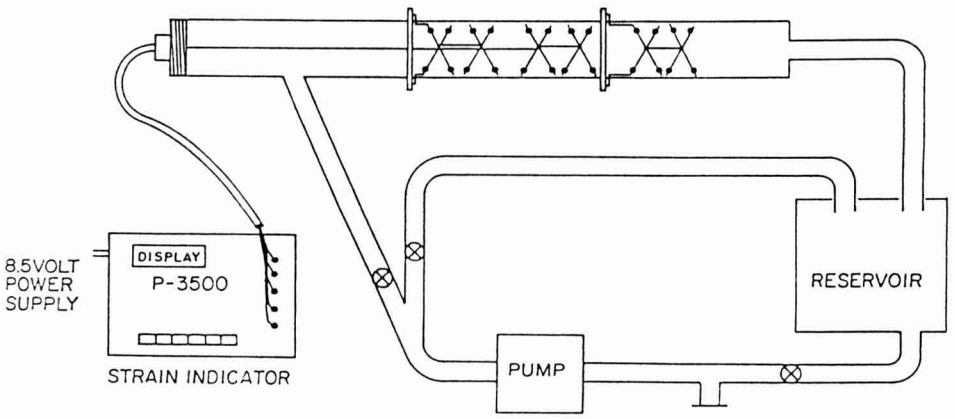

FIG. 1. SCHEMATIC DIAGRAM OF THE EXPERIMENTAL SYSTEM

The drag force on each of the above mentioned five assemblies were also measured under the presence of identical sphere assemblies fixed (to the flanges in the tube) at equal distances upstream and downstream from the assembly on which drag force measurements were taken (The distance between adjacent assemblies was the same as the distance between the two faces of an assembly). This experiment is supposed to better simulate a continuous system than the one with a single assembly of spheres. The experimental system used in both sets of experiments were the same as that used by Subramaniam and Zuritz (1994).

Drag force measurements were taken for different levels of viscosities and flow rates. Since a nondimensional analysis was to be performed, the viscosity and flow rate settings did not have to be maintained at the same level for different particle sizes and concentrations.

In order to obtain a better estimate of the drag force on a sphere, the drag force experienced by the frame and the string had to be subtracted. Therefore an experiment was also conducted to measure the drag force on a frame devoid of particles. From this experiment, the drag per unit length of the frame was computed. From this value, the drag force experienced by the portion of the frame exposed to the flow was calculated. Using this value, and the knowledge of the length of the exposed portion of the center sphere assembly, the force on the spheres and the string was computed. Another experiment was conducted to measure the drag force on the string alone. All these experiments were conducted at the same particle Reynolds number. The drag forces on the string and the empty frame were then subtracted from the drag force experienced by the sphere assemblies.

Arrangement (a)

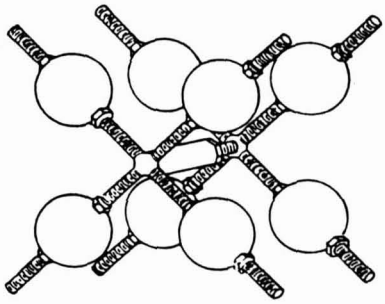

Arrangement (b)

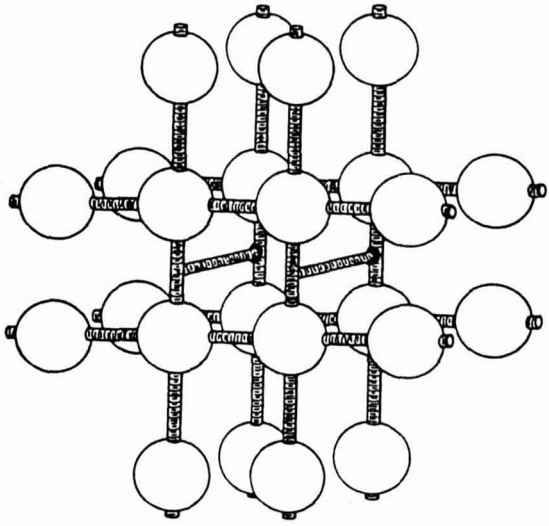

FIG. 2. SCHEMATIC DIAGRAM OF THE SPHERE ASSEMBLIES

DATA ANALYSIS AND RESULTS

The first part of the analysis involves single assemblies of spheres. The drag force experienced by each sphere in the assembly of spheres in arrange-

ment 'A' is assumed to be the same since all the particles are located at the same radial location in the tube. The drag force per sphere (F_d) was obtained by dividing the total corrected drag force by eight. The drag coefficient per sphere was then calculated using the following equation:

$$C_d = \frac{F_d}{\frac{1}{2}\rho v_s^2 A_p} \tag{5}$$

where,

$$A_p = \frac{\pi d^2}{4} \tag{6}$$

and

$$v_s = v_a \frac{3n+1}{n+1}\left[1 - \left(\frac{r}{R}\right)^{\frac{n+1}{n}}\right] \tag{7}$$

The fluid streamline velocity at the radial position of the spheres' centers, v_s, is used in this study since assembly 'B' has particles at different radial locations and is used to calculate the drag force on individual spheres as shown later.

The particle Reynolds number (Re_p) was calculated at different particle sizes, concentrations and fluid viscosities, flow rates using the following equation:

$$Re_p = \frac{\rho\, v_s^{2-n}\, d^n}{m} \tag{8}$$

The same procedure was adopted to calculate the drag coefficient and Reynolds number for the three-assembly experiment for arrangement 'A'. Graphs of C_d vs Re for both the single and the three-assembly experiments for arrangement 'A' are shown in Fig. 3, 4, and 5, respectively. From the figures, it can be seen that the drag coefficient for the three-assembly is higher than that for the single assembly at each concentration. Based on the findings of Satish and Zhu (1992) and Jaiswal *et al.* (1993), the data were separated by flow behavior index and regressional analyses were performed. However, the results of this study showed that the flow behavior index did not significantly influence the drag correction factor. This is probably due to the fact that the range of flow behavior indices in the present study was small ($n=0.73$ to $n=0.82$).

A regressional analysis on the experimental data was performed using Eq. (2) in order to determine the drag correction factors K. It was found that the three-assembly experiment yielded a 14% higher K value for the lowest particle concentration experiment ($\Phi=0.0153$) and a 25% higher K value for the highest

particle concentration (Φ=0.110) as compared to the single-assembly experiment. Therefore, it can be concluded that the presence of identical assemblies upstream and downstream has a significant influence on the drag force experienced by the test assembly. Since the three-assembly arrangement better represents continuous flow of particulate suspensions than the single assembly situation, further analysis was performed using the drag force measurements on the three-assembly configuration only.

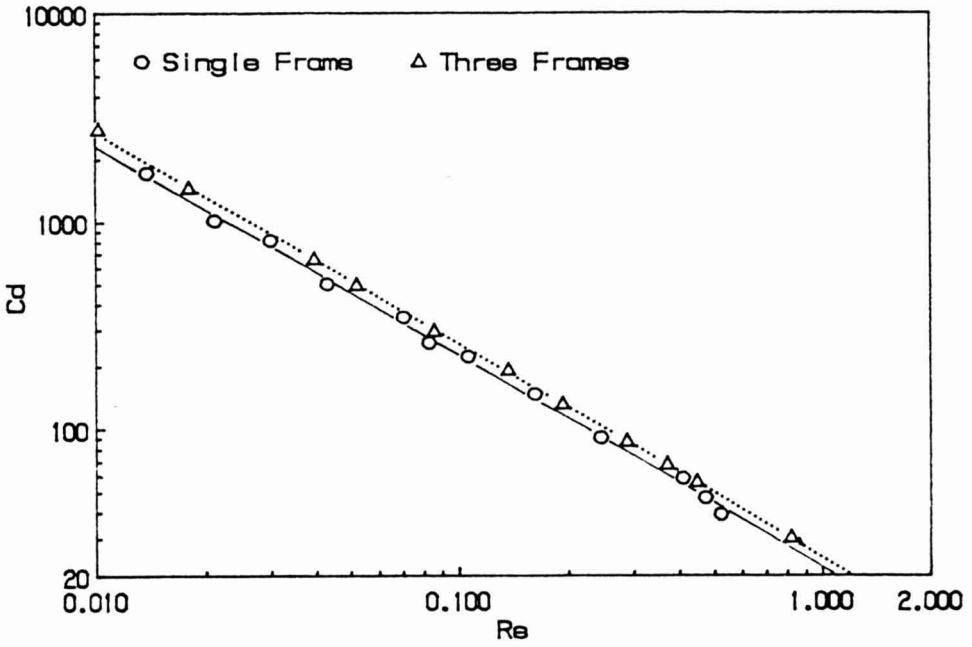

FIG. 3. Re VS C_d FOR ARRANGEMENT 'A' AT LOW CONCENTRATION

Once the K values for arrangement 'A' were determined, a linear regression was performed to obtain the following equation to predict K (with an r^2 value of 0.999) based on particle concentration:

$$K = 22.5\ \Phi + 0.773 \tag{9}$$

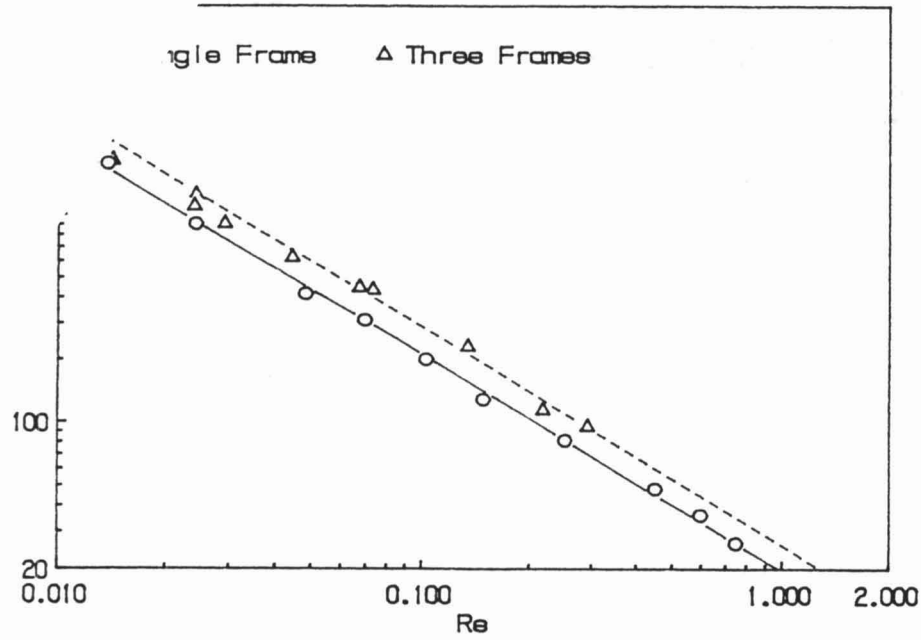

FIG. 4. Re VS C_d FOR ARRANGEMENT 'A' AT MEDIUM CONCENTRATION

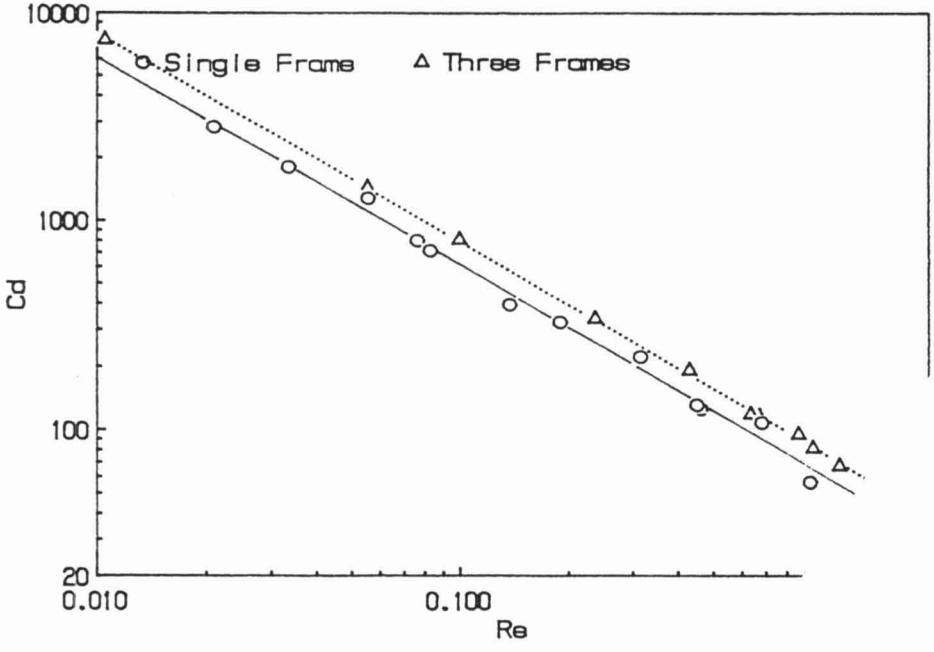

FIG. 5. Re VS C_d FOR ARRANGEMENT 'A' AT HIGH CONC

where, particle concentration is defined as (Subramaniam and Zuritz 1994):

$$\Phi = \frac{\frac{4}{3}\pi a^3 N}{2b\pi R^2} \tag{10}$$

Using Eq. (9), the K values for the 'B' arrangement were determined; the underlying assumption being that the drag correction factor for arrangement 'B' would vary with concentration as it does for arrangement 'A'.

In order to verify the validity of the above assumption, separate drag coefficients were calculated for the internal and external set of spheres in arrangement 'B' using Eq. (2). The total drag forces experienced by assemblies 'B' were then calculated using the following equation:

$$F_{d_{calc}} = (8c_{d_i}(\frac{1}{2}\rho A_p v_s^2) + (16C_{d_e})\ (\frac{1}{2}\rho A_p v_s^2) \tag{11}$$

where the subscripts 'i' and 'o' on C_d refer to the drag coefficient for the internal and external set of spheres, respectively.

A graph of the calculated and experimental drag forces is shown in Fig. 6. From this figure it can be seen that the calculated drag force is in close agreement with the experimental drag force, thereby validating the assumption that the drag correction factor for arrangement 'B' would vary in a manner similar to that for arrangement 'A' and that the K value can be determined as a function of the particle concentration alone.

This is a first step towards determining the drag coefficient on multiple sphere assemblies suspended in the flow regime of a non-Newtonian fluid and can be used as a first approximation for modeling continuous flow of particulate suspensions in aseptic processing.

CONCLUSIONS

(1) The drag force experienced by each sphere in an assembly suspended in non-Newtonian tube flow conditions increases with an increase in particle concentration.

(2) The presence of sphere assemblies upstream and downstream significantly increases the drag force on the test sphere assembly.

(3) Within the range of parameters studied, Eq. (9) can be used to account for the drag correction factor for the drag on a single sphere in multiple cubic assemblies in non-Newtonian tube flow.

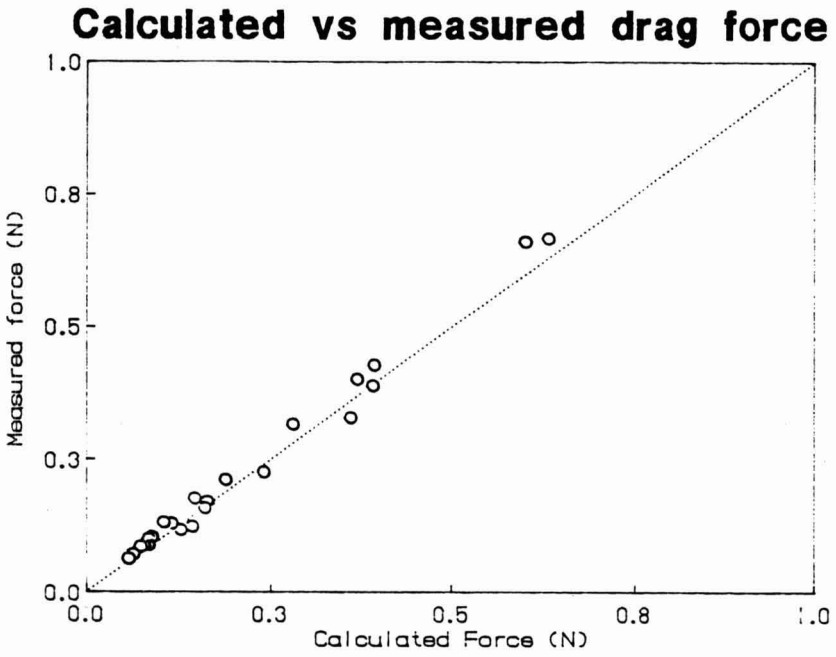

FIG. 6. CALCULATED VERSUS EXPERIMENTAL DRAG FORCE FOR ARRANGEMENT 'B'

NOMENCLATURE

- a Radius of particle, m
- A_p Projected area of sphere, m^2
- b Distance between spheres, m
- C_d Drag coefficient per sphere
- d Diameter of particle, m
- K Drag correction factor
- F_d Drag force per sphere, N
- m Consistency coefficient for a power-law fluid, $Pa\text{-}s^n$
- n Flow behavior index for a power-law fluid
- N Number of spheres in any assembly of spheres
- r Radial location of a sphere, m
- R Radius of the holding tube, m

Re Reynolds number
Re_p Particle Reynolds number
V_a Average velocity of the fluid, m/s
V_s Streamline velocity of the fluid, m/s
ρ Density of the fluid, kg/m^3
Φ Particle concentration on a volume basis (decimal)

REFERENCES

ACHARYA, A., MASHELKAR, R.A. and ULBRECHT, J. 1976. Flow of inelastic and viscoelastic fluids past a sphere - I. Drag coefficient in creeping and boundary-layer flows." Rheologica Acta. *15*, 454–470.

BURGERS, J.M. 1940a. Hydrodynamics -- On the application of viscosity data to the determination of the shape of protein molecules in solution. Koninklijke Akademie Van Wetenschappen (Amsterdam). Atdeling Natuurkundige. Proceed. Sect. Sciences *43*, 425–435.

BURGERS, J.M. 1940b. Hydrodynamics -- On the application of viscosity data to the determination of the shape of protein molecules in solution. Koninklijke Akademie Van Wetenschappen (Amsterdam). Atdeling Natuurkundige. Proceed. Sect. Sci. *43*, 645–652.

FRANKEL, N.A. and ACRIVOS, A. 1967. On the viscosity of a concentrated suspension of solid spheres. Chem. Eng. Sci. *22*, 847–853.

GOREN, S.L. 1983. Resistance and stability of a line of particles moving near a wall. J. Fluid Mech. *132*, 185–196.

GREENSTEIN, T. 1980. Interaction and wall corrections for the slow motion of two fluid or solid particles parallel to the axis of a circular cylinder through a viscous fluid. J. Mech. Eng. Sci. *22*, 243–249.

HASIMOTO, H. 1959. On the periodic fundamental solutions of the Stokes equations and their application to viscous flow past a cubic array of spheres. J. Fluid Mech. *5*, 317–328.

JAISWAL, A.K., SUNDARARAJAN, T. and CHHABRA, R.P. 1993. Hydrodynamics of creeping flow of power law fluids through particle assemblages. Internat. J. Eng. Sci. *31*, 293–306.

KAWASE, Y. and ULBRECHT, J.J. 1981. Motion of and mass transfer from an assemblage of solid spheres moving in a non-Newtonian fluid at high Reynolds numbers. Chem. Eng. Comm. *8*, 233–249.

SATISH, M.G. and ZHU, J. 1992. Flow resistance and mass transfer in slow non-Newtonian flow through multiparticle systems. J. Appl. Mech. *59*, 431–437.

SLATTERY, J.C. and BIRD, R.B. 1961. Non-Newtonian flow past a sphere. Chem. Eng. Sci. *16*, 231–241.

SMOLUCHOWSKI, M.S. 1912. On the practical applicability of Stokes' law of resistance, and the modifications of it required in certain cases. Fifth Intl. Congr. Math. 2, 192–201.

STOKES, G.S. 1901. Mathematical and physical papers III. (On the effect of the internal friction of fluids) pp 54–59, Cambridge University Press, Cambridge, U.K.

SUBRAMANIAM, G. and ZURITZ, C.A. 1990. A study of drag forces on solid spherical particles in power law bounded flow: Applications to aseptic processing. J. Food Process Engineering. *12*, 137–158.

SUBRAMANIAM, G. and ZURITZ, C.A. 1994. Drag on individual cubic assemblies of spheres in non-Newtonian tube flow. Can. J. Chem. Eng. *72*, 201–206.

SUBRAMANIAM, G., ZURITZ, C.A. and ULTMAN, J.S. 1991. A drag correlation for single spheres in Pseudoplastic tube flow. Transact. Am. Soc. Ag. Engineers. *34*, 2073–2078.

ZICK, A.A. and HOMSY, G.M. 1982. Stokes flow through periodic arrays of spheres. J. Fluid Mech. *115*, 13–26.

MODELING THE VIBRATIONAL RESPONSE OF PLANTAIN FRUITS

S.T.A.R. KAJUNA

Department of Agric. Engineering
Sokoine University of Agriculture
P.O. Box 3003, Morogoro, Tanzania

W.K. BILANSKI, G.S. MITTAL[1] and G.L. HAYWARD

School of Engineering
University of Guelph
Guelph, Ontario, Canada, N1G 2W1

Received for Publication October 2, 1995

ABSTRACT

Plantain fruits of the plantain subgroup (Musa AAB *Group) were obtained at a green stage and used in this study. The fruits were labelled for identification, and stored in a chamber maintained at a temperature of 20C and relative humidity of 90 ± 4%. On daily basis, for a period of 14 days, the fruits were removed from the storage chamber and each was weighed to record the mass. They were vibrated vertically on a vibration exciter through a range of frequencies from 10 to 2000 Hz. The frequency response was modeled by a single-degree-of-freedom Kelvin model. The mass of the fruit, the stiffness, the natural frequency and the critical damping all decreased significantly ($p < 0.01$) with storage time. There was no significant change ($p > 0.05$) in the damping coefficient of the fruit. The damping ratio decreased significantly ($p < 0.01$) with storage time. The models that described the changes in these parameters with storage time were obtained by stepwise regression, and are also presented. It was concluded that a single degree-of-freedom model provides satisfactory results of the vibrational characteristics of intact plantain fruit.*

INTRODUCTION

During transportation, fruits are subjected to dynamic forces which may lead to bruising. Bruising damage occurring to bananas and plantains due to

[1] Contact person: Dr. G.S. Mittal, Telephone: 519-824-4120, ext. 2431; Fax: 519-836-0227; Email: mittal@net2.eos.uoguelph.ca

Journal of Food Process Engineering **19** (1996) 185–200.

in-transit handling has not been addressed substantially. To quantify the extent of the damage, individual fruit's response to vibration should be established. This involves, among other things, determining the natural frequency of the fruits, because at this frequency, fruits may be subjected to excessively high amplitudes. This information could give a proper guide to the type of package for transportation. It has been reported (Thompson *et al.* 1972 quoted by Ferris *et al.* 1993) that fruits transported on the bunch ripen faster than fruits transported as individual fingers. This is perhaps due to more bruise susceptibility in fruits transported on a bunch. Thus, before recommending the packaging for transporting individual fingers, it is desirable to know the vibrational behavior of the individual fingers, and this has not been documented in literature.

Most agricultural materials are viscoelastic (Mohsenin 1986), and therefore it is customary to model the behavior of agricultural materials using elastic and viscous elements. Some researchers (Yong and Bilanski 1979; Bower and Rohrbach 1976) applied the one-degree-of-freedom kelvin element model to apples and blueberries, respectively, to explain the vibrational characteristics of intact fruits. Yong and Bilanski (1979) concluded that at the first natural frequency, it is likely that the fruit behaves mainly as a rigid body, except the cells of the skin and adjacent pulp tissues which together behave as a spring-damper system.

The objectives of this study were (1) to use the single-degree-of-freedom model to simulate the vibration of plantain fruits, and use the vibration technique to monitor the changes in textural properties over storage time and (2) to lay a ground work for the possibility of using a two degrees-of-freedom model to simulate the frequency response.

THEORY

For base excitation, the equation of motion for a mass suspended by an elastic element of stiffens K and damping element of damping coefficient c (single degree of freedom) (Fig. 1) can be written in the Laplace domain as (Cochin and Plass 1990):

$$(m\ s^2 + c\ s + K)\ Y\ (s) = (cs + K)\ X(s) \tag{1}$$

and the transfer function can be written as:

$$\frac{Y}{X}(s) = \frac{cs + K}{ms^2 + cs + K} \tag{2}$$

where X and Y are, respectively, input and output functions, and m is the mass of the vibrating system. The steady state frequency response to a sinusoidal input is obtained by letting $s = j\omega$, and separating real and imaginary parts, thus:

$$\frac{Y}{X}(j\omega) = \frac{K + jc\ \omega}{K - m\omega^2 + jc\ \omega}$$

Normalizing and dividing by ω_n^2, where ω_n $(= \{K/m\}^{1/2})$ is the natural frequency, and letting $\gamma = \omega/\omega_n$, we obtain

$$\frac{Y}{X}(j\omega) = \frac{1 + j\ 2\ \xi\ \gamma}{1 - \gamma^2 + j\ 2\ \xi\ \gamma} \tag{4}$$

where ξ is the damping ratio, c/c_c, and c_c $(= 2\{K.m\}^{1/2})$ is the critical damping.

The magnitude of the complex number in Eq. 4 may be written as

$$\frac{Y}{X} = \frac{\sqrt{1+(2\xi\gamma)^2}}{\sqrt{(1-\gamma^2)^2+(2\xi\gamma)^2}} \tag{5}$$

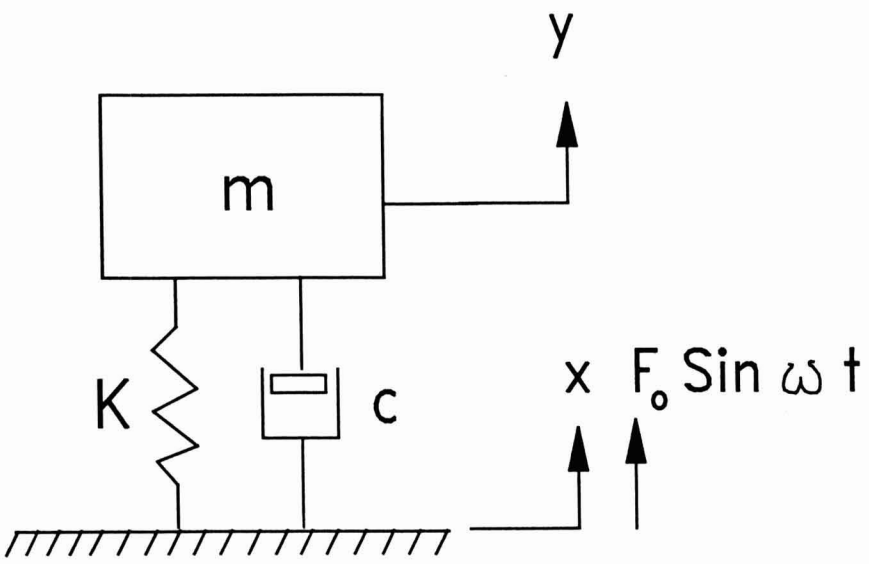

FIG. 1. ONE DEGREE OF FREEDOM MODEL

METHODOLOGY

Three different shipments from Costa Rica of Plantain fruits of the plantain subgroup (*Musa AAB* Group) were made through a fruit dealer (Meloripe Banana Company, Toronto, Canada) between May and July 1993, each shipment representing a replication for the experiment. When plantains arrived to Toronto, they looked dark green and were estimated at stage one on the color ripening chart. The plantains were in carton of 11.4 kg each, and stayed in the warehouse of the dealer for 3 days from receiving date to the delivery date. The 32 cartons for each shipments were delivered to the University of Guelph by a truck (1 h drive). Thus preliminary transportation treatment was same on all the batches used for the research. There was no visible transportation damage to the fruits. Upon arrival at Guelph, the fruits were estimated to be between stages 1 and 2 (dark to medium green) on the standard color ripening chart (Banana Retail Guide of Del Monte Tropical Fruit Company, USA). They were weighed, the mass recorded, and then sorted according to their mass and shape. Fairly straight ones which had a mass of approximately 300 ± 10 g were saved for the vibration experiments. The fruits were carefully labeled (to avoid scratching the peel) for identification, and were stored in a chamber maintained at a temperature of 20C and relative humidity of $90 \pm 4\%$. On a daily basis for a period of 14 days, the fruits were removed from the storage chamber and each was weighed to record the mass. Fruits were handled carefully to avoid bruising.

Two identical uniaxial accelerometers were attached by tape, one on to the mechanical exciter (vibration table) and the other on top of the fruit. The relatively straight fruit was placed in its most stable position on the exciter, and accelerometer was attached at the same geometrical location of the fruit each time and on each fruit. Care was always taken to ensure that each fruit would sit on the vibration table with the same orientation each time. This was to ensure approximately the same contact area on the vibration table. Each fruit was placed on the low-level mechanical-vibration exciter and vibrated in the vertical direction through a range of frequencies from 10 to 2000 Hz. In actual practice, vibrations from all sides will be acting randomly on the plantains. However, these are difficult to study systematically in the laboratory. The frequency-acceleration data were automatically plotted on a chart recorder (Fig. 2). This was later used to determine the resonant frequency from which the stiffness and coefficient of damping were calculated. The fruits were then returned to the storage chamber for future testing. The day-to-day vibration was considered to have a negligible effect on the texture of the fruits as they were subjected to low vibration levels. The acceleration peak level was 10 m/s^2 and vibrations were applied for 5 s in each treatment. The entire experiment was replicated twice.

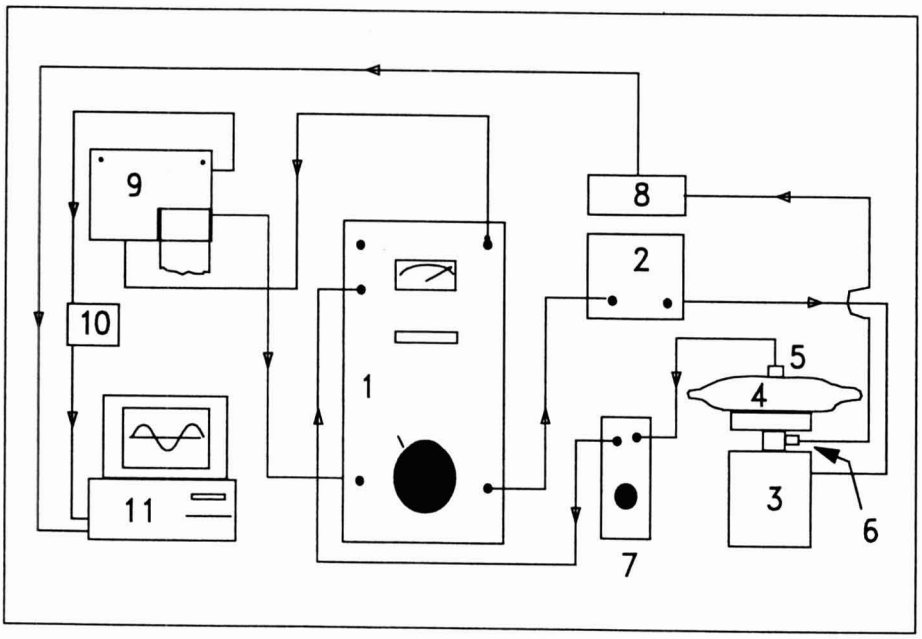

FIG. 2. SCHEMATIC REPRESENTATION OF THE VIBRATION INSTRUMENTATION

Instrumentation

The instrumentation set consisted of the following as indicated in Fig. 2:

(1) Heterodyne Analyzer, Bruel and Kjaer model 2010 (B&K, Naerum, Copenhagen, Denmark): This is a multi-function equipment that supplied the sinusoidal signal from its Beat Frequency Section. The signal was fed to the power amplifier.

(2) Power Amplifier, B&K model 2706: Amplified the sinusoidal signal from the heterodyne analyzer.

(3) Vibration exciter, B&K model 4809: Received the signal from the power amplifier and vibrated the plantain fruit. It had a Sine peak force of 44.5 N, a frequency range of up to 20 kHz, and a velocity limit of up to 1.65 m/s (peak).

(4) Plantain fruit.

(5) Fruit accelerometer, B&K type 4344: This is a light mass (2 g) sensor with a sensitivity of 2.5 mV/g. It was attached on top of the fruit to sense its vertical response during vibration.

(6) Exciter accelerometer: This is similar to the one explained above and was attached to the top of the exciter table for recording the acceleration of excitation.

(7) Charge amplifier, B&K type 2626: Amplified the signal from the fruit accelerometer.

(8) Charge amplifier, Sensotec model 060-3168-00 (A-Tech Instruments Limited, Scarborough, Ontario): Amplified the signal from the exciter.
(9) Level recorder, B&K type 2305: Received the amplified signal from the heterodyne analyzer, plotted it on the chart recorder and eventually sent it to the analog readout.
(10) Analog readout, B&K type ZR 0021: For receiving the acceleration signal from the level recorder and send it to the computer for recording.
(11) Computer: Received and recorded the acceleration signals for both accelerometers.
(12) Calibration exciter, B&K type 4294: Hand held vibration reference exciter, with fixed operating frequency of 159.2 Hz corresponding to 1000 rad/s, which produced a reference vibration level of 10 m/s^2 for calibrating the accelerometers (not shown in Fig. 2).

The acceleration-frequency data on the charts were digitized by the Geographical Information System, PC ARC/INFO (Environmental Systems Research Institute Inc., Redlands, CA, U.S.A). A Numonics Digitizer (Model No. 2200-0.90-G, Numonics Corporation, Montogomeryville, PA, U.S.A.), and ARC/INFO Digitizing System (ADS, PC ARC/INFO) were used. The digitized data were then edited by using the ARCEDIT (PC ARC/INFO). The data were then converted to ASCII files of x-y coordinates using the UNGEN command of the ARC/INFO. The data could now be replotted by QPRO software to obtain the difference in the curves between the exciter table and the fruit response and hence the amplitude ratio and the natural frequency.

Stiffness and Damping

The steady state solution of the vibrating fruit may be written as

$$y = Y \sin (\omega t - \theta) \tag{6}$$

where Θ is the phase angle by which the fruit top lags the motion of the vibrating table. The acceleration associated with this sinusoidal vibration is given by the second time derivative, thus:

$$\ddot{y} = -Y \omega^2 \sin (\omega t - \theta) \tag{7}$$

Since the sign is not important when measuring vibration (Cochin and Plass 1990), the only difference between the amplitude of the fruit displacement (Y) and that of its acceleration ($- Y \omega^2$) is the multiplier ω^2. Thus we can readily obtain the amplitude of the displacement for the table and the fruit from the acceleration signals given by the accelerometers.

The damping of the fruits was obtained from the experimental data by considering the damped forced vibration of a single-degree-of-freedom model.

At resonance, the damping ratio is obtained from Eq. 5 as

$$\xi = \frac{1}{2\sqrt{\{\frac{Y}{X}\}^2 - 1}} \tag{8}$$

and the damping is obtained as

$$c = \frac{C_c}{2\sqrt{\{\frac{Y}{X}\}^2 - 1}} \tag{9}$$

where the critical damping is given by

$$c_c = 2\ m\ \omega_n \tag{10}$$

The stiffness, K, is obtained from the mass and the natural frequency as

$$K = m\ \omega_n^2 \tag{11}$$

RESULTS AND DISCUSSION

Fruit Mass

The mass of the plantain fruits decreased significantly ($p < 0.01$) with storage time (Table 1). The decrease in mass was found to be linear (Fig. 3) throughout the storage period, described by the equation

$$W = 304.72 - 4.69\ D \tag{12}$$

where W is the mass of the fruits (g) and D is the storage time (days). The solid line in Fig. 3 is the fitted line with $R^2 = 0.99$. The possible causes of reduction in mass would be through moisture loss, an inevitable process that takes place when the relative humidity drops below 100%. Other causes of moisture loss would be the respirational and biochemical reactions.

A similar observation was reported by Asiedu (1987) and Ferris *et al.* (1993). Asiedu (1987) reported a decrease in the crude fiber of plantain fruits (the main components of which are cellulose, hemicellulose and insoluble protopectin) of almost 50% of the value originally present in the fruits after they were stored at 27C and RH 82%. Asiedu related the decrease in crude fiber with the loss of dry matter which exceeded 10% over the storage period of about 2 weeks. However, Izonfuo and Omuaru (1988) reported that the crude fiber in plantain pulp increased 3 fold and the dry matter increased by about 1% when

ripe, and they associated this increase with the transpiration during storage. This discrepancy between the Asiedu (1987) and Izonfuo and Omuaru (1988) results could perhaps be due to the differences in methodology used as the latter did not explain the method nor the conditions of temperature and RH used.

TABLE 1.
ANOVA FOR THE VIBRATIONAL PARAMETERS IN PLANTAINS

		Mean sum of squares					
Source	df	Mass	Natural frequency	Stiffness	Critical damping	Damping coefficient	Damping ratio
Rep.	1	5018**	12520**	2100622**	0.31	2.98	0.02**
Day	13	807**	8257**	6750047**	53.30**	2.98	0.02**

**p < 0.01, df = degrees of freedom.

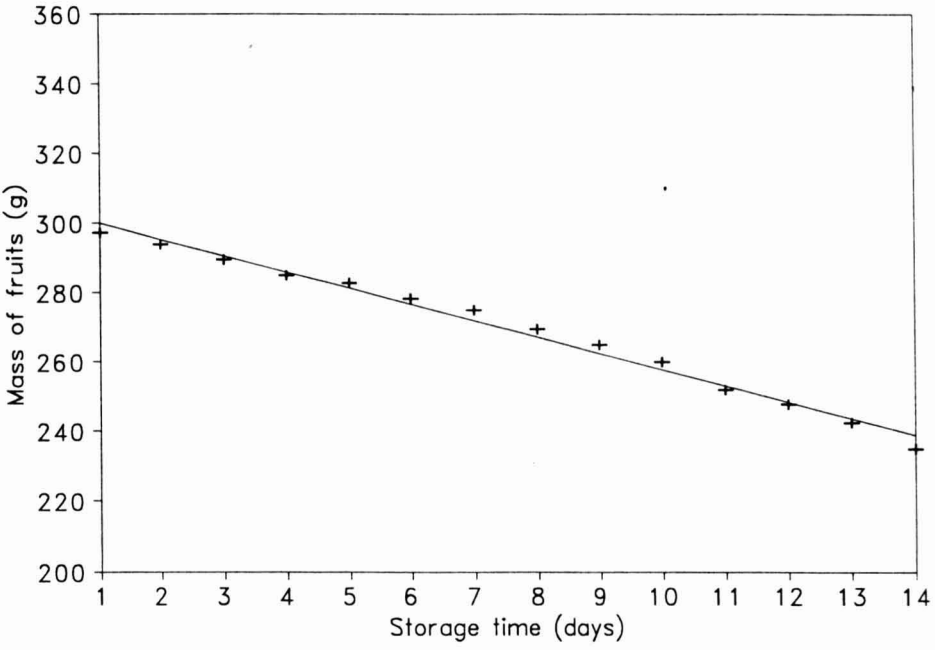

FIG.3. CHANGE IN MASS OF PLANTAIN FRUITS AS A FUNCTION OF STORAGE TIME
Each point is a mean of 12 observations in 2 replications

Ferris *et al.* (1993) reported that the loss in mass of plantain fruits is due to water loss as the RH is reduced from 100%, and that between 1.3 and 2.5% of the fruit mass is lost by respiration through conversion to carbon dioxide. Ferris *et al.* (1993) further demonstrated that peel damage by abrasion (without damaging the pulp) in plantain fruits resulted in loss in mass of more than 20% after storing for 11 days at the tropical temperature of 28C and RH of 82%, followed in between by quasi-static loading, and then impact which produced a loss in mass of about 16%, whereas the control produced a loss of about 15%.

The observed loss in mass in plantain in our study was about 20% (Fig. 3), and perhaps could be explained mainly by the natural loss of moisture by transpiration, the loss due to respiration and CO_2 release, and possibly some minor bruises on the skin during handling of the fruits in attaching the sensors and daily weighing. These bruises could have facilitated escape of moisture through the peel. Significant difference in original mass of the fruits used in different replications and treatments were noted, in spite of the care taken in selecting the fruits of similar masses.

Natural Frequency

The natural frequency of the fruits decreased significantly (Table 1) with storage time (Fig. 4). As the fruits became softer, the natural frequency became lower, following the equation of the form:

$$\omega_n = 94.0D^{-0.203}, \qquad R^2 = 0.95 \tag{13}$$

As the plantain fruit softens, the polymeric chains in the cell walls get broken down increasing the fluidity of the cell walls contents (Sakurai 1991). This has a corresponding reduction to the frequency at which the fruit resonates. Our results agree with the report by Abbot *et al.* (1968) who studied the vibration of apples and concluded that the riper the apple, the lower the natural frequency. The shape of the decay curve for the natural frequency with storage time obtained in this study is very similar to the one obtained by Liljedahl and Abbot (1994) for the second resonance in apples.

Since plantain fruits subjected to resonance in the frequency range between 50 and 100 Hz depending on the stage of ripeness, this range should be avoided when transporting plantains. However, for individual plantain fingers transported in packages, the natural frequency of the packaged fruits is likely to be lower. O'Brien and Guillou (1969) suggested that tight packing of fruits would elevate the natural frequency of the packaged fruits, hence the resonance frequency of the fruits would be well above the range of the truck's natural frequency. In peaches, when the truck frequency is about 10 Hz, the bottom layer of fruits would have an acceleration of about 0.2 'g' (approx 2 m/s^2) and this is the maximum reported acceleration of the bottom layer of fruits for a track traveling

on a paved road (O'Brien and Guillou 1969). Truck frequencies of vibration have been reported to reach as high as 20 Hz, in which case top layers of fruits could have amplitudes large enough to give accelerations of up to about 1 'g' (9.81 m/s^2).

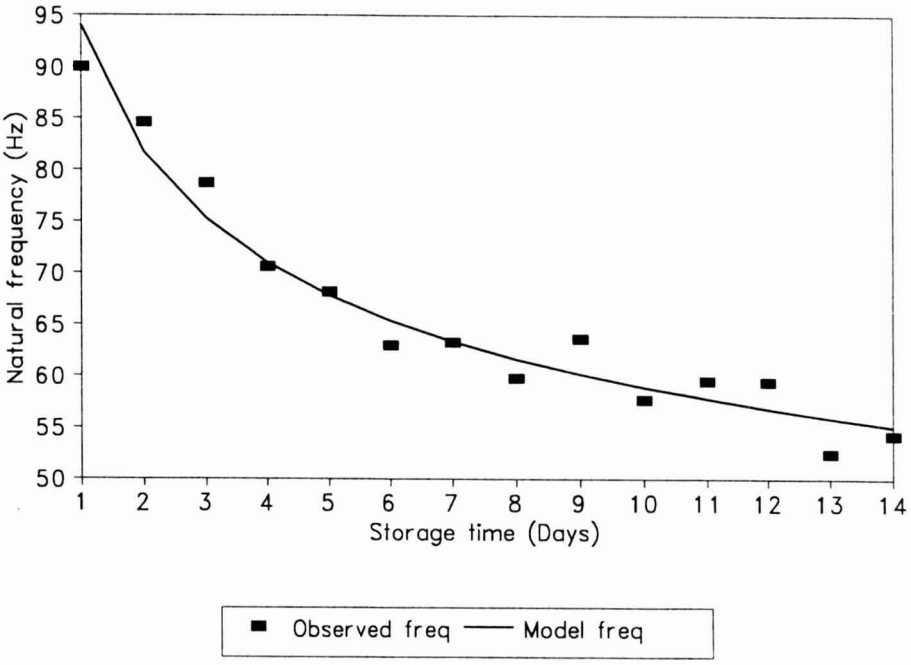

FIG. 4. CHANGE IN NATURAL FREQUENCY OF PLANTAINS WITH STORAGE TIME, MODELLED BY $\omega_{1c} = 94\ D^{-0.203}$, $R^2 = 0.95$
Each point is a mean of 12 observations in 2 replications

Stiffness (K)

The stiffness, K, decreased significantly with time (Table 1). It followed an equation of the form:

$$K = 12312.37 - 4186.63\ \sqrt{D} + 420.72\ D \qquad (14)$$

with $R^2 = 0.99$ (Fig. 5). The highest average value of K for plantains on day 1 was 8456.2 N/m (84.6 N/cm) while the lowest average value was 2465.5 N/m (24.7 N/cm) on day 14. The stiffness is a direct reflection of the firmness of the fruit, thus the trend in which the stiffness decreased could be a good indicator of the decrease in fruit firmness. The shape of the curve followed by the change in K is similar to the shape of curves obtained for the change in Maxwellian decay modulus, E, which was obtained in the quasi-static study (Kajuna *et al.* 1994). This signifies the strong correlation in the change of K with the pulp

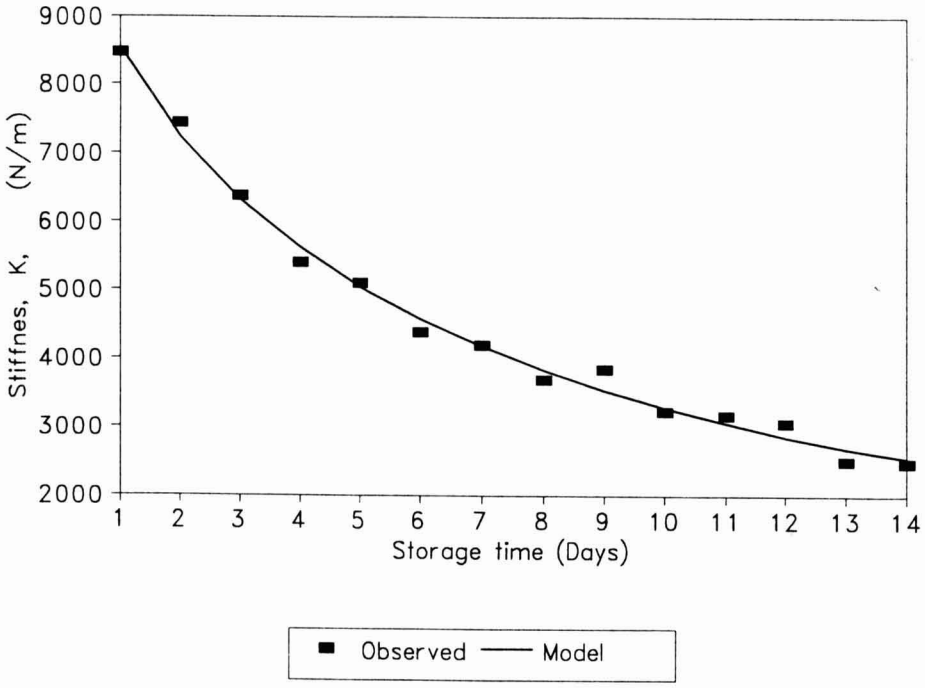

FIG. 5. CHANGE IN STIFFNESS OF PLANTAINS WITH STORAGE TIME
$K = 12312.4 - 4186.6\ D^{0.5} + 420.7\ D$, $R^2 = 0.99$. Each point is a mean of 12 observations in 2 replications

firmness. Bower and Rohrbach (1976) reported the stiffness constant for berries between 83.2 and 97.0 N/cm, which is on the higher side compared with our results. Cheson and O'Brien (1971) reported that the elasticity of fruits usually decreases as the time from date of harvest increases. This explains why K in our study decreased with storage time. In bananas, the hydrolysis of starch to sugar during ripening and the associated solubilization of pectinaceous materials between cells cause an increase in osmotic pressure which is usually associated with a decrease in turgor pressure. These account for softening during ripening, and would cause the elastic modulus to decrease (Finney *et al.* 1967).

Critical Damping (c_c)

The critical damping in the plantain fruit is the damping when the mass of the fruit would move from its extended position to its static equilibrium position in the minimum time without oscillating. It decreased significantly ($p < 0.01$) with storage time (Table 1). The mean value decreased from 32.12 Ns m^{-1} (0.32 Ns cm^{-1}) on day one to about 15.46 Ns m^{-1} (0.15 Ns cm^{-1}) on day 14 (Fig. 6). Since the critical damping was obtained from Eq. 10, and both m and ω_n

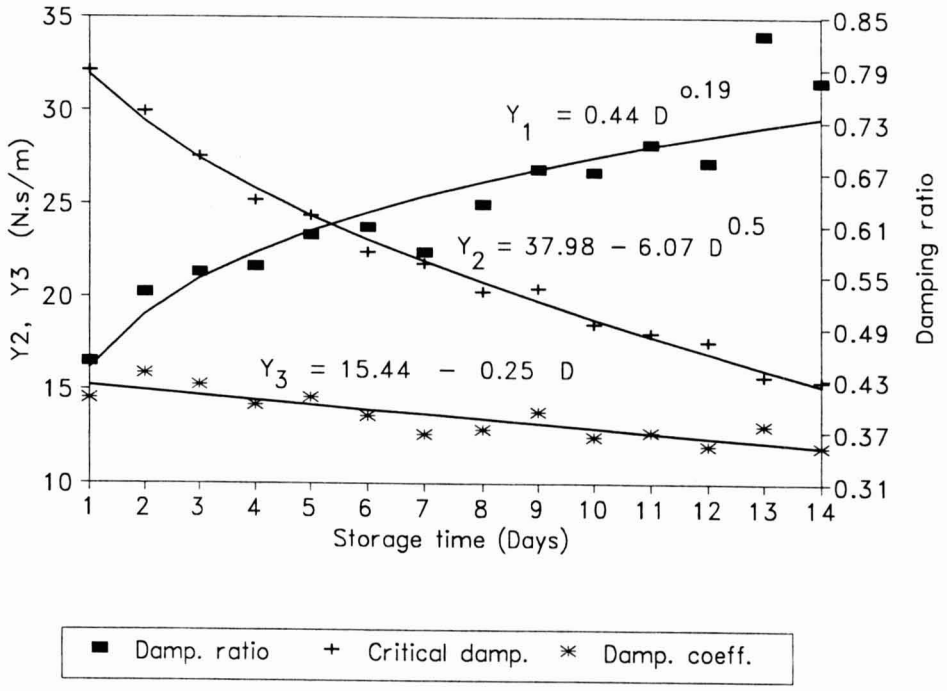

FIG. 6. DAMPING RATIO (Y_1), CRITICAL DAMPING (Y_2) AND DAMPING COEFFICIENT (Y_3) AND MODEL FITS FOR PLANTAINS
R^2 are respectively, 0.87, 0.99 and 0.74. D = Storage time (days).

decreased with storage, the critical damping could only follow suit. Regression showed that the critical damping decreased according to the equation:

$$c_c = 37.98 - 6.07\sqrt{D} \tag{15}$$

with $R^2 = 0.99$.

Damping Coefficient (c)

There was no significant change (Table 1) in the damping coefficient with storage time, although there was a slight tendency for a linear decrease with time (Eq. 16 and Fig. 6):

$$c = 15.44 - 0.25D, \qquad R^2 = 0.74 \tag{16}$$

The average value of the damping coefficient for plantains ranged between 15.9 Ns m^{-1} (0.15 Ns cm^{-1}) for green fruits and 11.97 Ns m^{-1} (0.12 Ns cm^{-1}) after storage for 2 weeks. Bower and Rohrbach (1976) reported that the mean value of the damping coefficient for berries was between 0.0193 and 0.0202 N.s cm^{-1}.

This represents a difference of about six times. The difference may be attributed to the difference in contents of the tissues, e.g., starch or the difference in the peel thickness.

Damping Ratio

The damping ratio increased significantly ($p < 0.01$) with storage time (Table 1) according to the equation:

$$\xi = 0.44D^{0.19} \tag{17}$$

with $R^2 = 0.87$ (Fig. 6). This seems to be in agreement with the assertion by Finney (1970) who reported that as a fruit softens, its viscous or damping properties may increase. The difference between the damping coefficient and the critical damping continued to narrow down as the storage time advanced. This had a significant influence on the amplitude ratio (Fig. 7). The amplitude ratio (Y/X) was simulated by Eq. 5 using the damping ratio predicted by Eq. 17. The curves obtained for the various storage days (Fig. 7) are in agreement with the curves that have been obtained for various damping ratios in mechanics (Tse *et al.* 1963).

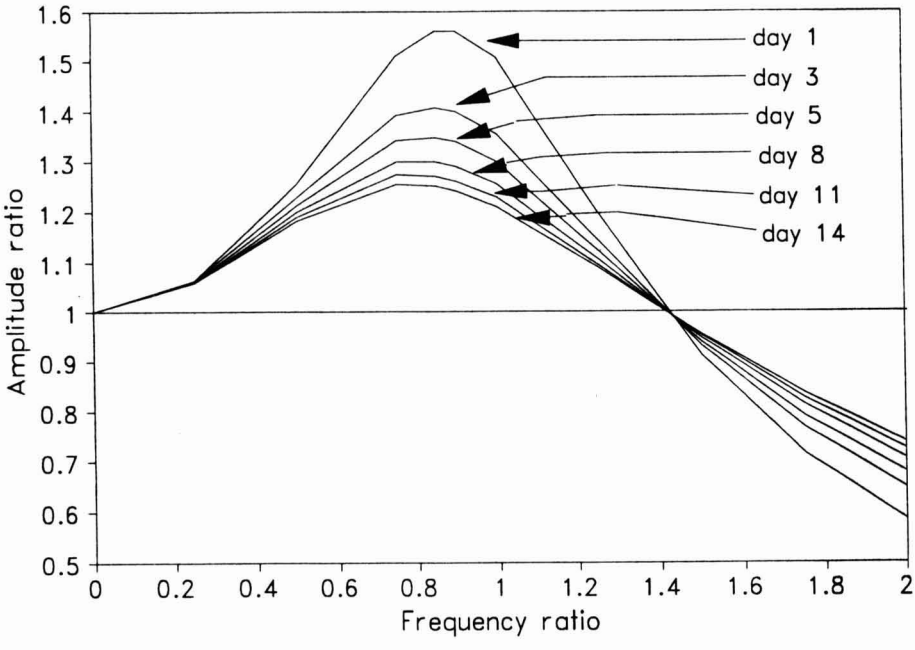

FIG. 7. PREDICTED CHANGE IN AMPLITUDE RATIO FOR THE VIBRATION OF PLANTAINS DURING STORAGE

When the vibration frequency was in the neighborhood of the natural frequency ($\omega/\omega_n = 1$), green plantains exhibited a higher value of amplitude ratio than when they had been stored for 2 weeks. As the storage time increased, the damping ratio also increased and consequently the amplitude ratio lowered. There was a higher drop in the amplitude ratio in the first storage days as compared to the later storage days. Thus, with longer storage time, the fluidity of the cell walls increased increasing the damping. The increased damping increased the loss coefficient of the fruit which resulted in more energy being absorbed (lost) as heat in the viscous element of the model. This is in agreement with Crede (1965) that addition of damping to a vibrating element decreased the response at resonance. By the same token, the stiffness or the elasticity of the cell walls decreased (Fig. 5) resulting in less energy being stored in the elastic element of the model.

Further Discussion

The results show that the single degree-of-freedom model is satisfactory in relating the relative displacement of the fruit to the stiffness and damping properties of the fruit. In this case homogeneity of the fruit is assumed. From the physiological point of view however, the peel of the plantain fruit has different properties from those of pulp. Thus, the results obtained using the single-degree-of-freedom model represent the average of the composite fruit. The plantain pulp is made of parenchymatous tissues which are mainly starchy when green, while the peel in made up of some starch and fiber. Crude fiber in plantains is ten times higher in the peel than in the pulp. It would therefore be of interest to investigate the possibilities of separating the vibration characteristics of the pulp from those of the peel. Thus, it is recommended that further investigation be attempted to see the suitability of using a two-degree-of-freedom model. This investigation has been undertaken, and the results are reported in Kajuna *et al.* (1995).

CONCLUSIONS

(1) The single degree-of-freedom model has satisfactorily explained the vibrational behavior of plantains through a range of frequencies.

(2) The natural frequency, stiffness and critical damping in plantain fruits decreased with storage time while the damping ratio increased.

(3) During transportation, the vibration of plantain fruits between 50 and 100 Hz would bring the fruits to resonance, hence this range should be avoided.

ACKNOWLEDGMENT

The partial support of this study by the International Development Research Center, Ottawa, Ontario, Canada is appreciated.

NOMENCLATURE

c, Y3	Damping coefficient, N.s/m
c_c, Y2	Critical damping, N.s/m
D	Storage time, day
j	Imaginary operator
K	Stiffness, N/m
m, W	Mass of fruit, g
s	Laplace operator
t	Time, s
Y/X	Amplitude ratio (fruit to vibration table)
ξ, Y1	Damping ratio
γ	Frequency ratio (ω/ω_n)
Θ	Phase angle, rad
ω	Frequency, rad/s
ω_n	Natural frequency, rad/s

REFERENCES

ABBOTT, J.A., BACHMAN, G.S., CHILDERS, R.F., FITZGERALD, J.V. and MATUSIK, F.J. 1968. Sonic techniques for measuring texture of fruits and vegetables. Food Technol. *22*, 101–112.

ASIEDU, J.J. 1987. Physicochemical changes in plantain (*Musa paradisiaca*) during ripening and the effect of degree of ripening on drying. Trop. Sci. *27*, 249–260.

BOWER, D.R. and ROHRBACH, R.P. 1976. Application of vibrational sorting to blueberry firmness separation. Trans. ASAE *19*, 185–191.

CHESON, J.H. and O'BRIEN, M. 1971. Analysis of mechanical vibration of fruit during transportation. Trans. ASAE *14*, 222–224.

COCHIN, I. and PLASS Jr., H.J. 1990. *Analysis and Design of Dynamic Systems*. Harper and Row Publishers, New York.

CREDE, C.E. 1965. *Shock and Vibration Concepts in Engineering Design*. Prentice-Hall, Englewood Cliffs, N.J.

FERRIS, R.S.B., HOTSONYAME, G.K., WAINWRIGHT, H. and THOMPSON, A.K. 1993. The effects of genotype, damage, maturity and environmental conditions on the post-harvest life of plantain. Trop. Agric. *70*(1), 45–50.

FINNEY, E.E. Jr. 1970. Mechanical resonance within red delicious apples and its relation to fruit texture. Trans. ASAE *13*, 177–180.

FINNEY, E.E. Jr., BENGERA, I. and MASSIE, D. 1967. An objective evaluation of changes in firmness of ripening bananas using a sonic technique. J. Food Sci. *32*, 642–646.

IZONFUO, W.L. and OMUARU, V.O.T. 1988. Effect of ripening on the chemical composition of plantain peels and pulps (*Musa paradisiaca*). J. Sci. Food and Agric. *45*, 333–336.

KAJUNA, S.T.A.R., BILANSKI, W.K. and MITTAL, G.S. 1994. Characterization of stress relaxation behavior of banana and plantain flesh using different models. NABEC/ASAE paper no. 94-222, presented at the Northeast Agr/Bio-Engineering Conf. of the Amer. Soc. Agric. Eng., University of Guelph, Guelph, Ontario, Canada.

LILJEDAHL, L.A. and ABBOT, J.A. 1994. Changes in sonic resonance of 'Delicious' and 'Golden Delicious' apples undergoing accelerated ripening. Trans. ASAE *37*, 907–912.

MOHSENIN, N.N. 1986. *Physical Properties of Plant and Animal Materials*. Gordon Breach Sci. Pub., New York.

O'BRIEN, M. and GUILLOU, R. 1969. An in-transit vibration simulator for fruit handling studies. Trans. ASAE *12*, 94–97.

SAKURAI, N. 1991. Cell wall functions in growth and development - physical and chemical point of view. Botanical Mag. Tokyo *104*, 235–251.

TSE, F.S., MORSE, I.E. and HINKIE, R.T. 1963. *Mechanical Vibrations*. Allyn and Bacon, Boston, MA.

YONG, Y.C. and BILANSKI, W.K. 1979. Modes of vibration of spheroids at the first and second resonant frequencies. Trans. ASAE. *22*, 1463–1466.

DYNAMICS OF FAT/OIL DEGRADATION DURING FRYING BASED ON PHYSICAL PROPERTIES

S. PAUL and G.S. MITTAL[1]

School of Engineering, University of Guelph
Guelph, Canada, N1G 2W1

Received for Publication November 22, 1995

ABSTRACT

The dynamics of fat/oil degradation were studied by measuring the concentrations of major degradation products, polymers, decomposition products, free fatty acids and total polar materials. Regression models were fitted to predict the changes in physical properties, specific gravity, viscosity, surface tension, specific heat, dielectric constant and capacitance with fat degradation. Fat degradation affected specific heat, specific gravity and viscosity. The dielectric constant or capacitance predicts fat degradation, independent of the food fried. A parallel plate capacitor of larger capacitance was found to produce better correlation with total polar materials in the high polar region.

INTRODUCTION

About 96 to 99% of the fresh frying fat/oil is triglycerides. During frying, the frying fat is exposed to 160C to 180C in the presence of air and moisture. As a result, hundreds of complex chemical reactions take place in the fat and it gets chemically altered during frying (Perkins 1988). More than 400 different chemical compounds including 220 volatile products have been identified in deteriorated frying fat (Gere 1982). The frying fat in the presence of oxygen, moisture and heat undergoes mainly three different types of alterations. They are hydrolytic alteration caused by moisture, oxidative alteration caused by oxygen and thermal alteration caused by heat (White 1991). At elevated frying temperatures steam reacts (hydrolysis) with triglycerides to form free fatty acids, monoglycerides, diglycerides and glycerol (glycerine). The atmospheric oxygen reacts with the fat at its surface causing oxidative alterations. Oxidation produces hydro-per-oxides which can further undergo three major types of degradations (1) 'fission' which produces alcohols, aldehydes, acids and hydrocarbons; (2)

[1] Send depositions to Dr. G.S. Mittal, Tel.: 519-824-4120, ext. 2431; Fax.: 519-836-0227; email: mittal@net2.eos.uoguelph.ca

Journal of Food Process Engineering **19** (1996) 201–221. *All Rights Reserved.*

'dehydration' which produces ketones; (3) 'free radical formation' which produces oxidized monomers, oxidative dimers and polymers, trimers, epoxides, alcohols, hydrocarbons, nonpolar dimers and polymers (Gutierrez *et al.* 1988; Stevenson *et al.* 1984; Lumley, 1988). Thermal alteration takes place because of heat and results in the formation of cyclic monomers, dimers and polymers through polymerization (White 1991). Cyclic monomers which are potentially harmful, originate from the intra-molecular cyclization of C_{18} polyunsaturated fatty acids. The hydrolytic, oxidative and thermal alterations are interrelated as well as superimposed (Gutierrez *et al.* 1988). The polymers formed as a result of oxidative and thermal alterations cause foaming which traps the steam bubbles longer in the fat to accelerate hydrolysis. All the degradation products other than nonpolar fraction is collectively called 'polar fraction'. The polar fraction is broadly grouped into polymers and decomposition products. Polymers refer to the group of all the degradation products with molecular weight higher than that of triglycerides. Decomposition products refer to the group of all the degradation products with molecular weight less than that of triglycerides.

There are a large number of factors that influence the deterioration of frying fat, turnover rate, type of the frying process, temperature, intermittent heating and cooling, degree of unsaturation of frying fats/oils, type of food material, design and maintenance of fryer, light, and use of filters. Many of the degradation products of frying fat are harmful to human health as they destroy vitamins, inhibit enzymes, potentially cause mutations or cause gastrointestinal irritations (Clark and Serbia 1991). As the fat degrades, more surfactants are formed. They increase the contact time between food and fat. As a result, the quantity of fat absorbed by the food and the rate of heat transfer to the food increase (Bluementhal 1991).

To determine the time when frying fats reach their maximum safe levels of deterioration, is a challenging task. No satisfactory and easy method of sensing the frying fat quality has been developed so far. Usually, in restaurants, the cooks with their experience, decide the discarding time of the fat by observing the color, odor, excessive foaming and smoking (Morton and Chidley 1988). An experienced cook may also evaluate the quality of the food products by tasting them. Obviously, these are not reliable methods because of their subjective nature. On the other hand, some restaurants and large scale fast food manufacturers have concerns about the public health, as well as their commitment to the high quality of food products. They discard the fat, based on the above described subjective evaluations. This often leads to the early discarding of safe fat, causing considerable financial losses to the restaurants. Thus, inaccurate monitoring of frying fat quality can either risk the public health or cause financial losses to the restaurants.

The harmful compounds forming in the deteriorated fat can be identified and their quantity measured by using chemical analysis. However, chemical analysis

require costly equipment such as gas chromatograph, different titrations, precise weighing arrangements and skilled labor. As a result, chemical methods are not generally preferred for restaurant conditions.

Therefore, the objective of this paper is to measure the changes in physical properties of the frying fat and find out their correlations with the changes in chemical composition of the fat so that an economical and reliable method to measure its quality during frying can be developed.

METHODS AND MATERIALS

Collection of Samples

In much of the past research, the degraded fat samples were prepared under laboratory conditions (Vijayan *et al.* 1993; DaSilva *et al.* 1993; El-Shami *et al.* 1992; Rojo and Perkins 1987; Sebedio *et al.* 1987). The simulated frying operations in most of these experiments were far too simple compared to the complexity of heat and mass transfer involved in the actual frying operation in restaurants. Various kinds of real-life conditions, associated with the frying of different types of foods, can add to the complexity of chemical reactions, physical interactions and hence the degradation characteristics. For example, Gwo *et al.* (1985) reported that the conjugated diene hydroperoxide (CDHP) values of fats used to fry chicken in the actual commercial fryers were lower than that of the fat/oil used in simulated frying tests.

All the fat samples were collected from one of the outlets of a large North American fast food chain in Ontario, Canada. Canola oil based shortening was used for frying. Samples were collected from four different fryers each for different type of deep fat fried food. The food products are named chicken product 1, chicken product 2, fish product and potato french fries. Eight samples including the fresh fat were collected for the chicken product 1 over a period of 7 days. Then, 10 samples including fresh fat were collected for the chicken product 2 over a period of 9 days. Ten samples including fresh fat were collected for the fish product over a period of 9 days. Ten samples were collected including fresh fat for the potato french fries over a period of 9 days. Thus, 38 samples were collected altogether. The samples were collected at the end of each day between 12:00 AM (midnight) and 1:00 AM. The collection was on a daily basis until the fat in the fryer was discarded. The bulk fat in the fryer at about 160C was mixed well using a stainless steel spoon to ensure the homogeneity. Then, each spoonful of fat was collected from different locations within the bulk fat in the fryer to make sure of the random nature of the sample collection.

The samples were always kept in air-tight glass jars at -4C. They were melted to conduct various experiments and analysis, and were maintained within

a temperature range of 45 to 60C. The samples were neither overheated nor allowed to be in the melted state for a long time. Each sample was kept melted only for the minimum duration required for the experiments. Contact of the samples with any sort of plastic containers was avoided to prevent polymer contamination. All the containers and stirrers used were made of either glass or stainless steel. The glass jars used for storage were almost full with the samples, leaving practically no space for air. The samples were kept in the dark inside the fridge to prevent photo-oxidation due to sunlight and fluorescent lights. These precautions were taken to minimize the further deterioration of the collected samples.

Chemical Composition

The maximum quantity of cyclic monomers detected in degraded fats is of the order of 0.5% by mass. Thus, the quantification of cyclic monomers is not important from the practical point of view. Quantities of polymers, decomposition products, unaltered triglycerides and free fatty acids present in the samples were determined.

The HPLC method described by Burkow and Henderson (1991) was slightly modified to get the better results. Waters 712 WISP HPLC system was used with Waters 510 Millipore brand HPLC pump, Waters 410 Millipore brand differential refractometer, and Waters 745B Millipore brand data module and digital integrator. Three of the Waters Ultrastyragel columns in series were used as the stationary phase, one linear column, one 500 A° unit column and one 100 A° unit column. HPLC grade tetrahydrofuran of molecular weight 72 daltons was used as the mobile phase and as the solvent for sample preparation. Fat samples were dissolved in tetrahydrofuran and diluted to be injected into the HPLC system. A number of trial and error analysis were done initially to optimize the ratio of solvent to sample, to achieve the best resolution of separation. For fat samples of lesser deterioration, a solvent/sample ratio of 1.4/0.2, for moderately deteriorated samples, a ratio of 1.4/0.143, and for highly deteriorated samples, a ratio of 1.4/0.09 were found to be the best.

After connecting three columns in series, 6M nitric acid was pumped continuously for about 6 h, to clean the columns. HPLC grade methanol was pumped for about 2 h to remove any traces of the nitric acid from the columns. Then tetrahydrofuran, the mobile phase was pumped through the columns. The pressure of pumping was adjusted to 6000 psi. An external temperature of 40C and an internal temperature of 35C were set. The flow rate of tetrahydrofuran was set to 1 mL/min. The system was run until the steady base line was obtained. The 15 μL samples were injected for analysis. The total running time for one sample analysis was 40 min. Three peaks were obtained for polymers, triglycerides and decomposition products, respectively. The retention times for

polymers, triglycerides and decomposition products were around 21.5 min, 22.5 min and 24.8 min, respectively.

The standard A.O.C.S. method #Ca 5a-40 (AOCS 1989) was used to determine the quantity of free fatty acids present in the samples. This is a simple titrimetric method. The percentage of free fatty acids was calculated as oleic acid.

Physical Properties

Specific Gravity. The A.O.C.S. method To-la-64 (AOCS 1989) was used to determine the specific gravity of the samples. But, the sample temperature was 45C in place of 25C for convenience of measurement.

Surface Tension. Surface tension of a liquid is defined as the force per unit length that acts across any line in the liquid surface, tending to pull the surface open. The surface tension of the samples were determined using a DuNouy Tensiometer (model #70535, CSC Scientific Company Inc., Fairfax, Virginia, USA). The procedure of measurement was as instructed by the manufacturer. All the readings were taken at 61C sample temperature.

Viscosity. The viscosities of the samples were determined using the Digital Viscometer (model RVDT, Brookfield Engineering Laboratories Inc., Stoughton, MA, USA). Samples were melted and poured into 100 mL beakers. The beakers were placed in a water bath kept at 45C. Spindle #1 and 50 rpm were chosen for better results. The spindle was placed in the beaker concentrically, rotated and stopped many times before the readings were taken, to ensure that no air bubble was sticking to the spindle. Then, the spindle was rotated in the sample for one min before the readings were taken. This was to stabilize the agitation of fat in the beaker.

Specific Heat. The specific heat values of the samples were determined using the adiabatic calorimeter developed by Mittal *et al.* (1989). The instrument, made of stainless steel, has four 40 Ω resistors connected in parallel. Initial temperature of both the sample and the instrument was maintained the same by keeping them at room temperature for 30 min. A current of 1.7 A at 18 V was passed through the resistors for 5 min. Temperature after 35 min was observed as the final temperature. The specific heat of the sample was calculated by using the following equation:

$$Q = m_{fat}C_{pfat}\Delta T + m_{app}C_{papp}\Delta T \quad (1)$$

where m_{fat} is the mass (kg) of the sample, C_{pfat} is the specific heat (J/(kgC)) of the sample, m_{app} is the mass of the apparatus, C_{papp} is the specific heat (J/(kgC))

of stainless steel, ΔT is the difference between initial and final equilibrium temperatures (°C), and Q is the total heat input (J) calculated as follows:

$$Q = I^2R\Delta t \tag{2}$$

where I is the current in ampere, R is the total resistance and Δt is the heating time, s.

Dielectric Constant. Dielectric constant is a measure of the ability of a substance to store electric charge. The dielectric constant of the fat increases with the increase in total polar materials. Food Oil Sensor (FOS) manufactured by Northern Instruments Corp., Lino Lakes, MN, USA, indirectly measures the dielectric constant of the frying fat. A few drops of frying fat are placed in the cup of the instrument maintained at a constant temperature of about 63C. The fat acts as a dielectric material in a small capacitor, and the FOS gives a reading proportional to the dielectric constant of the fat. Samples were filtered before test using grade 5 filter papers to ensure that no large solid particles were present.

Capacitance. All the parameters such as area of overlap (0.01007 m^2), distance between the plates (0.0001755 m) and the temperature of measurement (55C) were kept constant. An LCR meter (model 4261A, Hewlett Packard Co., Palo Alto, CA, USA) was used to measure the capacitance. Samples were filtered using grade 5 filter paper to ensure that no large solid particles were present. The capacitor was completely immersed in the sample and precautions were taken to ensure that no air bubble was sticking between the parallel plates. The area of overlap (A) was calculated using the following equation with air as the dielectric medium. The dielectric constant (K) of air was assumed to be 1.0006 (Giancoli 1985):

$$A = \frac{C.d}{\varepsilon_o(1.0006)} \tag{3}$$

where C is capacitance, d is distance between the parallel plates, ε_o is the permittivity of air. The following equation was used to calculate the dielectric constant of the samples:

$$\text{Dielectric Constant, } K = \frac{C.d}{\varepsilon_o A} \tag{4}$$

Data Analysis

Analysis of variance and correlation were done using ANOVA procedure of the Statistical Analysis System (SAS 1992). The Least Significant Difference (LSD) method was used for the comparison of means.

RESULTS AND DISCUSSION

Degradation Products

ANOVA (not shown) showed no replication effect on any of the degradation product or property. Significant increase in polymer formation with frying time was observed. However, the maximum amount of polymers formed was dependent on the food fried. This may be due to the variations in temperature, frying time, heat capacity or product composition. The polymer formed in somewhat regular increments of 0.6 to 2.5% by mass over the days, rather than sudden or accelerated increments. This was independent of the foods fried. Lower increase in polymer concentration was observed on a less busy day, when the heater was off for longer durations. This suggests that longer heating and the quantity of food fried may increase the polymer formation. DaSilva *et al.* (1993) also reported that the polymer concentration increased with larger quantities of food fried. The polymer concentration decreased when a higher turnover ratio was used.

Significant increase in the free fatty acid formation with frying time was observed gradually after three days of frying. It continued to increase every day until the oil was discarded, independent of high turnover rates and foods fried. The highest concentrations of free fatty acids in all the samples were observed at the discarding time.

The formation of decomposition products over the first 3 to 5 days was in small quantities ($<1\%$). But, their quantity suddenly increased to 5 to 7% by mass on fifth or sixth day and continued to increase until the fat was discarded independent of the high turnover rates and food fried. This may be due to the increasing accumulation of degradation products catalyzing further degradation.

Free fatty acids were found to constitute the major portion (49 to 69%) of the decomposition products in highly degraded fat. The decomposition products formed during the initial stages of degradation (up to 4 - 5 days) were almost entirely free fatty acids. However, the sudden increase of decomposition products from less than 1% to 5 - 7% by mass on fifth or sixth day is not accounted by the free fatty acids. It is due to the sudden increase in other decomposition products such as monoglycerides, diglycerides, volatile compounds, etc. The sudden increase could be due to the catalytic effect of degradation products on further decomposition.

The formation of total polar materials showed a steady and significant increase with frying time independent of the foods fried. However, their concentration reduced with high turnover ratios.

Decomposition products showed a poor correlation (0.53) with polymers. Figure 1 shows two distinct groups of scattered points due to the sudden increase in decomposition products concentration. Free fatty acids also showed a poor

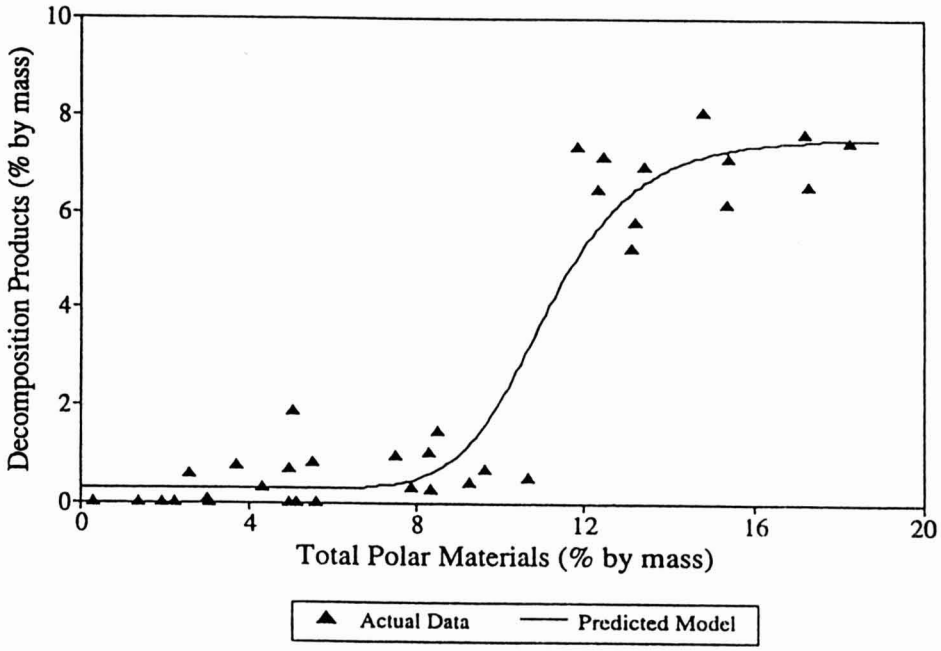

FIG. 1. RELATIONSHIP BETWEEN DECOMPOSITION PRODUCTS AND TOTAL POLAR MATERIALS IN FRYING FAT

correlation (0.63) with polymers. Total polar materials showed a good correlation (0.87) with polymers. Even though, total polar materials showed a good correlation (0.88) with decomposition products. Figure 2 shows two distinct groups of scattered points because of the sudden increase in decomposition products. Free fatty acids also showed a good correlation (0.90) with total polar materials (Fig. 3). Despite the two distinct groups of data points, the free fatty acids produced a good correlation (0.94) with the decomposition products.

The following regression models were fitted between total polar material (TPM), free fatty acids (FFA), and decomposition products (DP):

TPM = 2.80 + 2.66 FFA; R^2 = 0.81, standard error of estimate (SSE) = 0.56 and 0.21, respectively, and Pr > t was less than 0.0001.

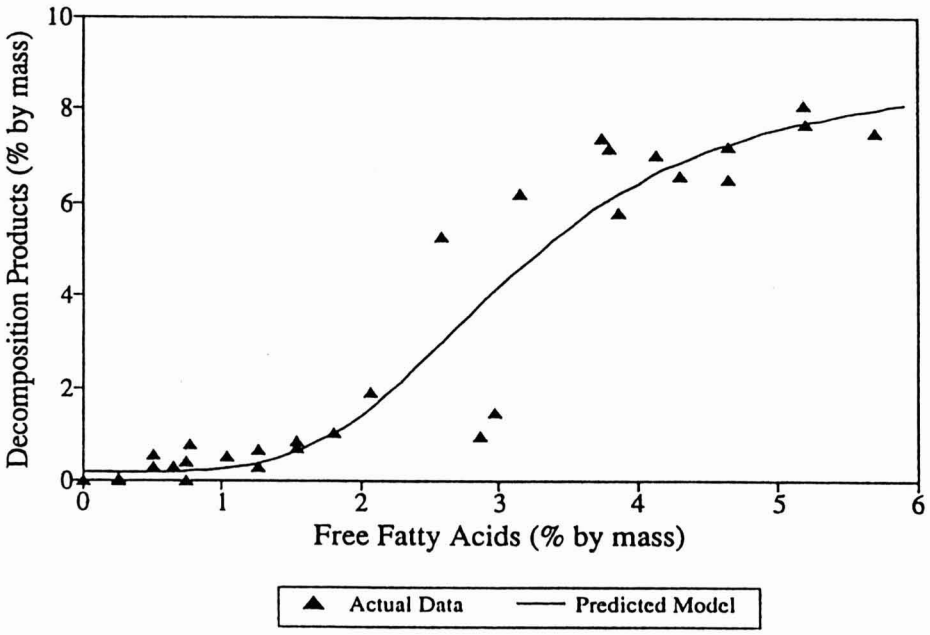

FIG. 2. RELATIONSHIP BETWEEN DECOMPOSITION PRODUCTS AND FREE FATTY ACIDS IN FRYING FAT

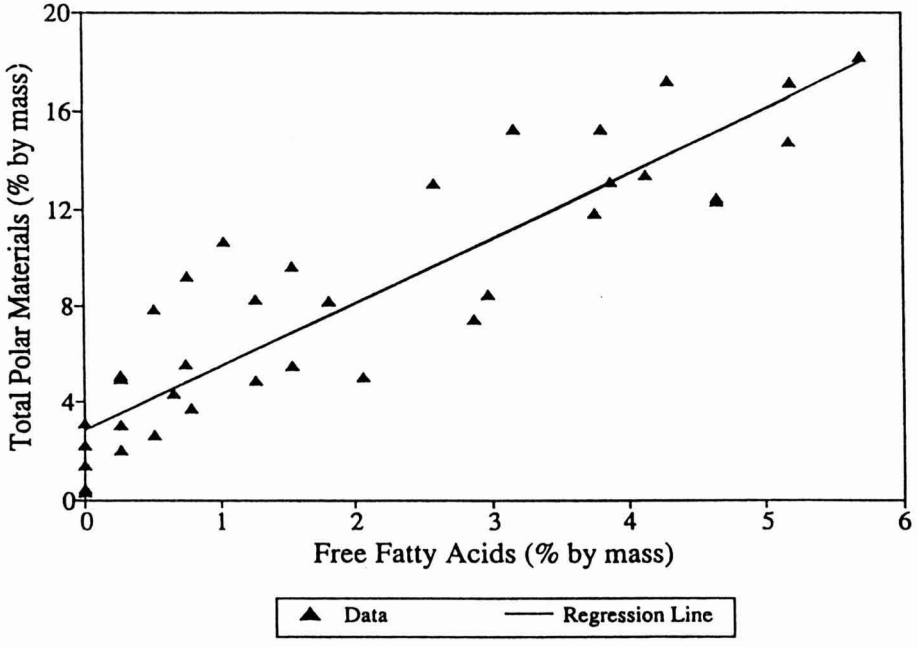

FIG. 3. RELATIONSHIP BETWEEN TOTAL POLAR MATERIAL AND FREE FATTY ACIDS IN FRYING FAT

$$DP = 0.272 + \frac{7.310}{[1 + (0.091TPM)^{-10.01}]^{1.1}} \quad (5)$$

with $R^2 = 0\ 95$.

$$DP = 8.875 - \frac{8.686}{[1+(0.349FFA)^{4.265}]^{0.766}} \quad (6)$$

with $R^2 = 0.95$.

The above results generally agreed with the findings of other researchers (Lumley 1988; Gutierrez *et al.* 1988; Smith *et al.* 1986; Wu and Nawar 1986; Croon *et al.* 1986; Gere 1982). Smith *et al.* (1986) suggested that the scattering of the data points may be due to the dilution effects from higher turnover ratios. In general, the longer the duration of frying was, the greater was the degradation. Higher turnover rates reduced the degradation in all the samples because of dilution effects. Greater lipid exchange was reported with longer durations of frying.

Physical Properties

Table 1 lists the correlation coefficients of physical properties with the major degradation products. Change in specific gravity correlated well with polymers (Fig. 4). But, the change in specific gravity was significant only at the fourth decimal. The following regression equation was fitted between specific gravity (γ) and polymers (POL) with $R^2 = 0.99$:

$$\gamma = 0.50 + 0.41POL^{0.003} \quad (7)$$

Surface tension did not show any significant change with frying time. The viscosity increased by 25% with an increase in polymer formation by 6.2%. The change in kinematic viscosity poorly correlated with the change in polymers (0.77) and total polar materials (0.65), the data points were rather scattered (Fig. 5 and 6). Higher correlations between the changes in viscosity and polymer formation have been reported by Wu and Nawar (1986) and DaSilva *et al.* (1993). But their results were based on simulated frying experiments conducted in the laboratory, while the present study was based on the samples collected from actual restaurant fryers, where the degradation process was more complex. This may be the reason for the lower correlations in the present study. The following regression models were fitted between kinematic viscosity (ν) and POL and TPM:

$$\nu = 42.31 + 5.28POL - 1.41(POL)^2 + 0.14(POL)^3; R^2 = 0.77 \quad (8)$$

$$\nu = 43.95 + 2.46TPM - 0.33(TPM)^2 + 0.01(TPM)^3; R^2 = 0.65 \quad (9)$$

TABLE 1.
CORRELATION BETWEEN CHEMICAL COMPOSITION AND PHYSICAL PROPERTIES OF FRYING FAT

Property	Polymers	Triglycerides	Decomposition products	Total polar materials	Free fatty acids
Specific gravity	0.813 (0.0001)	-0.683 (0.0036)	0.580 (0.0184)	0.683 (0.0036)	0.666 (0.0049)
Surface tension	0.078 (0.7685)	0.061 (0.8212)	-0.140 (0.6057)	-0.061 (0.8212)	-0.042 (0.8780)
Viscosity	0.727 (0.0001)	-0.737 (0.0011)	0.651 (0.0063)	0.737 (0.0011)	0.778 (0.0004)
Kinematic viscosity	0.84 (0.0001)	-0.74 (0.001)	0.65 (0.0061)	0.74 (0.001)	0.78 (0.0004)
Specific heat	-0.875 (0.0001)	-0.758 (0.0007)	0.660 (0.0054)	0.758 (0.0007)	0.747 (0.0009)
Capacitance	0.970 (0.0001)	-0.948 (0.0001)	0.898 (0.0001)	0.948 (0.0001)	0.960 (0.0001)
FOS reading	0.977 (0.0001)*	-0.984 (0.0001)	0.948 (0.0001)	0.984 (0.0001)	0.994 (0.0001)

* - Confidence level of the probability that there is no correlation.

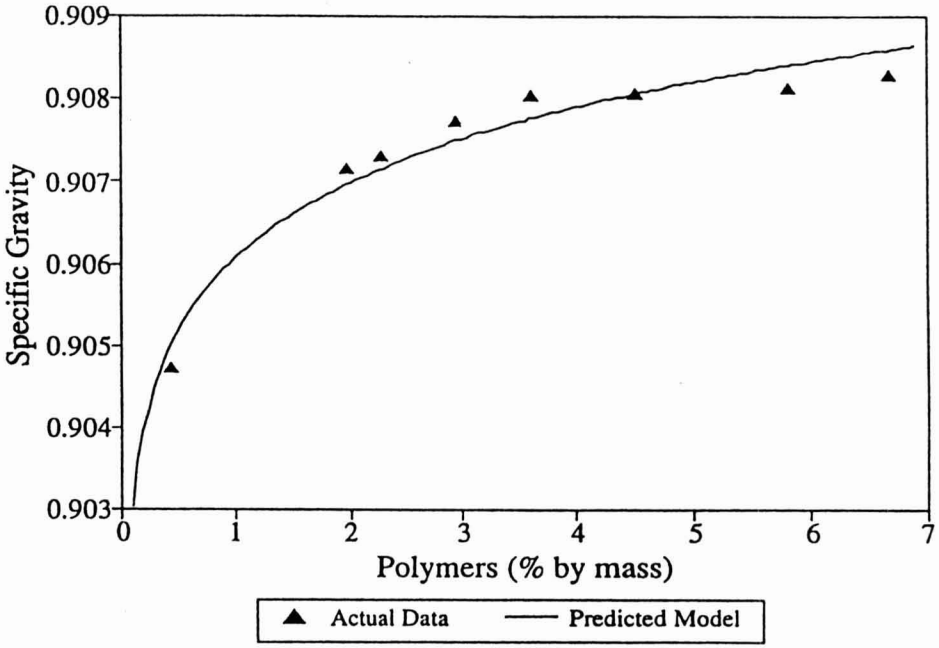

FIG. 4. RELATIONSHIP BETWEEN SPECIFIC GRAVITY AND POLYMERS IN FRYING FAT

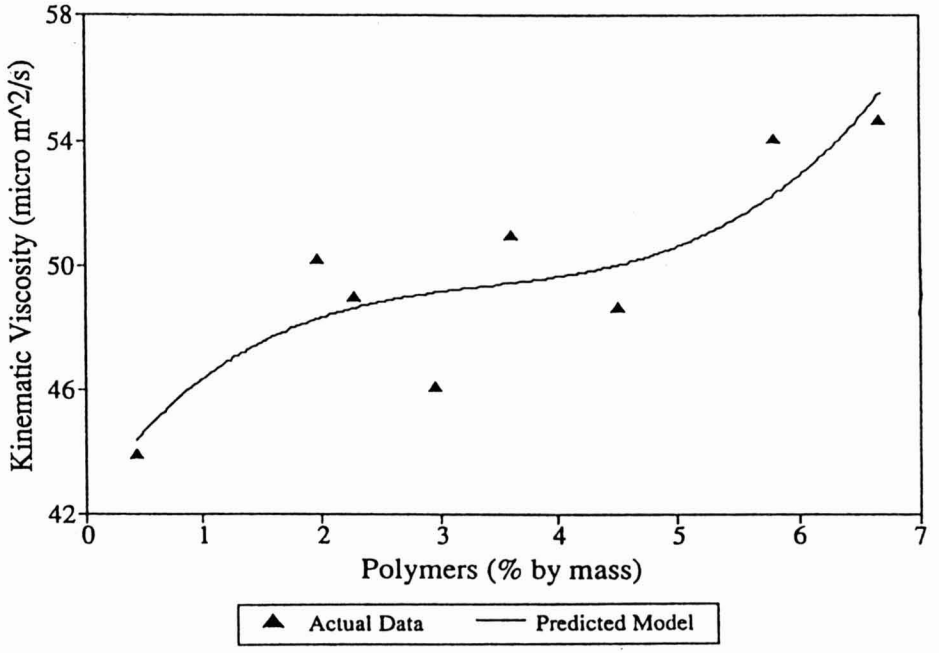

FIG. 5. RELATIONSHIP BETWEEN KINEMATIC VISCOSITY AND POLYMERS IN FRYING FAT

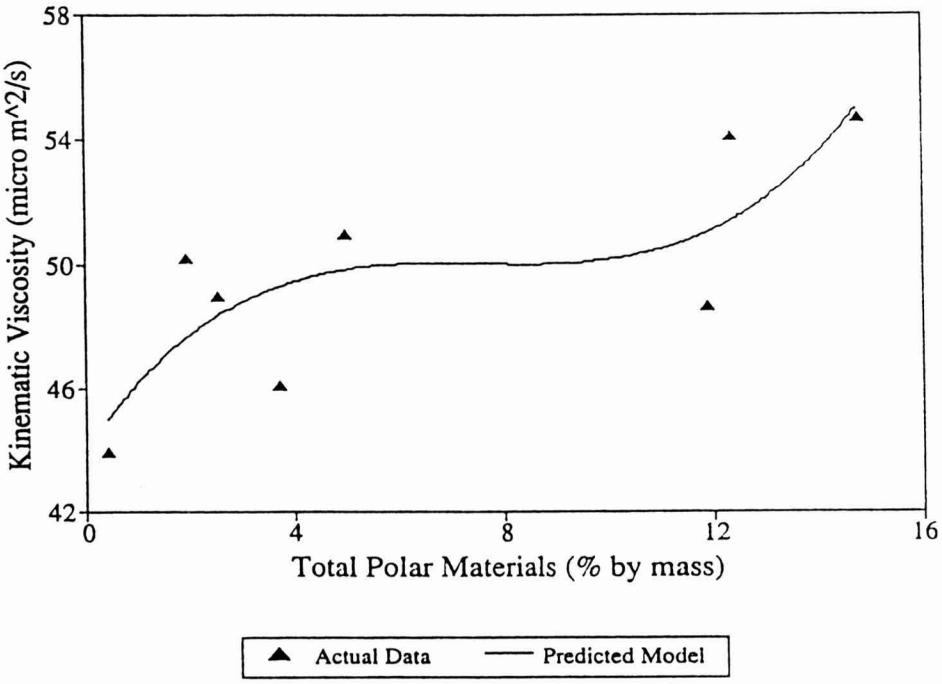

FIG. 6. RELATIONSHIP BETWEEN KINEMATIC VISCOSITY AND TOTAL POLAR MATERIAL IN FRYING FAT

Significant decrease in specific heat was observed only with higher levels of fat degradation. Even though the specific heat decreased by 14%, it did not produce a high correlation with the total polar materials.

Significant increase in the dielectric constant was observed with increase in the frying time. The dielectric constant increased by 9% with an increase in total polar materials by 14.3%. Both FOS readings and parallel plate capacitance produced high correlations with all the major degradation products. The polymers showed a reasonable fitting (FOS = 0.19 + 0.48 POL; R^2 = 0.83) with FOS reading (Fig. 7) and not good fitting (R^2 = 0.77) with parallel plate capacitance (Fig. 8). The FOS reading and the parallel plate capacitance showed similar trends of changes with polymers. The decomposition products showed poor regression (R^2 = 0.59) with FOS readings (Fig. 9) and a slightly better (R^2 = 0.77) with parallel plate capacitance (Fig. 10). Both FOS reading and parallel plate capacitance showed similar trends of changes with decomposition products. However, both of these cannot predict decomposition products concentration due to a large scatter of data.

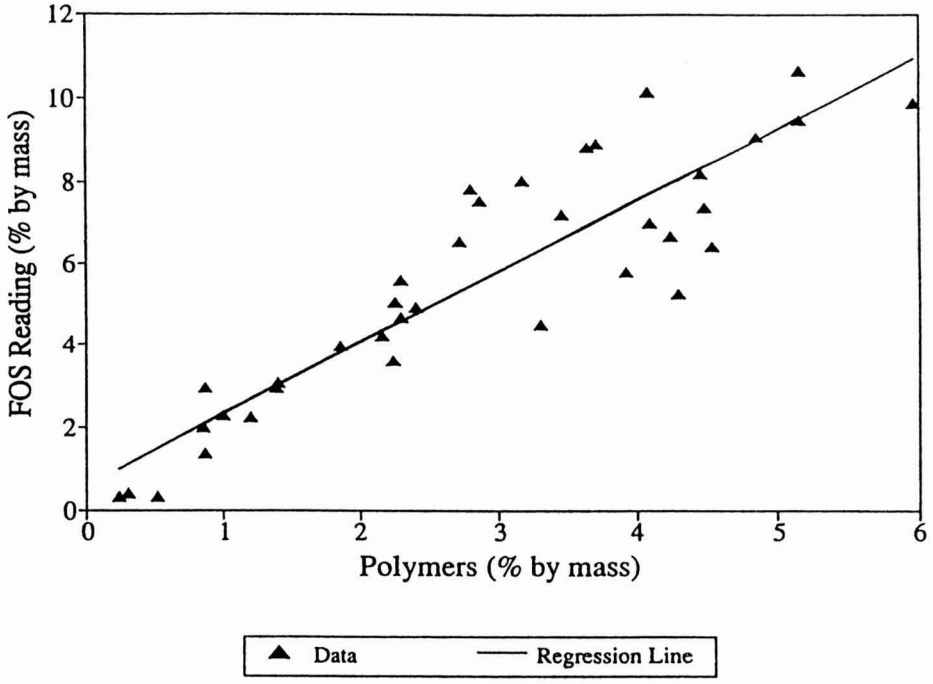

FIG. 7. RELATIONSHIP BETWEEN FOS (FOOD OIL SENSOR) READING AND POLYMERS IN FRYING FAT

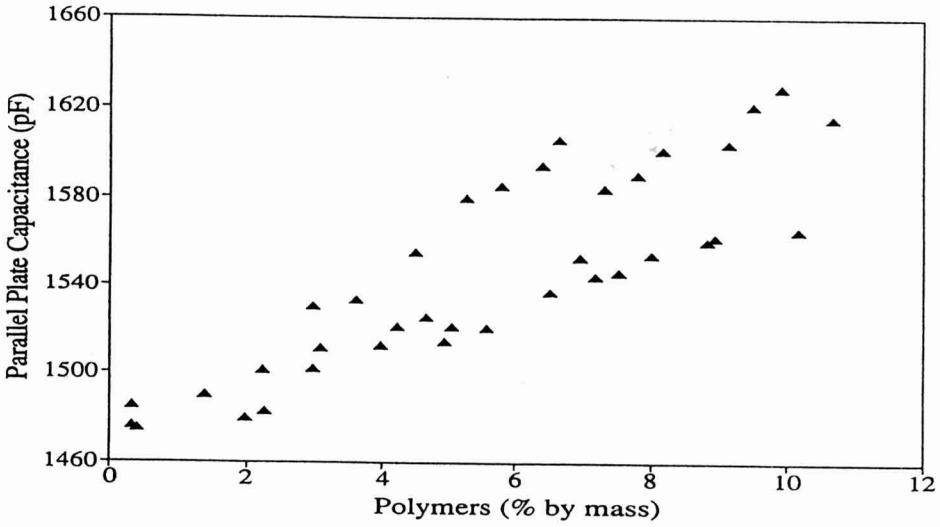

FIG. 8. RELATIONSHIP BETWEEN CAPACITANCE AND POLYMERS IN FRYING FAT

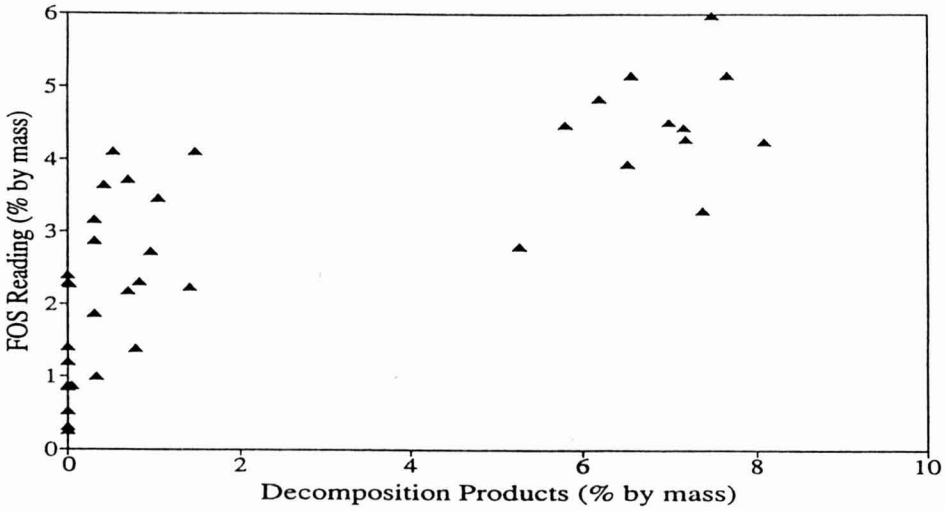

FIG. 9. RELATIONSHIP BETWEEN FOS (FOOD OIL SENSOR) READING AND DECOMPOSITION PRODUCTS IN FRYING FAT

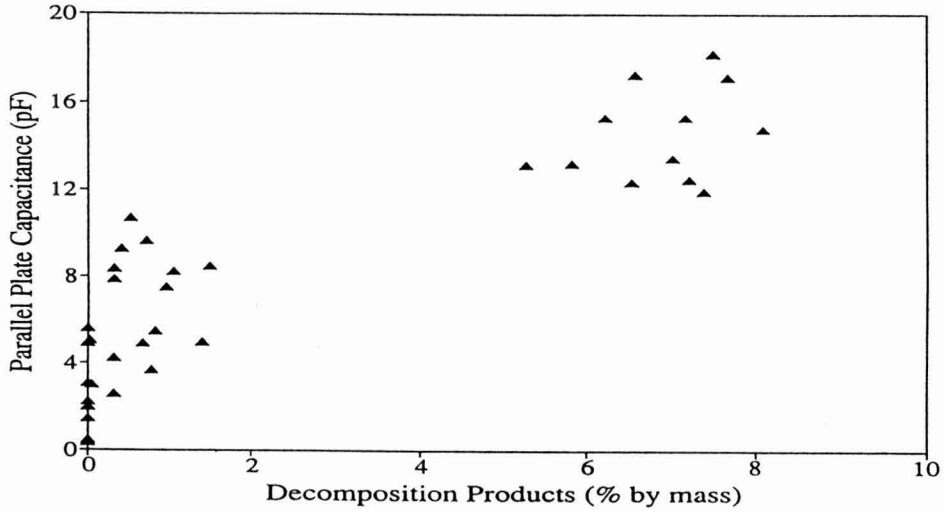

FIG. 10. SCATTER PLOT BETWEEN CAPACITANCE AND DECOMPOSITION PRODUCTS IN FRYING FAT

The free fatty acids showed a poor fit ($R^2 = 0.73$) with FOS reading (Fig. 11) and a slightly better fit ($R^2 = 0.79$) with parallel plate capacitance (Fig. 12) due to large scattering in the data. Both FOS reading and parallel plate capacitance showed very similar trends of changes with free fatty acids.

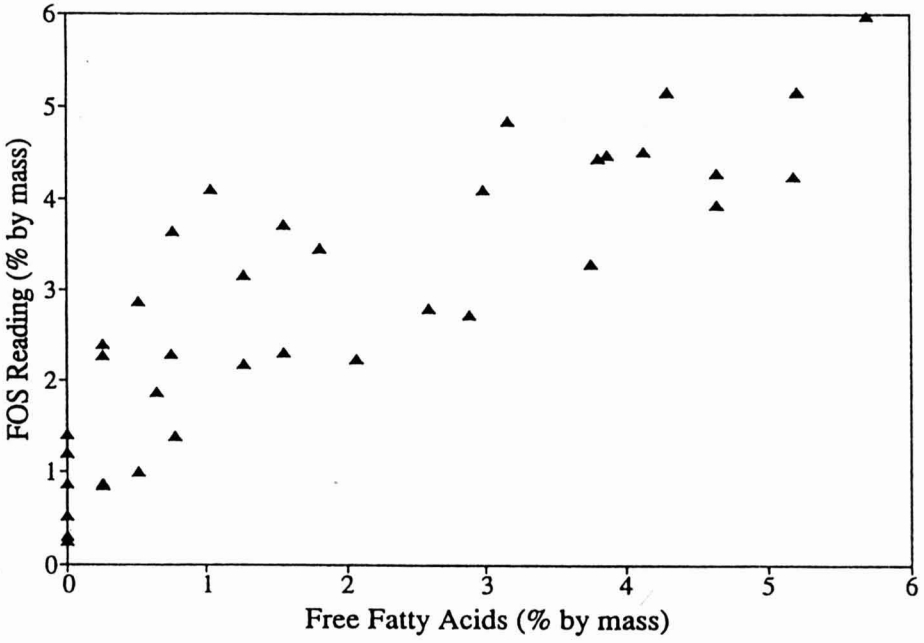

FIG. 11. SCATTER PLOT BETWEEN FOS (FOOD OIL SENSOR) READING AND FREE FATTY ACIDS IN FRYING FAT

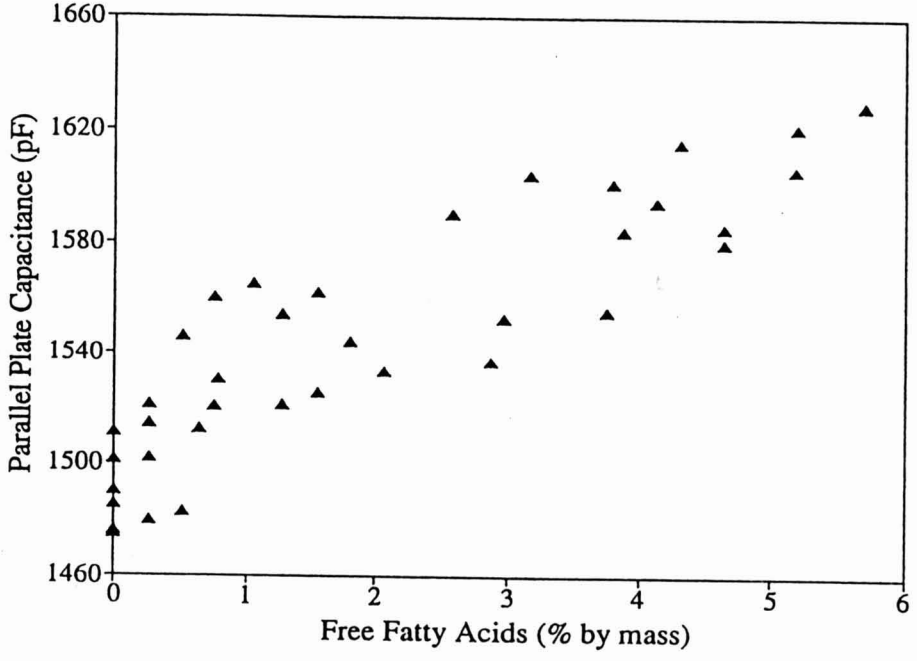

FIG. 12. SCATTER PLOT BETWEEN CAPACITANCE AND FREE FATTY ACIDS IN FRYING FAT

The total polar materials showed a good fit (FOS = 0.54 + 0.29 TPM; R^2 = 0.94) with FOS reading (Fig. 13) and a slightly better fit (C = 1477.81 + 8.30 TPM; R^2 = 0.97) with parallel plate capacitance (Fig. 14). Both FOS reading and parallel plate capacitance showed similar trend of changes with total polar materials. Croon *et al.* (1986) reported similar correlation (r = 0.94) between the FOS reading and the total polar materials for 100 oil samples collected from restaurant fryers in Scandinavian countries. Smith *et al.* (1986) also reported a slightly higher correlation (r = 0.95) between the total polar materials and the dielectric constant, for 60 oil samples collected from restaurant fryers in California. Only Graziano (1979) reported a higher correlation (r = 0.99) between the FOS reading and the total polar materials. But this report was based on only 24 samples collected from a simulated frying experiment conducted in the laboratory.

The presence of contaminants such as moisture, spices from the food, etc. also contributes greatly to the scattering of data points. The overall scattering of data points in the FOS reading plots, were slightly higher than that of the parallel plate capacitance. This may be due to: (1) The sensing capacitor used

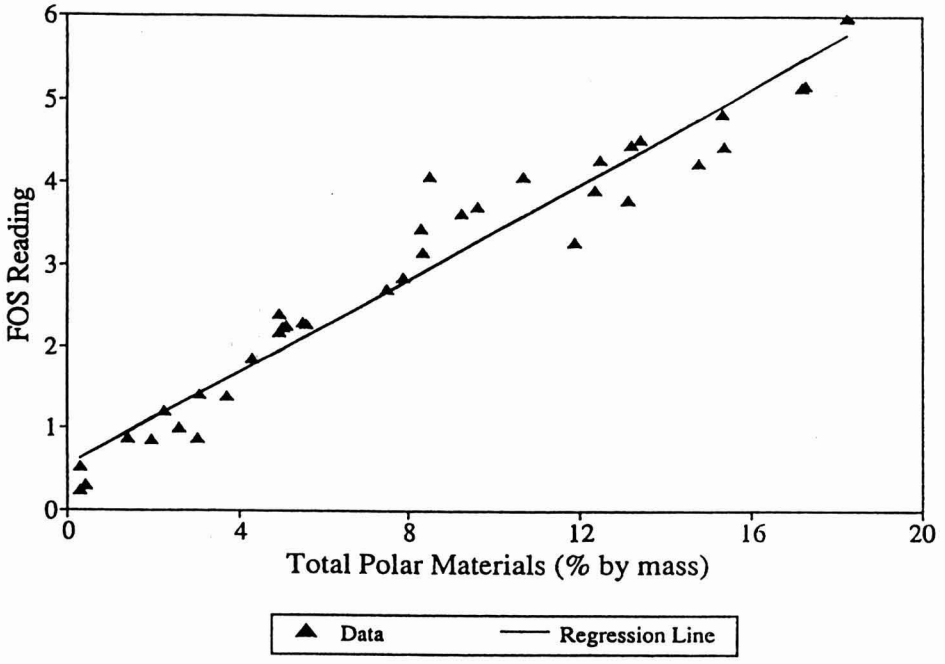

FIG. 13. RELATIONSHIP BETWEEN FOS (FOOD OIL SENSOR) READING AND TOTAL POLAR MATERIAL IN FRYING FAT

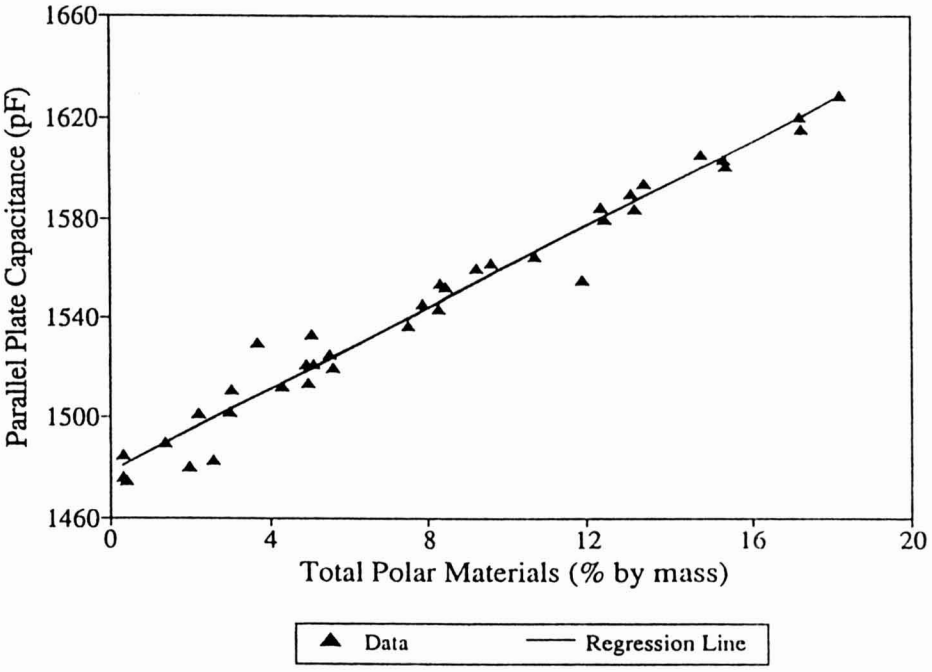

FIG. 14. RELATIONSHIP BETWEEN CAPACITANCE AND TOTAL POLAR MATERIAL IN FRYING FAT

in the FOS is very small. Therefore, the area of capacitor in contact with the fat is very small. This increases the error in measurements. (2) The volume of fat used in the FOS is approximately 1 mL. Such a small volume is less accurate in representing the overall polarity and dielectric constat of the fat.

More scattering of FOS readings and parallel plate capacitances was observed at lower concentrations of total polar materials. The scattering became less as the concentration of total polar materials in the fat increased. In the plot of total polar materials against the FOS reading reported by Wu and Nawar (1986), 7 data points corresponding to the higher concentrations of polar compounds showed much less scattering than the other data points. In the plot of total polar materials against the dielectric constant reported by Smith *et al.* (1986), 10 data points corresponding to the higher dielectric constants showed lower scattering than the rest of the data. The decreased scattering of data with

the increase in total polar materials may be because the decomposition products have relatively higher effective polarity than the polymers and hence they have a stronger influence on the overall polarity of the fat. Therefore, the scattering should become less as the concentration of the decomposition products increases, relative to that of the polymers.

SUMMARY AND CONCLUSIONS

(1) The polymer concentration in the fat increases from 0.33 - 0.44% to 5 - 9.6% by mass in 9 days of frying. The polymer concentration decreases with high turnover ratio.

(2) The concentration of decomposition products in the fat increases from 0% to 5.8 - 8.3% by mass in 9 days of frying. This increase is independent of high turnover ratio.

(3) The concentration of free fatty acids in the fat increases from 0% to 3.9 - 5.7% by mass in 9 days of frying. This increase is independent of high turnover ratio.

(4) The concentration of total polar materials in the fat increases from 0.33 - 0.44% to 12.5 - 18.3% by mass in 9 days of frying. The total polar materials concentration decreases with high turnover ratio.

(5) The decomposition products formed during the initial stages of degradation (up to 4 to 5 days) are almost entirely free fatty acids. The free fatty acids constitute the major portion (49 - 69%) of the decomposition products in highly degraded fat. Free fatty acids correlate well with decomposition products.

(6) Specific gravity correlates well with polymers.

(7) Viscosity increases by 25% with an increase in polymer formation by 6.2% by mass.

(8) Specific heat decreases by 14.1% in 7 days of frying.

(9) The dielectric constant of the fat increases from 2.90 - 2.92 to 3.15 - 3.21 in 9 days of frying. The dielectric constant increases by 6.7 - 9% with an increase in total polar materials by 12.1 - 17.9%.

The results show that except for dielectric constant, other measured physical properties are indirectly measuring mainly one chemical concentration. For example, changes in viscosity indicate mainly the changes in polymer content. But the measurement of polymers alone is not a reliable indication of overall oil degradation. Moreover, correlations in the region of high polar concentration is more important in the sensor development. Therefore, more physical properties of the fat, such as optical, are needed to be measured during frying. These and other physical properties dynamics data will assist in developing a suitable oil quality sensor. However, further work is required in this direction.

ACKNOWLEDGMENTS

This research was financially supported by the Natural Sciences and Engineering Research Council of Canada, and the Ontario Ministry of Agriculture, Food and Rural Affairs, Ontario, Canada.

REFERENCES

AOCS. 1989. *Official Methods and Recommended Practices of the American Oil Chemists' Society*, (D. Firesone, ed.) American Oil Chemists' Society, Champaign, IL.

BLUMENTHAL, M.M. 1991. A new look at the chemistry and physics of deep-fat frying. Food Technol. *45*(2), 68–94.

BURKOW, I.C. and HENDERSON, R.J. 1991. Isolation and quantification of polymers from autoxidized fish oils by high-performance size-exclusion chromatography with an evaporative mass detector. J. Chromatography *552*, 501–506.

CLARK, W.L. and SERBIA, G.W. 1991. Safety aspects of frying fats and oils. Food Technol. *45*(2), 84–94.

CROON, L.B., ROGSTAD, A., LETH, T. and KIIJTAMO, T. 1986. A comparative study of analytical methods for quality evaluation of frying fat. Jahrgang *88*(3), 87–91.

DASILVA, M.G., VIJAYAN, J. and SINGH, R.P. 1993. Changes in viscosity of corn oil subjected to thermal degradation. In *Annual Meeting/Book of Abstracts*. pp. 229, Institute Food Technologists, Chicago, IL.

EL-SHAMI, S.M., SELIM, I.Z., EL-ANWAR, I.M. and EL-MALLAH, M.H. 1992. Dielectric properties for monitoring the quality of heated oils. J. Amer. Oil Chemists' Soc. *69*(9), 872–875.

GERE, A. 1982. Studies of the changes in edible fats during heating and frying. Die Nahrung *26*(10), 923–932.

GIANCOLI, D.C. 1985. Electric charge and electric field; electric potential and electric energy. In *Physics Principles with Applications*. pp. 353–391. Prentice Hall, Englewood Cliffs, NJ.

GRAZIANO, V.J. 1979. Portable instrument rapidly measures quality of frying fat in food service operations. Food Technol. *33*(9), 54–57.

GUTIERREZ, R., GONZALEZ, Q. and DOBARGANES, M.C. 1988. Analytical procedures for the evaluation of used frying fats. In *Frying of Food, Principles, Changes, New Approaches*, (G. Varela, A.E. Bender and I.D. Morton, eds.) pp. 141–154, Ellis Horwood, Chichester, England.

GWO, Y.Y., FLICK Jr., G.J., DUPUY, H.P., ORY, R.L. and BARAN, W.L. 1985. Effect of ascorbyl palmitate on the quality of frying fats for deep frying operations. J. Amer. Oil Chemists' Soc. *62*(12), 1666–1671.

LUMLEY, I.D. 1988. Polar compounds in heated oils. In *Frying of Food, Principles, Changes, New Approaches*, (G. Varela, A.E. Bender and I.D. Morton, eds.) pp. 166–173. Ellis Horwood, Chichester, England.

MITTAL, G.S., WANG, C.Y. and USBORNE, W.R. 1989. Thermal properties of emulsion type sausages during cooking. Can. Inst. Food Sci. Technol. J. *22*(4), 359–363.

MORTAN, I.D. and CHIDLEY, J.E. 1988. Methods and equipment in frying. In *Frying of Food, Principles, Changes, New Approaches*, (G. Varela, A.E. Bender and I.D. Morton, eds.) pp. 37–51, Ellis Horwood, Chichester, England.

PERKINS, E.G. 1988. The analysis of frying fats and oils. J. Amer. Oil Chemists' Soc. *65*(4), 520.

ROJO, J.A. and PERKINS, E.G. 1987. Cyclic fatty acid monomer formation in frying fats. I. Determination and structural study. J. Amer. Oil Chemists' Soc. *64*(3), 414–421.

SAS. 1992. SAS/STAT User's Guide, Vol. 2. Statistical Analysis System Inst., Inc., Cary, NC.

SEBEDIO, J.L., PREVOST, J. and GRANDGIRARD, A. 1987. Heat treatment of vegetable oils I. Isolation of the cyclic fatty acid monomers from heated sunflower and linseed oils. J. Amer. Oil Chemists' Soc. *64*(7), 1026–1032.

SMITH, L.M., CLIFFORD, A.J., HAMBLIN, C.L. and CREVELING, R.K. 1986. Changes in physical and chemical properties of shortenings used for commercial deep-fat frying. J. Amer. Oil Chemists' Soc. *63*(8), 1017–1023.

STEVENSON, S.G., VAISEY-GENSER, M. and ESKIN, N.A.M. 1984. Quality control in the use of deep frying oils. J. Amer. Oil Chemists' Soc. *61*(6), 1102–1108.

VIJAYAN, J., SINGH, R.P. and SLAUGHTER, D. 1993. Changes in optical properties of the corn oil during frying. *Annual Meeting/Book of Abstracts* pp. 229, Inst. of Food Technologists, Chicago, IL.

WHITE, P.J. 1991. Methods for measuring changes in deep-fat frying oils. Food Technol. *45*(2), 75–80.

WU, P. and NAWAR, W.W. 1986. A technique for monitoring the quality of used frying oils. J. Amer. Oil Chemists' Soc. *63*(10), 1363–1367.

ESTIMATION OF CONVECTIVE HEAT TRANSFER BETWEEN FLUID AND PARTICLE IN CONTINUOUS FLOW USING A REMOTE TEMPERATURE SENSOR[1]

V.M. BALASUBRAMANIAM[2] and S.K. SASTRY[3]

Department of Food, Agricultural and Biological Engineering
The Ohio State University
590 Woody Hayes Drive
Columbus, OH 43210

Accepted for Publication April 12, 1996

ABSTRACT

The convective heat transfer coefficient (h_{fp}) between fluid and particle in continuous tube flow was estimated using a temperature pill, a remote electronic temperature sensor which uses a quartz crystal as the temperature sensing element. The temperature history of a particle (with temperature pill mounted within) was monitored as it moved through a test section. A finite element algorithm was then used to back calculate h_{fp} from the time-temperature data. The value of h_{fp} ranged from 134 W/m^{2}K to 669 W/m^{2}K (Nu=3.6 to 17.3) over a fluid generalized Reynolds number range (restricted by experimental constraints) from 19 to 196.8. As expected, h_{fp} decreased with increasing carrier medium viscosity and increased with increasing flow rates. Even with several conservative factors at play, the lowest Nusselt number was greater than the 2.0 expected for a spherical particle in a stagnant fluid. Potential applications of the technique include noninvasive measurement of the temperature (and h_{fp} values) of the particles moving within a fluid stream in otherwise inaccessible locations.

INTRODUCTION

Conventional canning is the most widely used technology for producing shelf-stable particulate low acid foods. As consumer expectations of quality and convenience increase, the food industry has considered alternative choices for

[1] Salaries and research support provided in part by State and Federal Funds appropriated to the Ohio Agricultural Research and Development Center, The Ohio State University, and in part by a grant from the Center for Aseptic Processing and Packaging Studies, North Carolina State University. References to commercial products and trade names is made with the understanding that no discrimination and no endorsement by The Ohio State University is implied.

[2] Present address: The National Center for Food Safety and Technology, Illinois Institute of Technology, Summit-Argo, IL 60501

[3] Corresponding author.

Journal of Food Process Engineering **19** (1996) 223–240. *All Rights Reserved.*

sterilization, including aseptic processing and packaging. This is essentially a continuous sterilization technology, wherein the food and the container are sterilized separately and then packaged together in a sterile environment. The liquid-solid mixture is heated to the sterilization temperatures using scraped surface or tubular heat exchangers, and then held in insulated tubes so that particles achieve the desired lethality. Two important design parameters for this technology are the residence time distribution and the convective heat transfer coefficient (h_{fp}) at the liquid-solid interface. A considerable body of literature has been accumulated on residence time distribution of liquid-solid mixtures over a period of time (e.g., Taeymans *et al.* 1985; McCoy *et al.* 1987; Dutta and Sastry 1990; Lee and Singh 1990; and Yang and Swartzel 1992). However, due to the technological challenge involved in measuring the temperature of a moving particle, few researchers have attempted to determine h_{fp} under continuous flow conditions. Some of the proposed methods include: (1) the microbiological approach (Heppell 1985), (2) moving thermocouple method (Sastry *et al.* 1990), (3) liquid crystal method (Stoforos and Merson 1991; Balasubramaniam and Sastry 1994), (4) time-temperature integrator (Hendrickx *et al.* 1992), (5) melting point indicators (Mwangi *et al.* 1993), and (6) relative velocity method (Balasubramaniam and Sastry 1994). Even though many of these methods are helpful in understanding the basic heat transfer mechanisms, each has its own limitations and inaccuracies, and none can be considered universally applicable for all conditions (Sastry 1992). Methods such as liquid crystal, relative velocity, and melting point indicator require transparent vessels and carriers. The moving thermocouple method could be used for conservative but realistic estimation of h_{fp} values in continuous tube flow conditions, but it either is difficult to implement with multiple-particle streams or inapplicable in scraped-surface heat exchangers. Hence there is a need to develop a remote sensor methodology to measure h_{fp} of moving particles under industrially significant process conditions.

Remote Temperature Sensors

Due to the technological challenges involved in miniaturized remote temperature measurements, there are a limited number of remote sensors commercially available such as CorTemp^R (Human Technologies,Inc., St Petersburg, FL) and Datatrace^R Micropack (Mesa Medical Inc., Wheat Ridge, CO) sensors. The temperature pill is a miniaturized temperature sensor originally developed by researchers at John Hopkins University's Applied Physics Laboratory in collaboration with NASA (Lesho and Hogrefe 1989) and manufactured and commercially marketed by Human Technologies, Inc. to hospitals for long-term monitoring of the internal body temperature of patients. It essentially consists of a silicone capsule encapsulating a telemetry system with

printed circuit board and electronic components, microbattery, and a quartz temperature sensor. The crystal resonates at a temperature-dependent frequency and invokes a coil circuit, which generates a magnetic signal. An external receiver converts the magnetic signal back to temperature readings. Dimensions and properties of the sensor are provided in Table 1. Micropack^R is another commercially available remote temperature sensor marketed by Mesa Medical, Inc. which functions based on a similar principle. It is said to have applications involving moving conveyors, retorts, ovens, freezers, and dryers (Ashley 1992). By placing a sensor at a known location within a particle, the temperature history of the particle can be recorded. Then, h_{fp} can be back calculated from time-temperature data using a mathematical model.

The use of the transmitter particle has been previously reported by Bhamidipati and Singh (1995), who used the CorTemp^R sensor to determine h_{fp} using the intact pill under its settling velocity within stagnant fluid in a tube. Since these studies were conducted under conditions far removed from process flow conditions, the results cannot be considered representative. Moreover, as will be shown, the temperature pill in the intact form is not well suited to measurement of rapid thermal responses due to its own slow thermal response and long logging interval.

The objectives of the present study were: (1) to noninvasively estimate h_{fp} for a moving particle in continuous tube flow using an appropriately designed remote temperature sensor and (2) to study the factors influencing h_{fp} under these conditions.

MATERIALS AND METHODS

Experimental Setup

The schematic diagram of the experimental setup is shown in Fig. 1. A tube of diameter 0.0508 m (2 in.) with 3.05 m (10 ft) length, inclined upwards at 2.08 cm/m (0.25 in./ft; as required of commercial holding tubes) was used as the test section. An antenna in the shape of a ring enclosing the test section was used to noninvasively receive signals from the temperature sensor. The antenna was capable of receiving magnetic signals from the pill within a range of 3 ft. Beyond this distance, weak signals and erroneous temperature readings would occur.

Preliminary Experiments

Preliminary experiments conducted during summer 1990 used a commercially available temperature pill (CorTemp^R, Human Technologies, St Petersburg, FL), the dimensions and properties of which are listed in Table 1. The sensor was tested in an agitated water bath as well as in continuous tube flow

TABLE 1.
DIMENSIONS AND PROPERTIES OF TEMPERATURE SENSORS

Sensor	Dimensions		Density	Temperature (°C).		Sampling	Time
	Diameter (m)	Length (m)	(kg/m^3)	Maximum	Accrcy.	time (s)	constant[1] (s)
Temperature pill, sensor in its intact form	0.01 (0.40 in.)	0.023 (0.925 in.)	1936	80C	0.1C	5	34.0
Micropack[R], sensor in its intact form	0.036 (1.4 in.)	0.053 (2.1 in.)	2101	85C	0.5C	1	N/a
Modified Temperature pill, sensor separated	0.011 (0.44 in.)	0.029 (1.145 in.)	1987	80C	0.1C	1	1.23

[1] Determined in the laboratory using an agitated water bath at 45C, and the sensor initially at 20C.

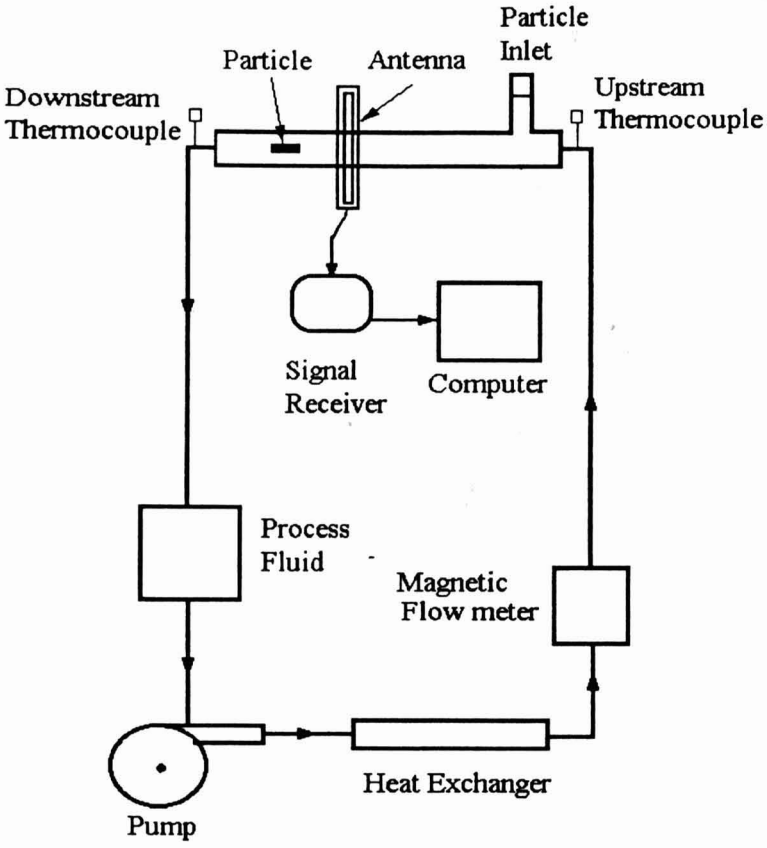

FIG. 1. SCHEMATIC DIAGRAM OF THE EXPERIMENTAL SETUP

conditions (fluid temperature was maintained at 45 $\pm$ 1C and the sensor was equilibrated to an initial temperature of 20C). Even though similar temperature response profiles were obtained under similar operating conditions, the sensor showed slow response to thermal changes (time constant of approximately 34 s over a temperature range of 20-45C). The quartz temperature sensing element was embedded within the pill along with the electronic components and its exact location within the sensor was unknown. Thus, it was not possible to accurately estimate the temperature at a known location within the particle.

The specific heat of the temperature pill, estimated using calorimetry, was found to be 5233 J/kgK. A subsequent heat transfer analysis of the temperature

response revealed that the sensor had a high internal resistance to heat transfer and was ill-conditioned for Biot number calculations. During preliminary studies under continuous flow conditions in tubes, difficulties were encountered in controlling sensor orientation, which could be either axial or perpendicular to the flow. As a result, weak signals were often received resulting in erroneous temperature readings. Since the receiver had a long logging interval (5 s), it became necessary to either use unrealistically low flow rates or an inordinately long test section to ensure that adequate data were collected for each experimental run. The latter solution was found impractical due to restrictions in laboratory space, and the logistics of mounting and supporting a tube assembly that would not interfere with free operator and antenna motion. A faster sampling rate was clearly necessary.

In a separate study (conducted during summer, 1991), an attempt was made to explore the application of the Micropack sensor (Mesa Medical Inc., Wheat Ridge, CO; dimensions and properties listed in Table 1) in the same application. The sensor was found inapplicable for the present situation due to its large dimensions (diameter 36 mm, length 53 mm) relative to food particles, and practical restrictions in the hold tube size commonly used in the industry (50 mm diameter).

The manufacturer of the temperature pill sensor (Human Technologies, Inc., St Petersburg, FL) was contacted with the following needs: (1) faster temperature sampling rate (1 s or less); and (2) separation of quartz temperature sensing element from microcircuitry; and (3) improved signal transmission capabilities for different orientations of the sensor. Subsequent discussions with the company led to the design of a modified sensor (Fig. 2) with the temperature sensing element protruding from the electronic composite. Due to the limitations in battery technology, the sensor could only be used up to a process temperature of 85C with a minimum sampling time of 1 s. The thermal conductivity and specific heat of different components of the modified temperature sensor were measured using a modified Fitch apparatus (Zuritz *et al.* 1989) and differential scanning calorimetry respectively. The dimensions of the modified sensor are given in Table 1 and the properties of different component parts are listed in Table 2.

Construction of the Transducer

Sastry *et al.* (1990) used a transducer particle made of aluminum whose density was adjusted to that of a food particle. The choice of a metallic particle with high thermal conductivity (and low Biot number) permitted rapid measurement of h_{fp} in continuous tube flow conditions. Since the temperature pill did not transmit signals through high conductivity metallic particles such as

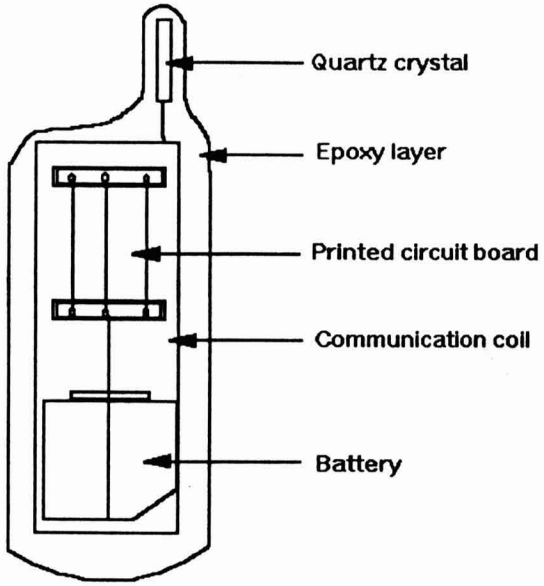

FIG. 2.SCHEMATIC DIAGRAM OF THE MODIFIED TEMPERATURE SENSOR

TABLE 2.
PROPERTIES OF BORON NITRIDE CYLINDER AND COMPONENTS OF THE MODIFIED TEMPERATURE SENSOR

Material	Specific Heat (kJ/kg°K)	Thermal Conduc. W/m°K
Boron Nitride[1]	0.59	161
Sensor[2]-Temperature sensing element	1.70	0.77
Epoxy layer	1.25	0.10
Electronics	1.08	0.39
Circuit wires	0.40	401

[1] Data taken from manufacturer's literature

[2] Mean values of three replicates determined using Differential Scanning Calorimetry for specific heat, and the modified Fitch apparatus for thermal conductivity

aluminum and copper, we attempted to use a nonmetallic particle with high thermal conductivity. Attempts to construct a silicon transducer failed due to difficulties in machining a hollow thin-walled (to adjust the effective density of particle with pill to that of a food particle) particle. Eventually, a specially fabricated hollow cylindrical particle made of boron nitride [diameter 0.0178 m (0.70 in.) and length 0.032 m (1.26 in.) with two end caps] was used (fabrication by Accuratus Ceramic Corporation, Washington, NJ). The shape and dimensions of the cylinder were chosen to ensure that the cylinder with the modified temperature pill within it would result in an effective density similar to that of a real food particle. Upon fabrication, installation of the pill and assembly, the effective density was measured as 1025.5 kg/m^3. The properties of the various components are given in Table 2. A diagram of the assembly is presented in Fig. 3.

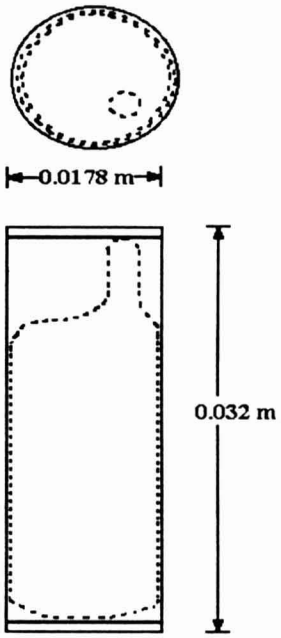

FIG. 3. PLAN AND ELEVATION OF TRANSDUCER WITH TEMPERATURE SENSOR INSTALLED

Experimental Conditions

Aqueous solutions of sodium carboxymethylcellulose (CMC,7HF, Aqualon, Wilmington, DE) were used as carrier media. Experiments were conducted

during the fall of 1993, at a fluid temperature of 60C, for two viscosities (0.5% and 0.8% CMC concentrations), and three flow rates of 0.000126, 0.000221, and 0.000315 m^3/s (2.0, 3.5, and 5.0 gal,min respectively). Experiments consisted of introduction of the transducer particle (with temperature pill embedded within) into the upstream end of the test section. As the particle moved through the test section, the external antenna was manually moved along with it to receive signals. Care had to be exercised to ensure that the antenna was always within three feet of the particle, to prevent inaccurate temperature readings.

Replications. Results were based on approximately 60 experimental runs (minimum of five replicates at the flow rate of 0.000126 m^3/s (2.0 gal/min) and 10 replicates for flow rates of 0.000221 and 0.000315 m^3/s (3.5 gal/min and 5.0 gal/min). At higher flow rates (e.g., 0.000505 m^3/s corresponding to 8 gal/min) manual movement of the antenna along with the particle was difficult, and weak signals were transmitted, resulting in erroneous temperature readings. Hence, only data from flow rates up to 0.000315 m^3/s (5 gal/min) could be considered. The method could be improved further by installing a series of antennae along the test section to receive signals as the particle moves through it.

Theory

The governing heat conduction equation for the temperature T of a solid when subjected to heat exchange with a surrounding fluid can be determined using the heat conduction equation:

$$\nabla.(k\nabla T) = \rho C_p \frac{\partial T}{\partial t} \tag{1}$$

with a convective boundary condition at the fluid-solid interface:

$$k\nabla T.\vec{n} = h_{fp} [T_s - T_f] \tag{2}$$

Equation (2) may be solved for three dimensional space using the Galerkin-Crank-Nicolson algorithm, which involves finite elements in space dimensions and finite differences in time. A modified version of the finite element algorithm developed by Sastry *et al.* (1985) was employed. The approach, outlined in Fig. 4, involved the following steps. An initial estimate of h_{fp} was first made and the average theoretically predicted temperature at the location that corresponded to that of the sensor was generated. The differences between observed and predicted temperatures were used to determine the error sum of square values. The procedure was then repeated with new values of h_{fp} until the error sum of squares was minimized with a maximum difference of 0.6C between observed and predicted temperature at any instant of time.

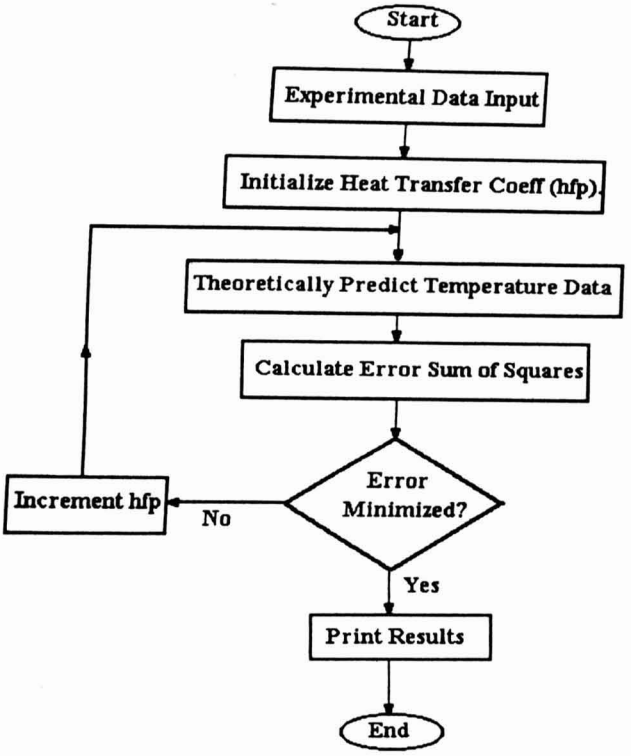

FIG. 4. PROGRAM FLOW CHART FOR FINITE ELEMENT ALGORITHM

Rheological Characterization

The rheological characteristics of the CMC solutions were studied using a coaxial cylinder type rotational viscometer (Contraves, RHEOMAT, MODEL 115, Contraves AG, Zurich, Switzerland) equipped with a jacket for temperature control. The data were fitted to the Ostwald-de Waele Power law model.

$$\tau = K\dot{\gamma}^n \tag{3}$$

Values of consistency coefficient (K) and flow behavior index (n) for different experimental conditions are presented in Table 3. The range of dimensionless parameters of the study are presented in Table 4.

TABLE 3.
RHEOLOGICAL CHARACTERISTICS OF CARRIER FLUID (CMC) AT 60C

Concentration of CMC %	Consistency Coefficient (K) Pas^n	Flow behavior index (n)
0.5	0.058	0.873
0.8	0.237	0.821

TABLE 4.
RANGE OF DIMENSIONLESS NUMBERS

Parameter	Maximum	Minimum
Generalized Fluid Reynolds number	196.8	19.0
Generalized Prandtl number	1014.0	245.0
Biot number	0.036	0.008

RESULTS AND DISCUSSION

A sample plot of measured and predicted temperature histories of the modified temperature sensor is shown in Fig. 5. The value of h_{fp} ranged from 134 W/m^2K to 669 W/m^2K (Nu = 3.6 to 17.3); standard deviations ranged from 10.2 to 93.0 W/m^2K. As expected, h_{fp} increased significantly with decreasing carrier medium viscosity and increased with increasing flow rate (Fig. 6) ($p < 0.05$ by F-test). These values were lower than those of our previous studies (Table 5), primarily because of the low (generalized) Reynolds numbers of this study. As indicated earlier, studies at higher Reynolds numbers were too difficult because of the need for accurate antenna positioning relative to the particle.

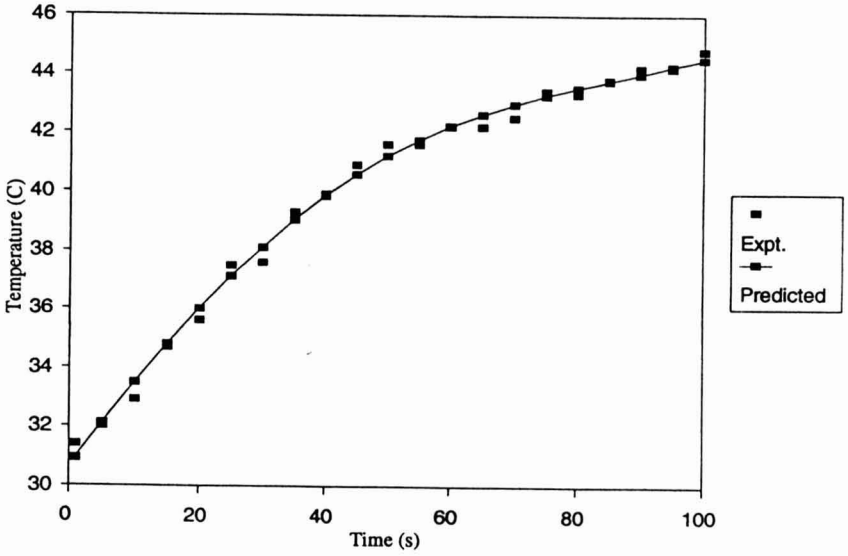

FIG. 5. SAMPLE PLOT OF MEASURED AND PREDICTED TEMPERATURE PROFILES (CMC con: 0.5%, Q=0.000221 m^3/s and h_{fp} = 423 W/m^2K)

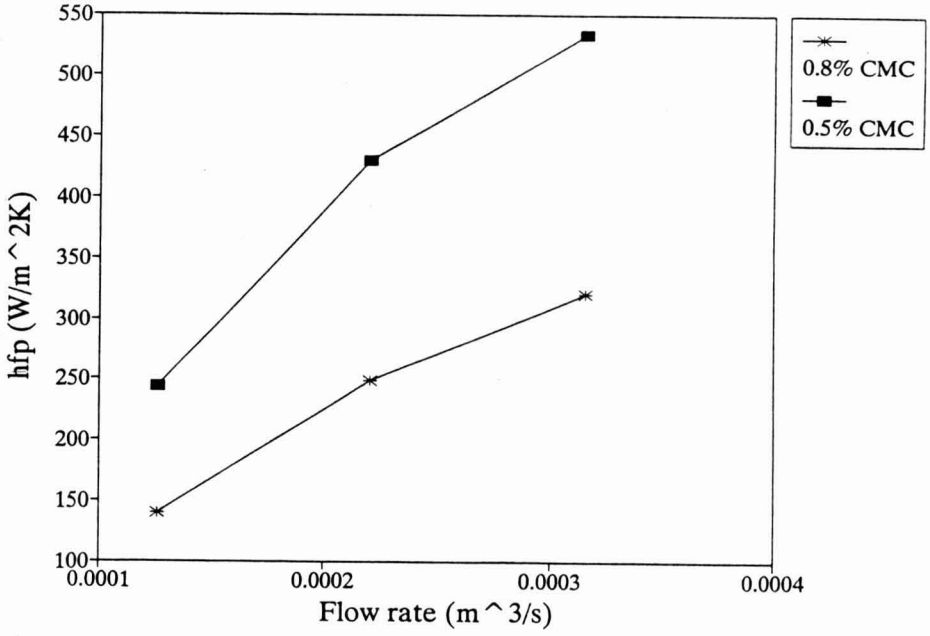

FIG. 6. EFFECT OF CARRIER MEDIUM VISCOSITY AND FLOW RATE ON h_{fp}

TABLE 5.
RANGE OF h_{fp} DATA REPORTED IN THE LITERATURE USING DIFFERENT EXPERIMENTAL APPROACHES

Source	Reynolds no.	Particle Geometry	h_{fp} (W/m^2K)	Remarks
Sastry *et al.* 1990	7,300-43,600	Spherical	688-3005	Moving thermocouple method
Balasubramaniam and Sastry 1994b	2,174-10,422	Cube	986-2270	Liquid crystal method
Zitoun and Sastry 1995	21.2-270	Cube	286-1277	Relative velocity method (& flat plate correlation)
Present study	19.0-196.8	Cylinder	134-669	Temperature pill method

Additional reasons for our lower values were likely the location of the temperature sensor, and the orientation of the particle relative to the flow. The earlier studies were conducted over wider ranges of fluid Reynolds number and were based on average surface temperature of particles. The present data were based on temperature measurement with the sensor at the downstream face of the cylinder (which was oriented with the length parallel to the flow, and moved along the bottom of the tube). For such a flow situation, forced convection effects are predominantly along the length dimension, with reduced effects on the downstream face, due to a stagnant region. A representation of this situation is illustrated in Fig. 7 for a particle moving at the center of the tube; the situation with a bottom flowing particle is qualitatively similar. Thus our present data likely represent local heat transfer coefficients at a relatively stagnant downstream location. We have verified this point using thermal visualization studies in our laboratory using a continuous flow ohmic heater, where it is apparent that the heat transfer from particle to fluid is greater on the sides than either the upstream or downstream faces. We should also note that as flow rates increase, vortices would occur at the downstream face, as well established from the fluid mechanics and convective heat transfer literature (e.g., Eckert and Drake 1959). Vortex formation and flow separation might change the situation to one of enhanced heat transfer on these faces.

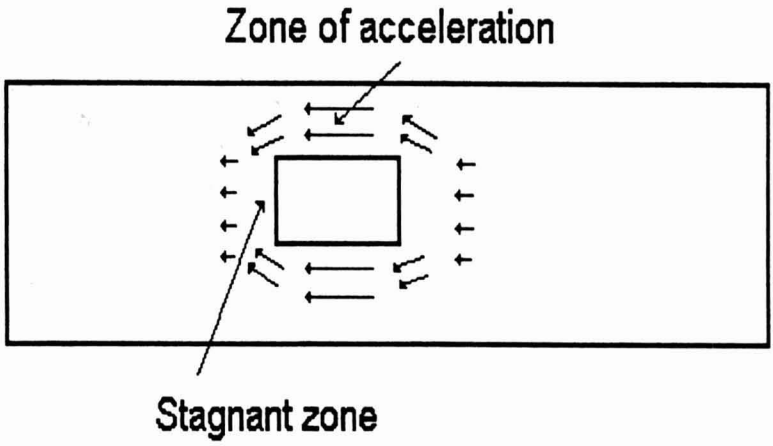

FIG. 7. ILLUSTRATION OF STAGNANT ZONES ABOUT A CYLINDRICAL PARTICLE IN TUBE FLOW

One final reason for low h_{fp} is the absence of particle rotation in these studies. The construction of the transducer resulted in an eccentric internal weight distribution, thus the particle did not rotate. This would be expected to result in lower h_{fp} than for a rotating particle. It may be noted that even with these many conservative factors at play, the lowest Nusselt number was higher than the value of 2 expected for a stagnant fluid surrounding a sphere.

Although the present setup requires a transparent carrier fluid and tube to maintain proximity between antenna and particle, it may be possible to eliminate this restriction by use of a multiple antenna arrangement. This would be more expensive, but could be considered if transparent model carriers cannot be used.

An ideal temperature sensor would (1) be small enough to not interfere with the particle dynamics; (2) be capable of either transmitting signals to an external receiver without interference or alternatively possess built-in data storage capabilities; and (3) be able to measure transient temperature changes up to the sterilization temperature range. It appears that none of the currently available sensors satisfy all these requirements. The temperature restriction is due to the difficulty in developing miniature sized batteries which operate at elevated temperatures. The physical dimensions of the sensor are dictated by battery dimensions; thus it is possible to achieve higher temperature operation at the expense of increased battery size. However, since the pill is already of significant size compared to many realistic food particles, increased size is not desirable. An alternate possibility is the development of a remote miniaturized temperature sensor with built-in data storage capabilities which could be powered by an external source (Hicks 1992); however this would require additional development effort and expenditure. If such a development occurs in the coming years, it may be possible to measure h_{fp} at elevated process temperatures, as well as monitor temperatures within particles.

CONCLUSIONS

Although some limitations exist, the temperature pill may be modified for measurement of temperature (and h_{fp}) of moving particles in continuous flow through aseptic processing systems. The maximum and minimum values of h_{fp} measured were 134 W/m^2K to 669 W/m^2K respectively, the relatively low (compared to our previous work) values being primarily attributable to the low fluid Reynolds numbers necessitated for the study. Even with these conservative factors, Nusselt numbers were found greater than the value of 2.0 expected for a stagnant fluid surrounding a spherical particle.

LIST OF SYMBOLS

Bi Biot number ($h_{fp}l/kp$)
C_p Specific heat (J/kgK)
d Diameter of the particle (m)
D Diameter of the holding tube (m)
h_{fp} Liquid-to-particle convective heat transfer coefficient (W/m^2K)
k_f Thermal conductivity of the fluid (W/mK)
k_p Thermal conductivity of particle (W/mK)
K Consistency coefficient (Pas^n)
l Characteristic dimension (m)
n Flow behavior index
Nu Nusselt number ($Nu = h_{fp}d/k_f$)
Pr_G Generalized Prandtl number ($Pr_G = [C_pK ((3n+1)/n)^n 2^{(n-1)}] / [4 k_f V_f^{(1-n)}D^{(n-1)}]$)
Re_G Generalized fluid Reynolds number ($Re_G = [8V_f^{(2-n)}D^n\rho]/[2^n ((3n+1)/n)^n]$
V_f Velocity of fluid (m/s)
t Time (s)
T_s Temperature of the particle surface (C)
T_f Temperature of the fluid (C)

Greek symbols:

γ Shear rate (s^{-1})
∇ Gradient
τ Shear stress (Pa)
ρ Density (kg/m3)

REFERENCES

ASHLEY, D.L. 1992. DATATRACE[R] - Personal Communication. Wheat Ridge, CO.

BALASUBRAMANIAM, V.M. and SASTRY, S.K. 1994a. Liquid-to-particle heat transfer in non-Newtonian carrier medium during continuous tube flow. J. of Food Engr. *23*, 169–187.

BALASUBRAMANIAM, V.M. and SASTRY, S.K. 1994b. Convective heat transfer at particle-liquid interface in continuous tube flow at elevated fluid temperatures. J. Food Sci. *59*(3), 675–681.

BHAMIDIPATI, S. and SINGH, R.K. 1995. Determination of fluid-particle convective heat transfer coefficient. Transactions of the ASAE, *38*(3), 857–862.

DUTTA, B. and SASTRY, S.K 1990. Velocity distributions of food particle suspensions in holding tube flow: Experimental and modeling studies on average particle velocities. J. Food Sci. *55*(5), 1448–1453.

ECKERT, E.R.G. and DRAKE, R.M. 1959. *Heat and Mass Transfer*. 2nd. Ed. McGraw-Hill Book Co., New York.

HENDRICKX, M., WENG, Z., MAESMANS, G. and TOBBACK, P. 1992. Validation of a time-temperature integrator for thermal processing of foods under pasteurization conditions. Int. J. Food Sci. Technol. *27*, 21–31.

HEPPELL, N.J. 1985. Measurement of the liquid-solid heat transfer coefficient during continuous sterilization of foodstuffs containing particles. IuFoST Symposium on aseptic processing and packaging of foods: proceedings. pp. 108–114. Sep 9-12. Tyløsand, Sweden.

HICKS, W.S. 1992. Personal communication. Human Technologies, Inc., St. Petersburg, FL.

LEE, J.H. and SINGH, R.K. 1990. Particle residence time distribution in scraped surface heat exchanger. Paper no. 90-6522. Presented at the International Winter Meeting of American Society of Agricultural Engineers, Dec 18-21, Chicago, IL.

LESHO, J.C. and HOGREFE, A.F. 1989. Indigestible size continuously transmitting temperature monitor pill. US Patent No. 4,844,076, 1989.

McCOY, S.C., ZURITZ, C.A. and SASTRY, S.K. 1987. Residence time distribution of simulated food particles in a holding tube: Paper no. 87-6536. Presented at the International Winter Meeting of American Society of Agricultural Engineers, Dec. 15-18, Chicago, IL.

MWANGI, J.M., RIZVI, S.S.H. and DATTA, A. 1993. Heat transfer to a particle in shear flow: application in aseptic processing. J. of Food Engr. *19*, 55–74.

SASTRY, S.K. 1992. Liquid to particle heat transfer coefficient in aseptic processing. Advances in Aseptic Processing Technologies. (P.E. Nelson and R.K. Singh, eds.) pp. 63-72, Elsevier App. Sci.

SASTRY, S.K., BEELMAN, R.B. and SPERONI, J.J. 1985. A three-dimensional finite element model for thermally induced changes in foods: Application to degrataion of agaritine in canned mushrooms. J. Food Sci. *50*(5), 1293–1299, 1326.

SASTRY, S.K, LIMA, M., BRIM, J., BRUNN, T. and HESKITT, B.F. 1990. Liquid-to-particle heat transfer during continuous tube flow: Influence of flow rate and particle to tube diameter ratio. J. Food Engr. 13, 239-253.

STOFOROS, N.G. and MERSON, R.L. 1991. Measurement of heat transfer coefficients in rotating liquid/particulate systems. Biotech. Prog. *7*, 267–271.

TAEYMANS, D., ROELANS, E. and LENGES, J. 1985. Residence time distribution in a horizontal SSHE used for UHT processing of liquids containing solids. Presented at the 4th International Congress on Engineering and Foods, July 7–10, Edmonton, Alberta, Canada.

YANG, B.B. and SWARTZEL, K.R. 1992. Particle residence time distribution in two-phase flow in straight circular conduit. J. of Food Sci. *57*(2), 497–502.

ZITOUN, K.B. and S.K. SASTRY. 1994. Determination of convective heat transfer coefficient between fluid and cubic particle in continuous tube flow using noninvasive experimental techniques. J. Food Process Engineering *17*, 209–228.

ZURITZ, C.A., SASTRY, S.K., McCOY, S.C., MURAKAMI, E.G. and BLAISDELL, J.L. 1989. A modified Fitch device for measuring the thermal conductivity of small food particles. Trans. ASAE. *32*(2), 711–718.

F N P PUBLICATIONS IN FOOD SCIENCE AND NUTRITION

Journals

JOURNAL OF FOOD LIPIDS, F. Shahidi
JOURNAL OF RAPID METHODS AND AUTOMATION IN MICROBIOLOGY, D.Y.C. Fung and M.C. Goldschmidt
JOURNAL OF MUSCLE FOODS, N.G. Marriott, G.J. Flick, Jr. and J.R. Claus
JOURNAL OF SENSORY STUDIES, M.C. Gacula, Jr.
JOURNAL OF FOODSERVICE SYSTEMS, C.A. Sawyer
JOURNAL OF FOOD BIOCHEMISTRY, J.R. Whitaker, N.F. Haard and H. Swaisgood
JOURNAL OF FOOD PROCESS ENGINEERING, D.R. Heldman and R.P. Singh
JOURNAL OF FOOD PROCESSING AND PRESERVATION, D.B. Lund
JOURNAL OF FOOD QUALITY, J.J. Powers
JOURNAL OF FOOD SAFETY, T.J. Montville
JOURNAL OF TEXTURE STUDIES, M.C. Bourne and M.A. Rao

Books

HACCP: MICROBIOLOGICAL SAFETY OF MEAT AND POULTRY, J.J. Sheridan, R.L. Buchanan and T.J. Montville
OF MICROBES AND MOLECULES: FOOD TECHNOLOGY AT M.I.T., S.A. Goldblith
MEAT PRESERVATION: PREVENTING LOSSES AND ASSURING SAFETY, R.G. Cassens
S.C. PRESCOTT, M.I.T. DEAN AND PIONEER FOOD TECHNOLOGIST, S.A. Goldblith
FOOD CONCEPTS AND PRODUCTS: JUST-IN-TIME DEVELOPMENT, H.R. Moskowitz
MICROWAVE FOODS: NEW PRODUCT DEVELOPMENT, R.V. Decareau
DESIGN AND ANALYSIS OF SENSORY OPTIMIZATION, M.C. Gacula, Jr.
NUTRIENT ADDITIONS TO FOOD, J.C. Bauernfeind and P.A. Lachance
NITRITE-CURED MEAT, R.G. Cassens
POTENTIAL FOR NUTRITIONAL MODULATION OF AGING, D.K. Ingram *et al.*
CONTROLLED/MODIFIED ATMOSPHERE/VACUUM PACKAGING OF FOODS, A.L. Brody
NUTRITIONAL STATUS ASSESSMENT OF THE INDIVIDUAL, G.E. Livingston
QUALITY ASSURANCE OF FOODS, J.E. Stauffer
THE SCIENCE OF MEAT AND MEAT PRODUCTS, 3RD ED., J.F. Price and B.S. Schweigert
HANDBOOK OF FOOD COLORANT PATENTS, F.J. Francis
ROLE OF CHEMISTRY IN PROCESSED FOODS, O.R. Fennema *et al.*
NEW DIRECTIONS FOR PRODUCT TESTING OF FOODS, H.R. Moskowitz
ENVIRONMENTAL ASPECTS OF CANCER: ROLE OF FOODS, E.L. Wynder *et al.*
FOOD PRODUCT DEVELOPMENT AND DIETARY GUIDELINES, G.E. Livingston, R.J. Moshy and C.M. Chang
SHELF-LIFE DATING OF FOODS, T.P. Labuza
ANTINUTRIENTS AND NATURAL TOXICANTS IN FOOD, R.L. Ory
UTILIZATION OF PROTEIN RESOURCES, D.W. Stanley *et al.*
VITAMIN B_6: METABOLISM AND ROLE IN GROWTH, G.P. Tryfiates
POSTHARVEST BIOLOGY AND BIOTECHNOLOGY, H.O. Hultin and M. Milner

Newsletters

MICROWAVES AND FOOD, R.V. Decareau
FOOD INDUSTRY REPORT, G.C. Melson
FOOD, NUTRITION AND HEALTH, P.A. Lachance and M.C. Fisher

GUIDE FOR AUTHORS

Typewritten manuscripts in triplicate should be submitted to the editorial office. The typing should be double-spaced throughout with one-inch margins on all sides.

Page one should contain: the title, which should be concise and informative; the complete name(s) of the author(s); affiliation of the author(s); a running title of 40 characters or less; and the name and mail address to whom correspondence should be sent.

Page two should contain an abstract of not more than 150 words. This abstract should be intelligible by itself.

The main text should begin on page three and will ordinarily have the following arrangement:

Introduction: This should be brief and state the reason for the work in relation to the field. It should indicate what new contribution is made by the work described.

Materials and Methods: Enough information should be provided to allow other investigators to repeat the work. Avoid repeating the details of procedures that have already been published elsewhere.

Results: The results should be presented as concisely as possible. Do not use tables *and* figures for presentation of the same data.

Discussion: The discussion section should be used for the interpretation of results. The results should not be repeated.

In some cases it might be desirable to combine results and discussion sections.

References: References should be given in the text by the surname of the authors and the year. *Et al.* should be used in the text when there are more than two authors. All authors should be given in the Reference section. In the Reference section the references should be listed alphabetically. See below for style to be used.

RIZVI, S.S.H. 1986. Thermodynamic properties of foods in dehydration. In *Engineering Properties of Foods*, (M.A. Rao and S.S.H. Rizvi, eds.) pp. 133–214, Marcel Dekker, New York.

MICHAELS, S.L. 1989. Crossflow microfilters ins and outs. Chem. Eng. *96*, 84–91.

LABUZA, T.P. 1982. *Shelf-Life Dating of Foods*, pp. 66–120, Food & Nutrition Press, Trumbull, CT.

Journal abbreviations should follow those used in *Chemical Abstracts*. Responsibility for the accuracy of citations rests entirely with the author(s). References to papers in press should indicate the name of the journal and should only be used for papers that have been accepted for publication. Submitted papers should be referred to by such terms as "unpublished observations" or "private communication." However, these last should be used only when absolutely necessary.

Tables should be numbered consecutively with Arabic numerals. The title of the table should appear as below:

TABLE 1.
ACTIVITY OF POTATO ACYL-HYDROLASES ON NEUTRAL LIPIDS, GALACTOLIPIDS AND PHOSPHOLIPIDS

Description of experimental work or explanation of symbols should go below the table proper. Type tables neatly and correctly as tables are considered art and are not typeset. Single-space tables.

Figures should be listed in order in the text using Arabic numbers. Figure legends should be typed on a separate page. Figures and tables should be intelligible without reference to the text. Authors should indicate where the tables and figures should be placed in the text. Photographs must be supplied as glossy black and white prints. Line diagrams should be drawn with black waterproof ink on white paper or board. The lettering should be of such a size that it is easily legible after reduction. Each diagram and photograph should be clearly labeled on the reverse side with the name(s) of author(s), and title of paper. When not obvious, each photograph and diagram should be labeled on the back to show the top of the photograph or diagram.

Acknowledgments: Acknowledgments should be listed on a separate page.

Short notes will be published where the information is deemed sufficiently important to warrant rapid publication. The format for short papers may be similar to that for regular papers but more concisely written. Short notes may be of a less general nature and written principally for specialists in the particular area with which the manuscript is dealing. Manuscripts that do not meet the requirement of importance and necessity for rapid publication will, after notification of the author(s), be treated as regular papers. Regular papers my be very short.

Standard nomenclature as used in the engineering literature should be followed. Avoid laboratory jargon. If abbreviations or trade names are used, define the material or compound the first time that it is mentioned.

EDITORIAL OFFICE: DR. D.R. HELDMAN, COEDITOR, *Journal of Food Process Engineering*, Food Science/Engineering Unit, University of Missouri-Columbia, 235 Agricultural/Engineering Bldg., Columbia, MO 65211 USA; or DR. R.P. SINGH, COEDITOR, *Journal of Food Process Engineering*, University of California, Davis, Department of Agricultural Engineering, Davis, CA 95616 USA.

JOURNAL OF FOOD PROCESS ENGINEERING VOLUME 19, NUMBER 2

CONTENTS